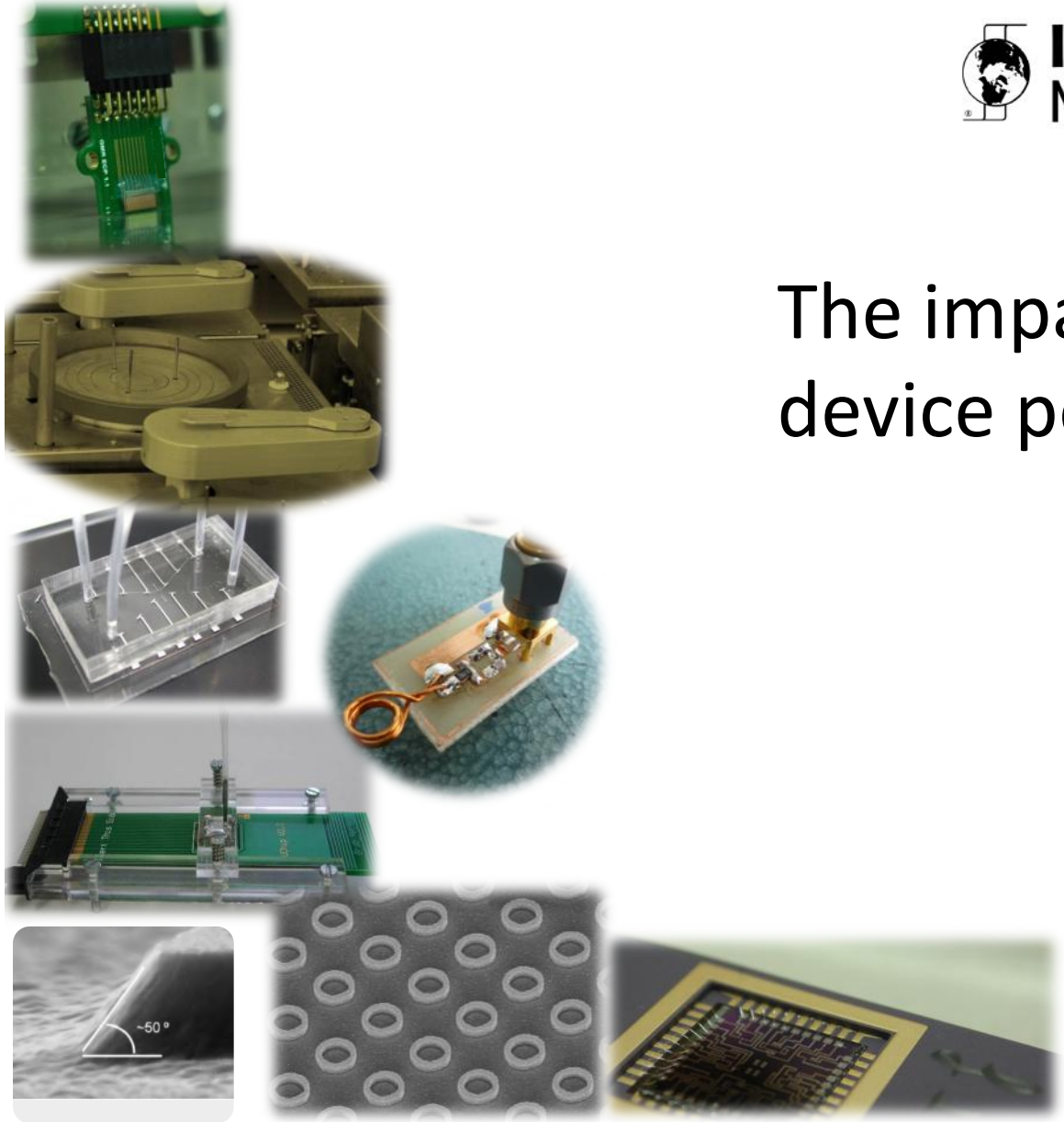

The impact of materials growth in device performance and scalability

Susana Cardoso de Freitas

Group leader Spintronics & Magnetic Sensors

INESC – Microsystems and Nanotechnologies
Lisbon, Portugal
www.inesc-mn.pt

INESC MN
Microsistemas &
Nanotecnologias

Outline

Magnetoresistive materials

- thin film materials
- thermal stability
- noise, SNR => detectivity

Magnetoresistive sensor applications

Magnetic sensors

INESC MN
Microsistemas & Nanotecnologias

Material optimization/ characterization

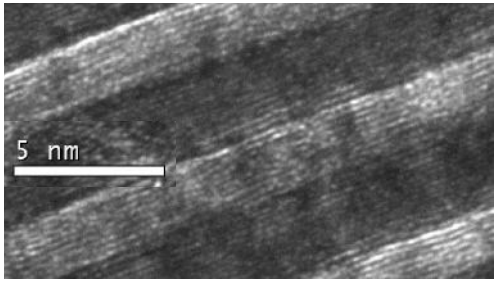

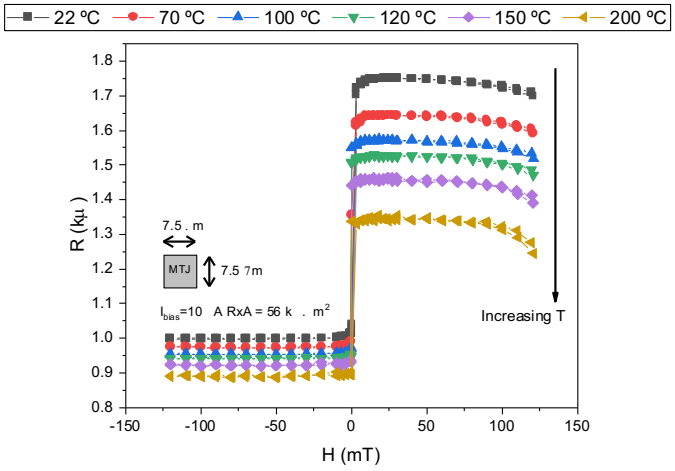

Sensor design and microfabrication

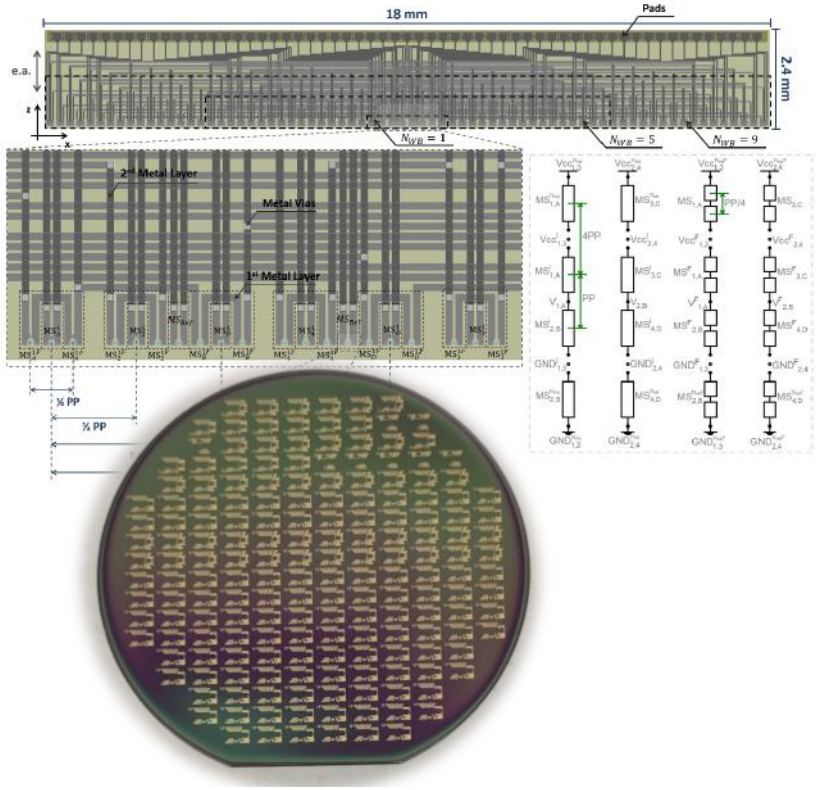

Sensor integration

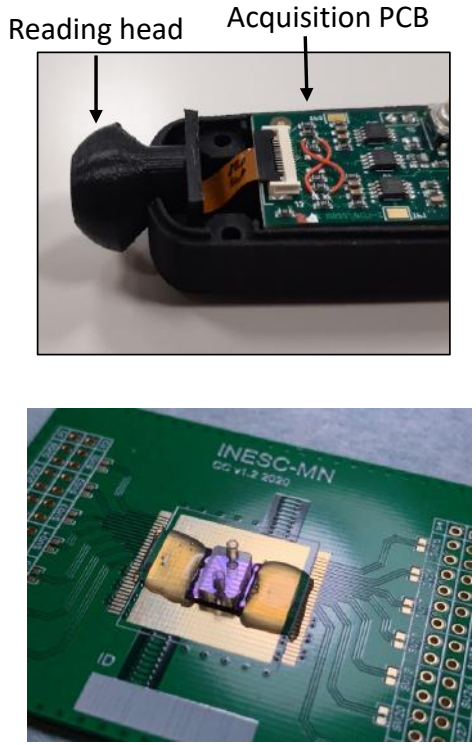

WHY MAGNETORESISTIVE SENSORS ARE CANDIDATES FOR MANY APPLICATIONS ?

INESC MN
Microsistemas & Nanotecnologias

Magnetoresistance $\mathrm{MR} = \dfrac{R_{max} - R_{min}}{R_{min}}$

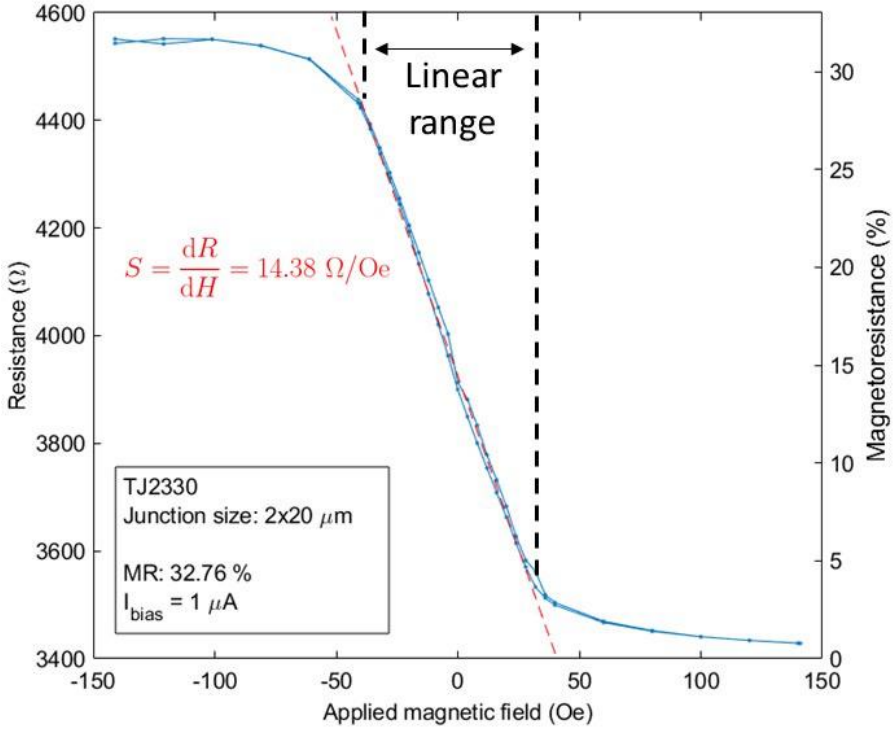

Typical MR values in sensors:

AMR: 2-5%
GMR: 6~15%
Al_2O_3 TMR: 20~40%
MgO TMR: 80~260%

- Work at room temperature
- Small sizes
- Thin films => in plane sensitive directions

Publications related with magnetic sensor applications

INESC MN
Microsistemas & Nanotecnologias

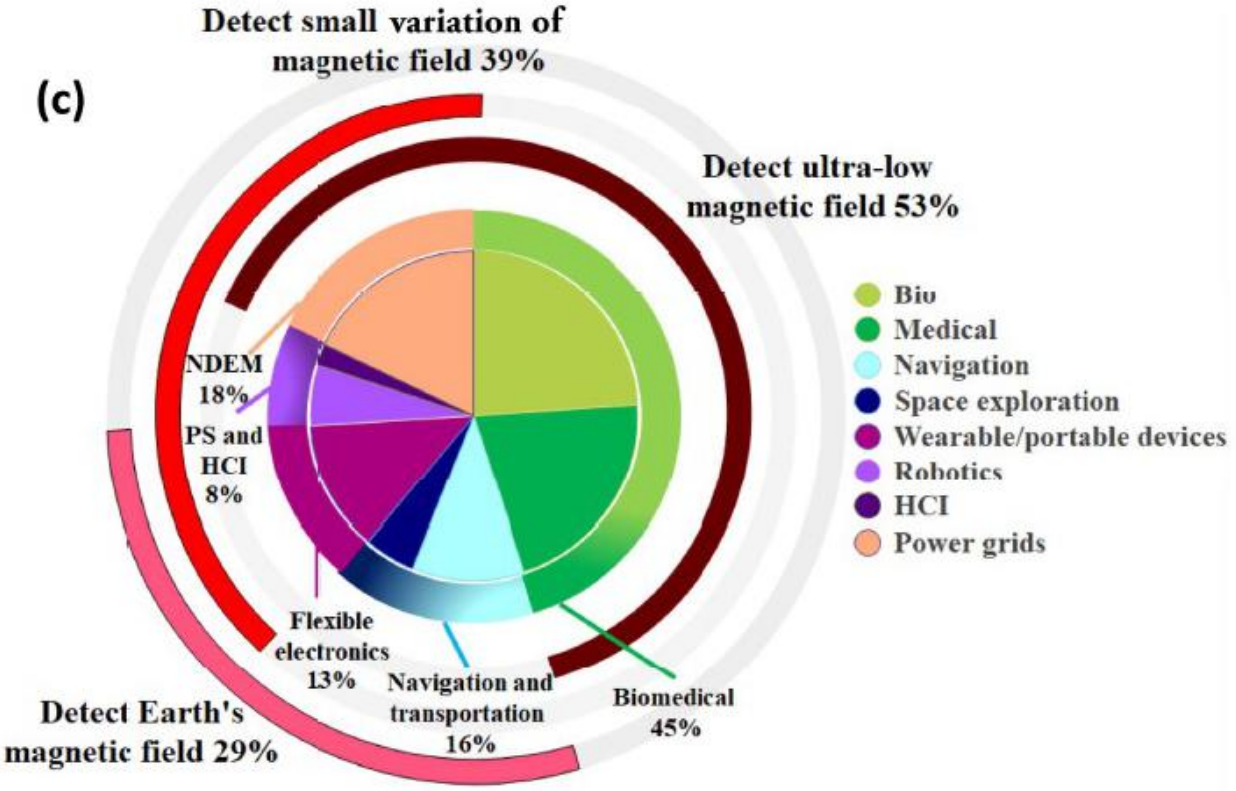

"Magnetoresistive Sensor Development Roadmap (Non-Recording Applications)"
IEEE Trans.Magn. (2019)

Integration with smart grid platforms

INESC MN

Microsistemas & Nanotecnologias

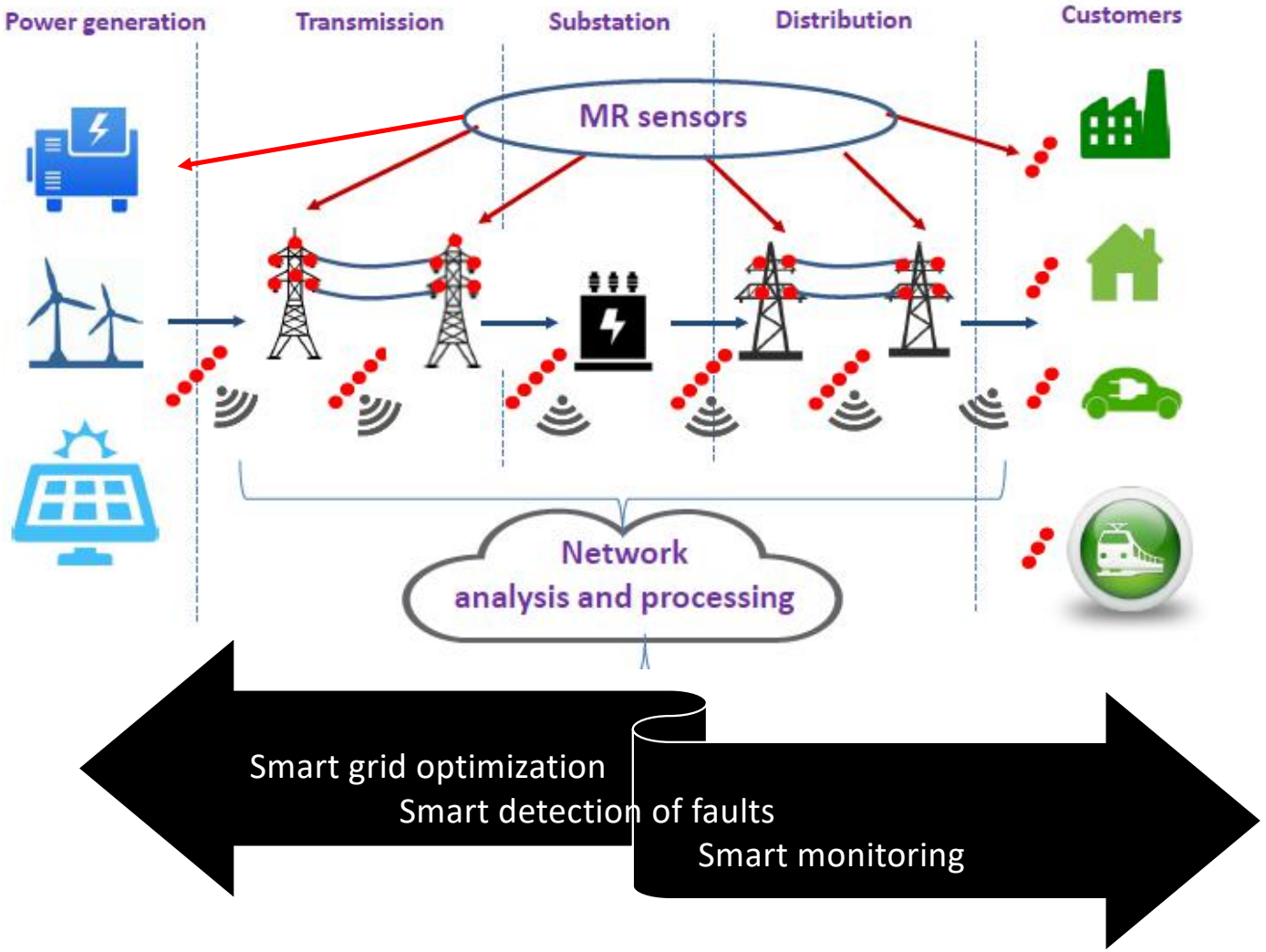

Developing path of magnetic sensing technology

Hall Sensor → AMR → GMR → TMR

Spinvalve

Hall effect	AMR effect	GMR effect	TMR effect
0.2 ~ 0.8 mV/V/Gs	0.1 ~ 0.3 mV/V/Gs	0.2 ~ 1 mV/V/Gs	2 ~ 10 mV/V/Gs

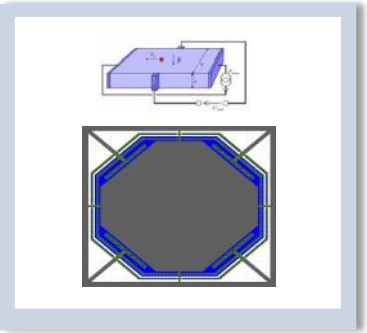

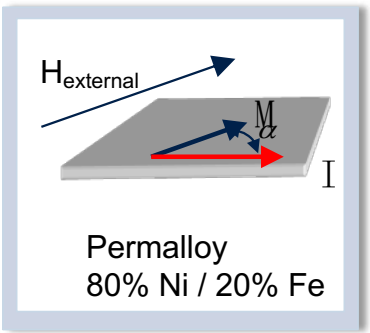

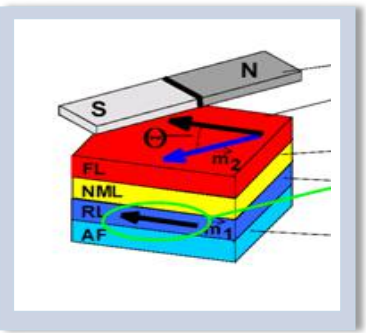

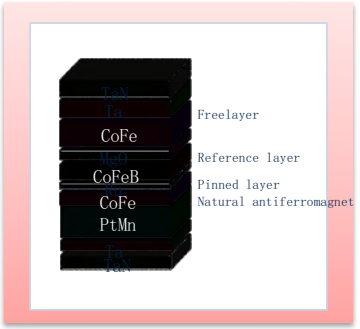

Hard Disks 1986 → 1996 → 2004 →

SENSORS Hall → AMR → GMR → TMR →

Magnetic tunnel junction - TMR

INESC MN
Microsistemas & Nanotecnologias

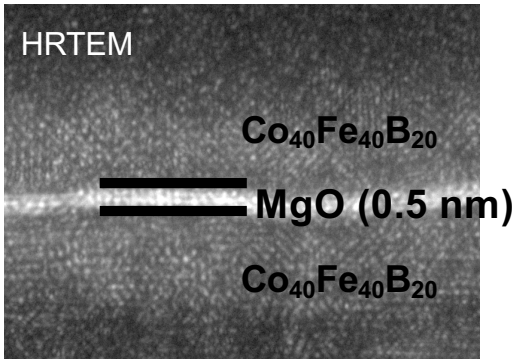

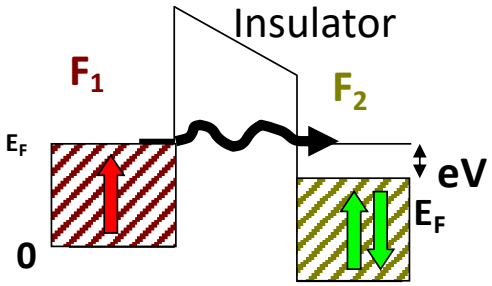

MIT, 1996
IBM, 1997
INESC, 1997

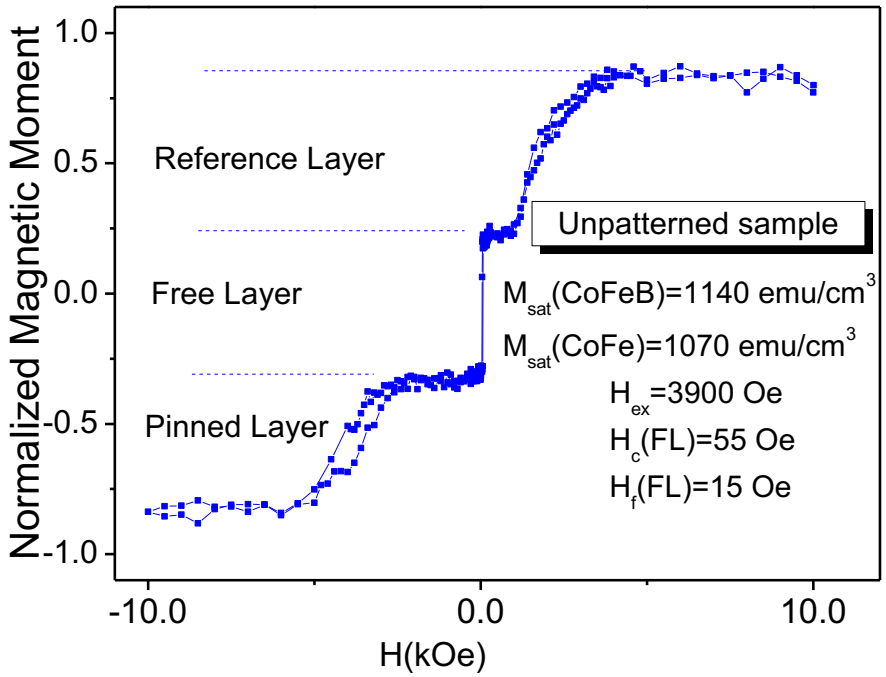

Electrons will tunnel if apply voltage between electrodes
Spin is conserved upon tunneling

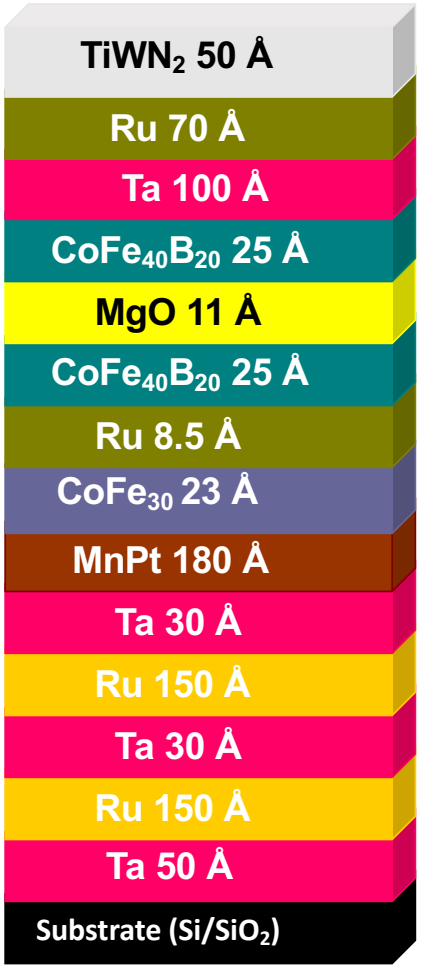

Micromagnetic and Analytical Models

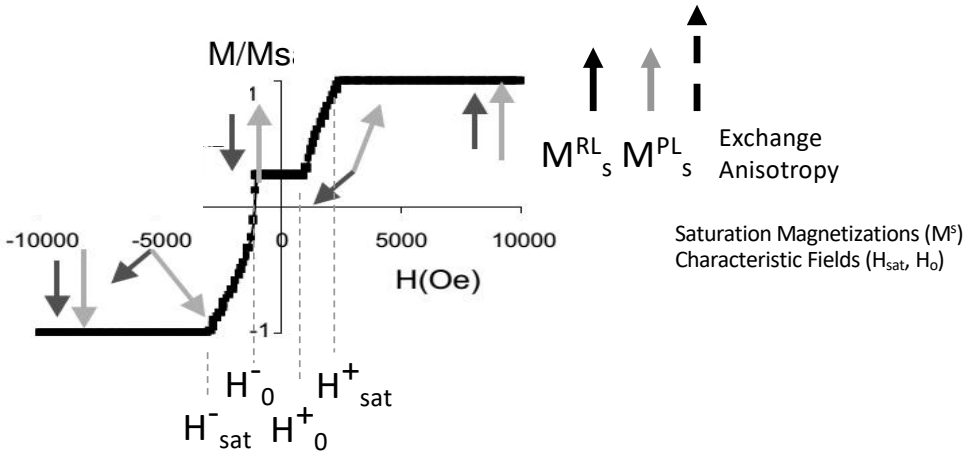

Saturation Magnetizations (M^s)
Characteristic Fields (H_{sat}, H_o)

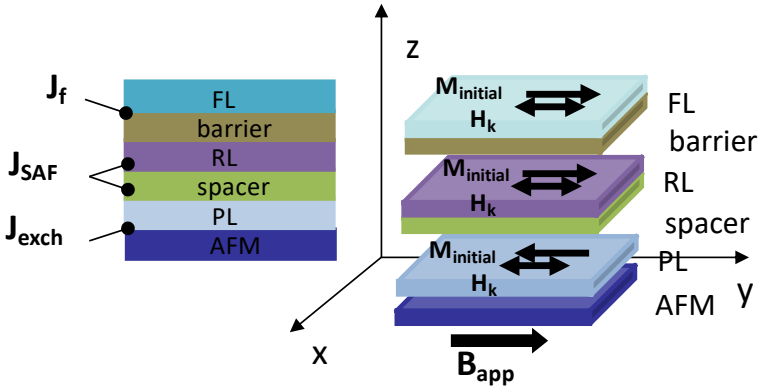

INESC MN
Microsistemas & Nanotecnologias

Nanotechnology 27, 045501 (2015)

Magnetoelectronics, Elsevier, Ed. Mark Jonhson, 2004

Experimental

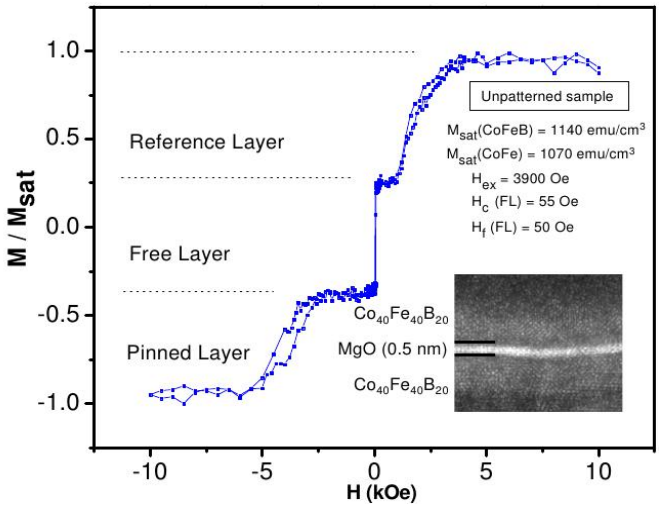

M_{sat}

J_{exch}
J_{SAF}
Jf

Simulation

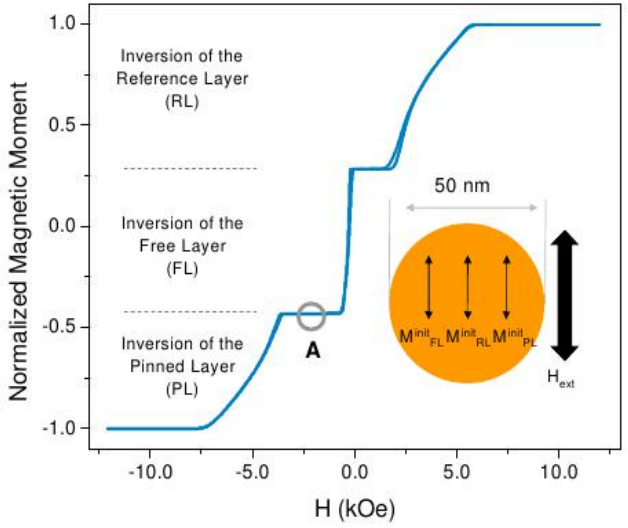

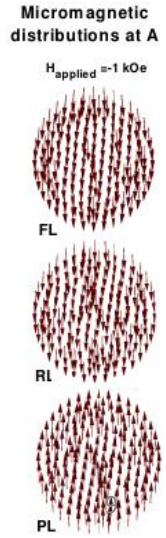

Modelling - micromagnetics

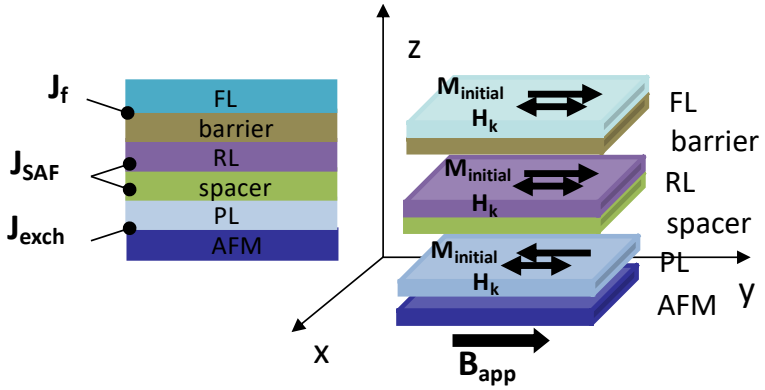

INESC MN
Microsistemas & Nanotecnologias

Magnetic volumic properties		
for all ferromagnetic volumes		
Saturation flux densities μ0Ms	*T*	*Initial M versor*
Uniaxial anisotropy flux density Hk	*T*	*Anisotropy versor*
for all micromagnetic volumes		

Surface Energy Coupling constants (erg/cm^2)	
Allmicromagnetic surfaces	
Exchange coupling between PL and AFM	J_{exch}
Néel Ferromagnetix Coupling	J_f
AntiFerromagnetic coupling trough spacer	J_{SAF}

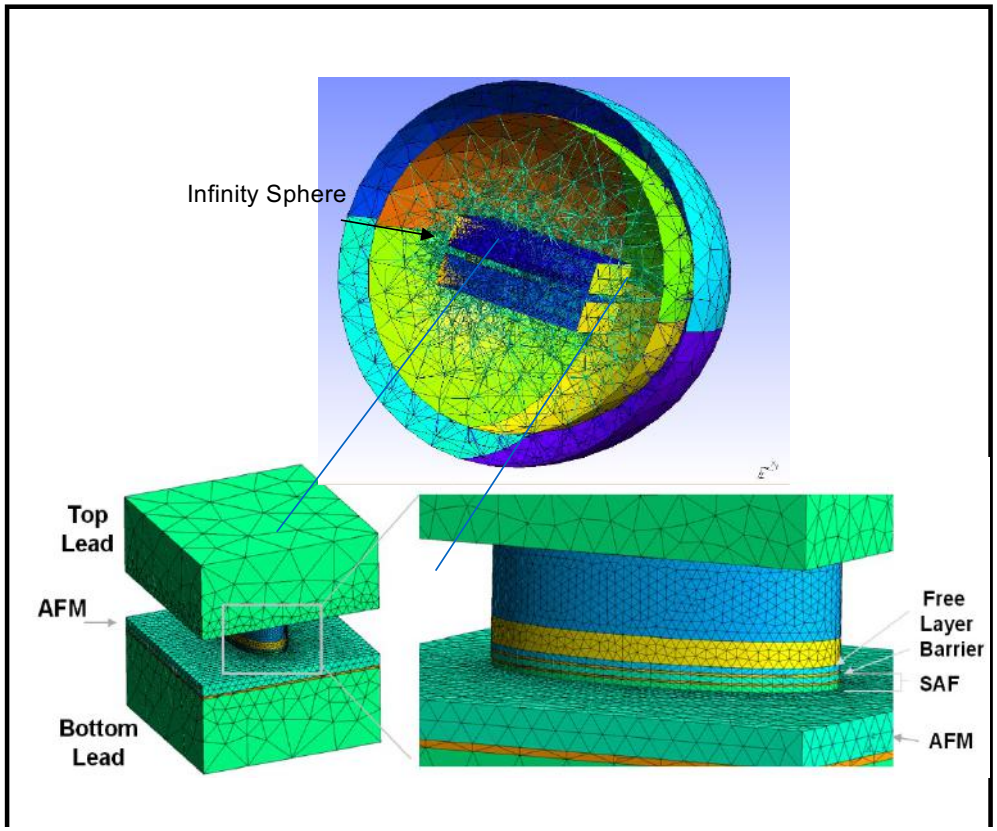

INESC MN
Microsistemas & Nanotecnologias

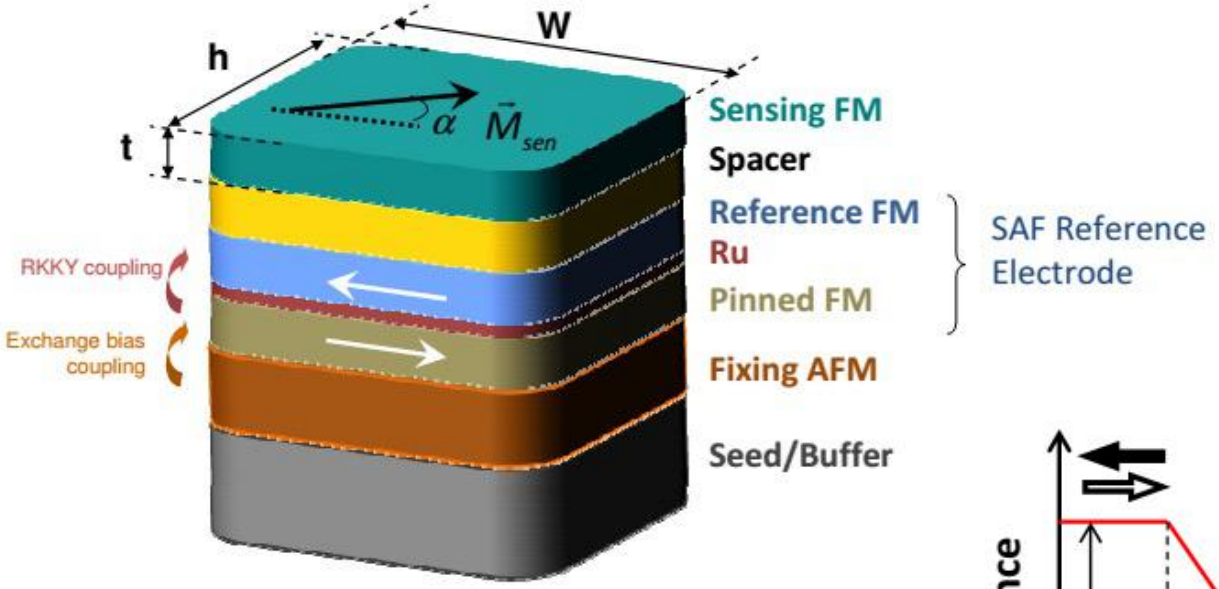

Linear range

ΔH ~ 10-100 Oe

(1-10 mTesla)

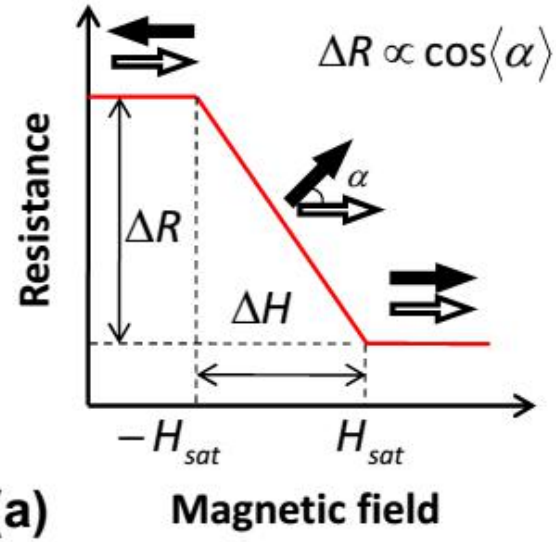

Eur. Phys. J. Appl. Phys. (2015) 72: 10601;

Magnetic Energy of a semi-infinite thin film **(w>>h,t)**

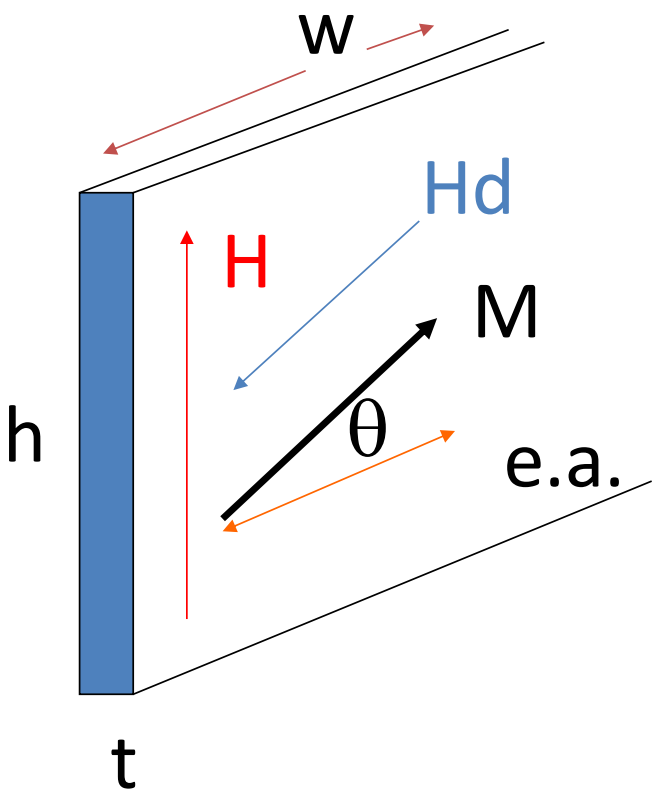

$$E/V=-\mu_o H.M + K \sin^2\theta - \tfrac{1}{2} \mu_o H_d.M$$

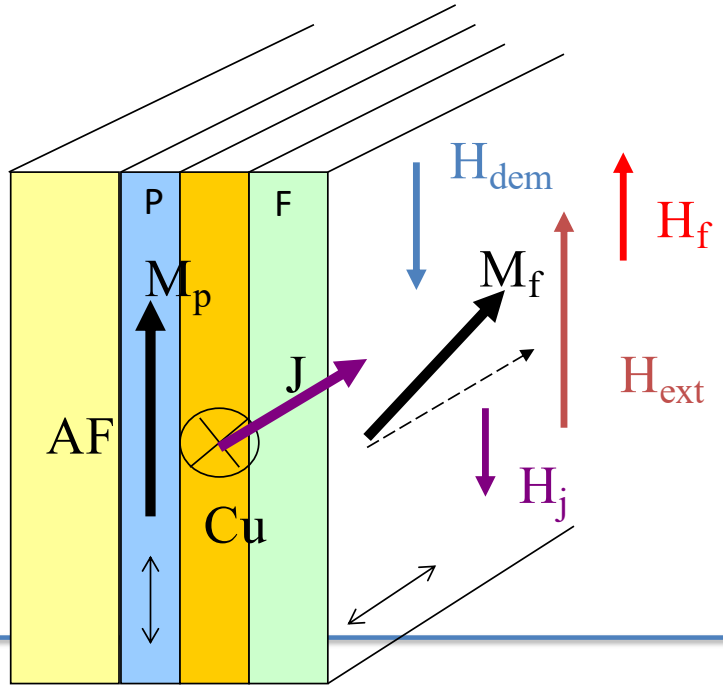

Theory Magnetic Recording, N.Bertram

B.D.Cullity(1972) Introduction to Magnetic Materials

1- C.Tsang, et.al, IEEE Trans.Magn., 30, 3801 (1994).

2- B.Dieny, et.al Phys.Rev.B, 43, 1297(1991).

3- D.E.Heim, et.al , IEEE Trans.Magn.., 30, 316 (1994);

4- P.P.Freitas, et.al , Appl.Phys.Lett., 65, 493 (1994);

Macrospin Model for MR sensors

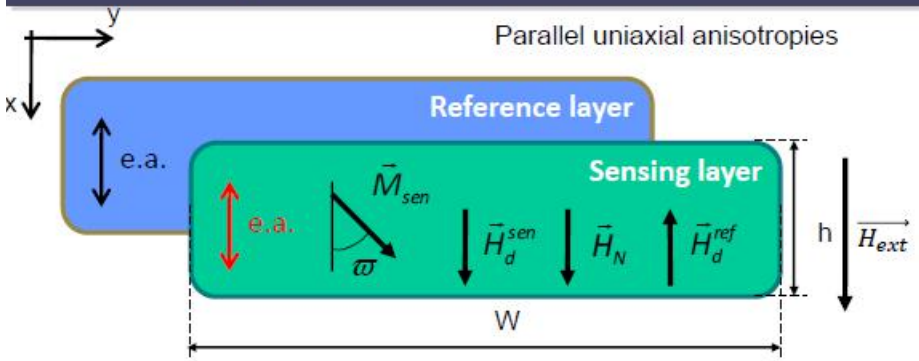

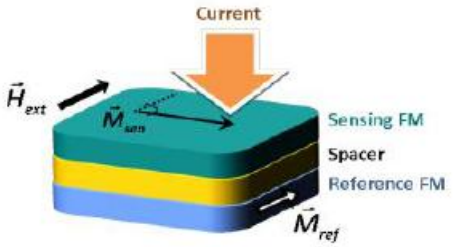

$t <<< h < W$

Energy minimization

When $H_{ap} < H^{ref}{}_d - H_N - |H_k - N_h M^{sen}{}_s|$

Minimum @ $\varpi = \pi$

When $H_{ap} > H^{ref}{}_d - H_N + |H_k - N_h M^{sen}{}_s|$

Minimum @ $\varpi = 0$

When $|H_{ap} - H^{ref}{}_d + H_N| < |H_k - N_h M^{sen}{}_s|$

2 situations can occur:
If $H_k > N_h M^{sen}{}_s$

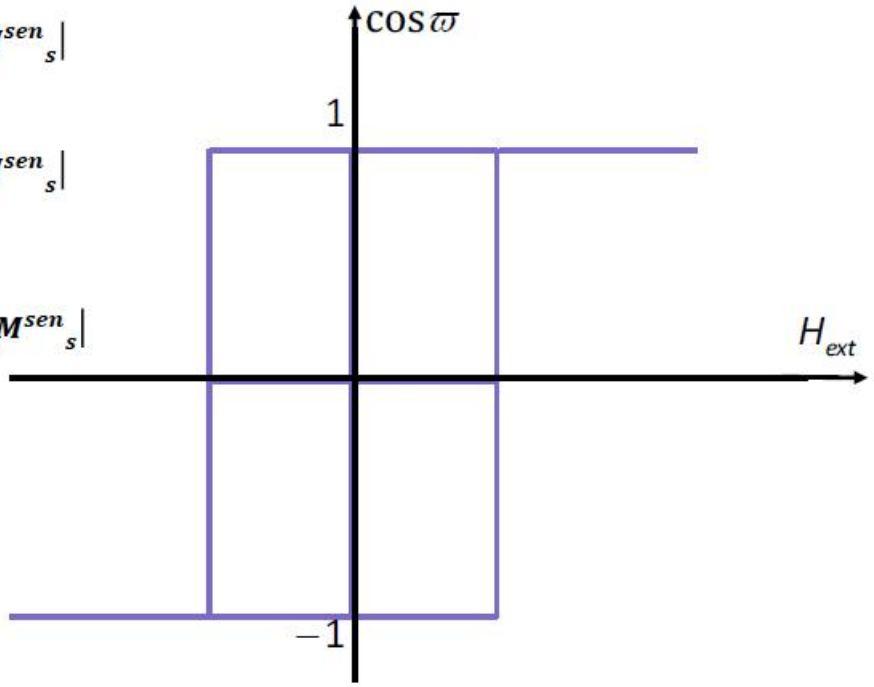

INESC MN

INESC MN
Microsistemas & Nanotecnologias

Macrospin Model for MR sensors

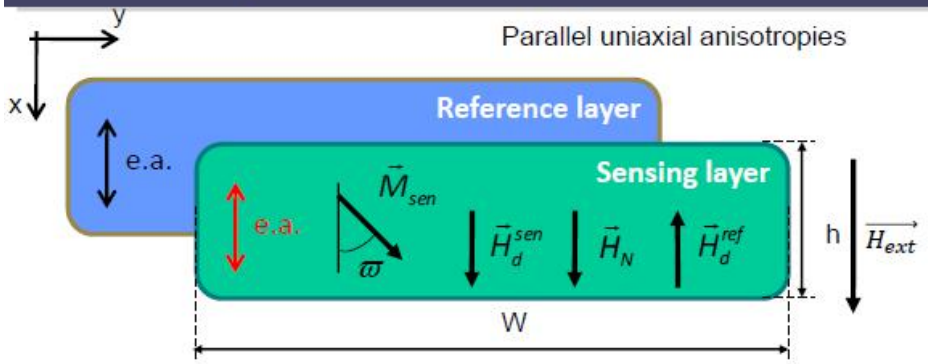

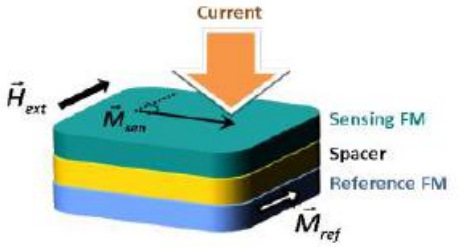

$t <<< h < W$

Energy minimization

When $H_{ap} < H^{ref}{}_d - H_N - |H_k - N_h M^{sen}{}_s|$

Minimum @ $\varpi = \pi$

When $H_{ap} > H^{ref}{}_d - H_N + |H_k - N_h M^{sen}{}_s|$

Minimum @ $\varpi = 0$

When $|H_{ap} - H^{ref}{}_d + H_N| < |H_k - N_h M^{sen}{}_s|$

2 situations can occur:

If $H_k < N_h M^{sen}{}_s$

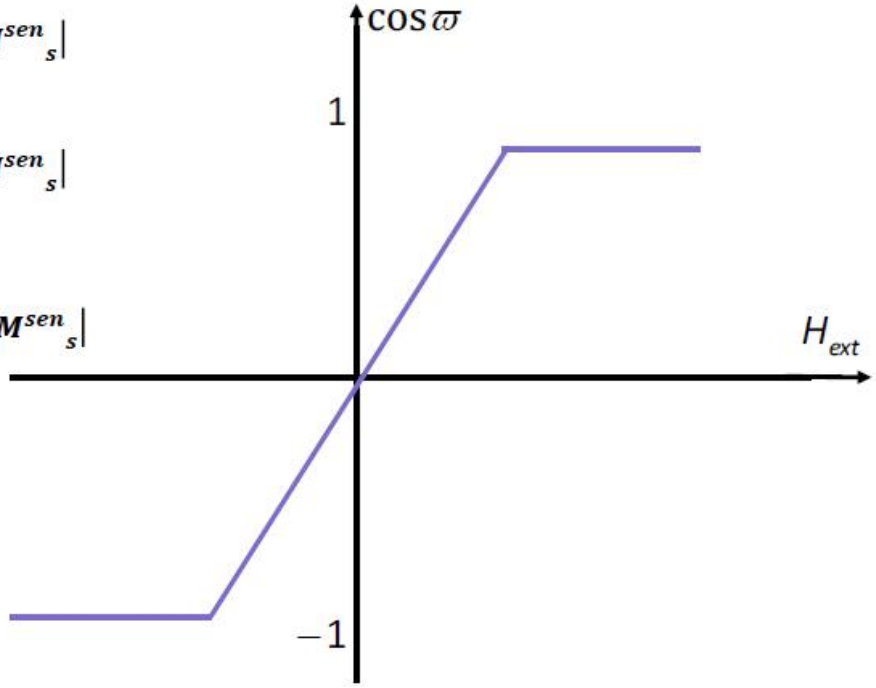

Macrospin Model for MR sensors

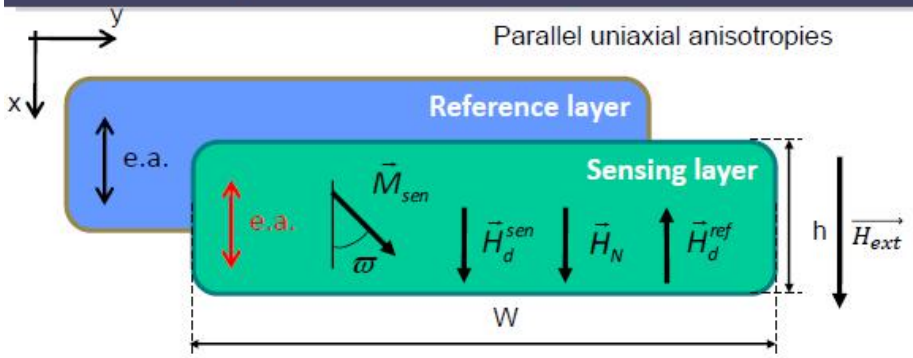

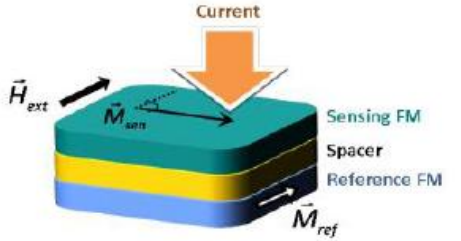

$t <<< h < W$

Final transfer curves

If $H_k > N_h M^{sen}{}_s$

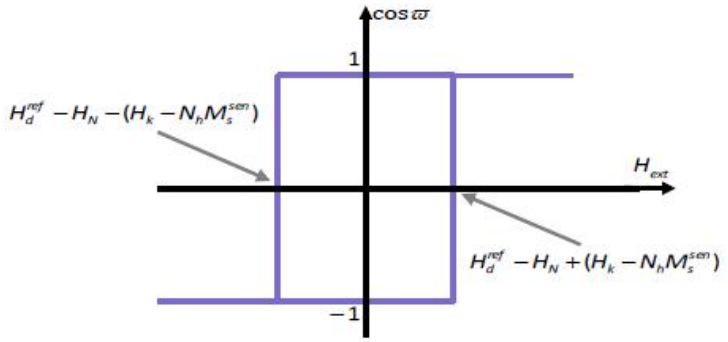

If $H_k < N_h M^{sen}{}_s$

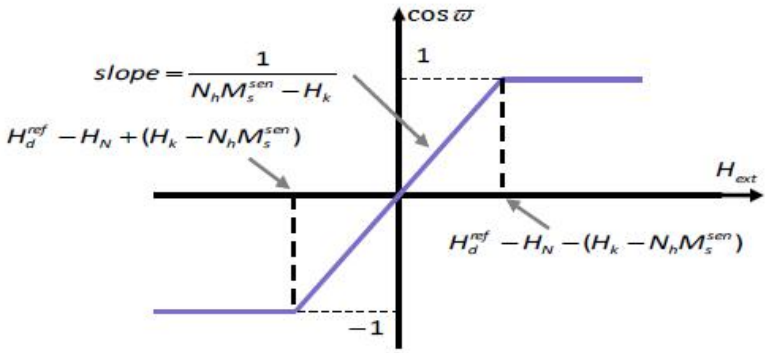

Memory applications:

Coercive field: $H_c = \frac{H_k - N_h M^{sen}}{2}$

Sensor applications:

Sensitivity ∝ *slope*

Highest sensitivity when $H_k = N_h M^{sen}{}_s$

INESC MN

INESC MN
Microsistemas &
Nanotecnologias

Current-perpendicular-to-plane (CPP) device fabrication

INESC MN
Microsistemas & Nanotecnologias

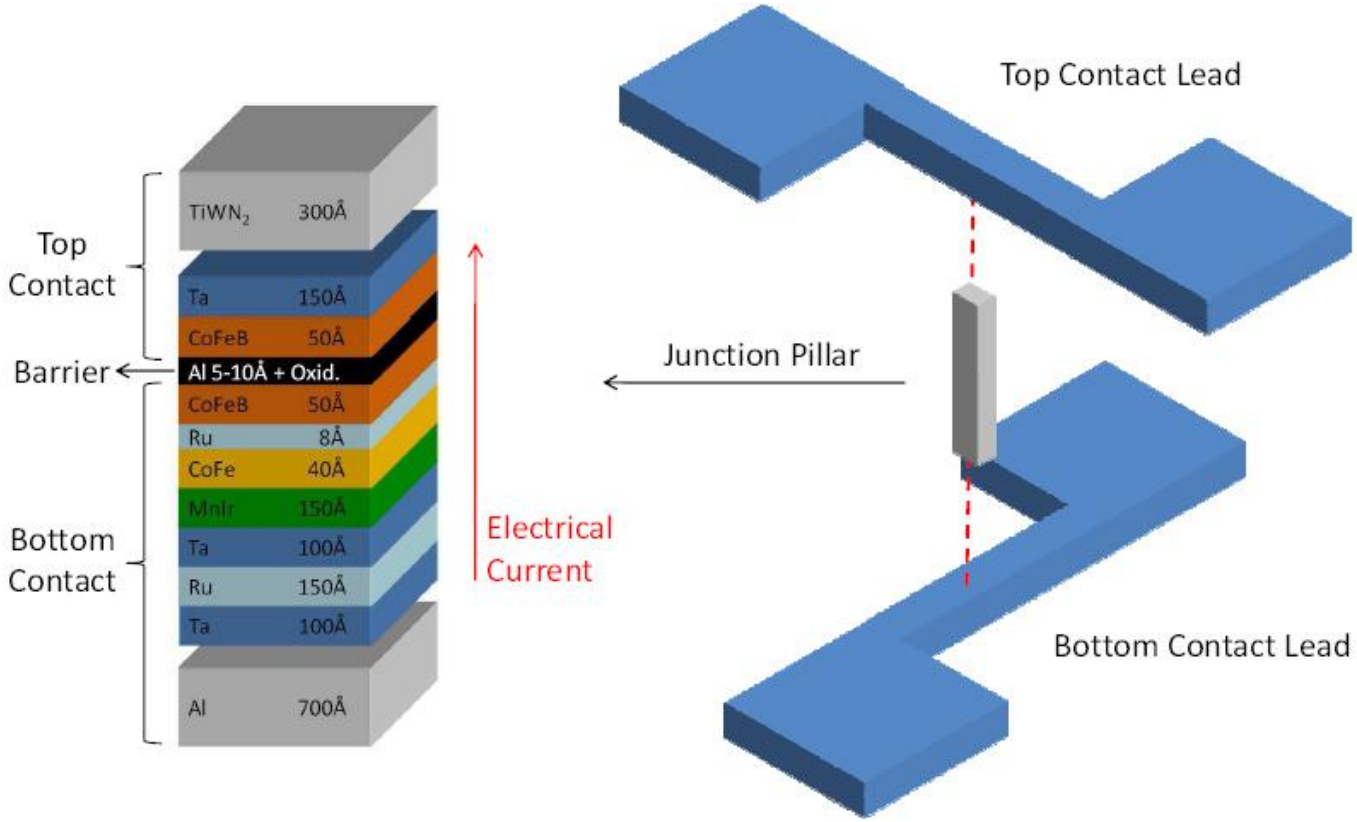

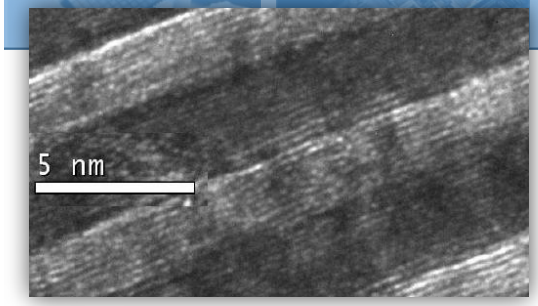

Film thickness:
Controlled at the atomic scale
1 Å = 0.1 nm

Multilevel device patterning

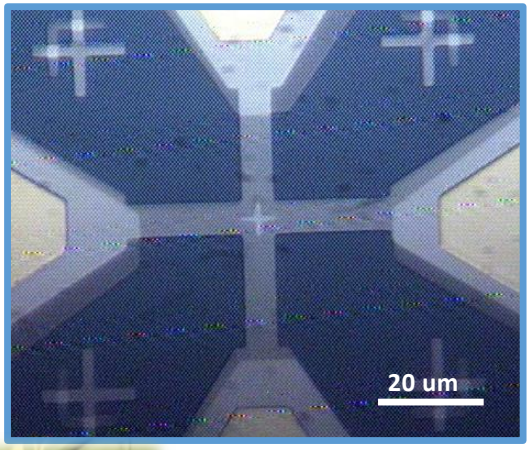

MgO target with Ar plasma

Wafer microfabrication in a Clean Room

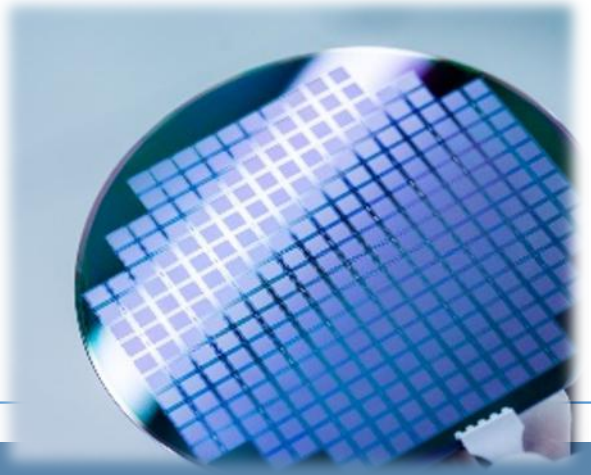

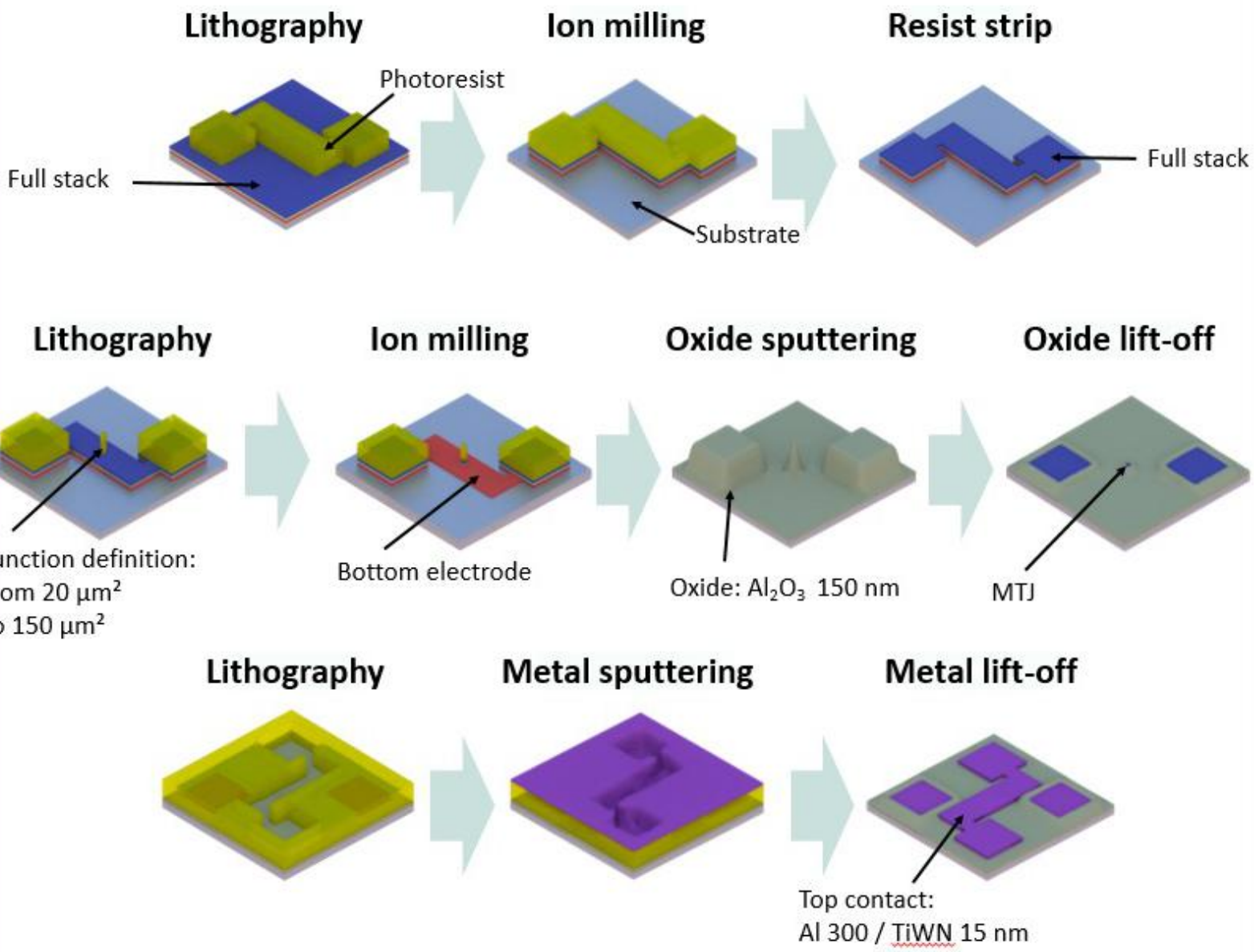
Lithography
Ion milling
Resist strip
Photoresist
Full stack
Substrate
Full stack
Lithography
Ion milling
Oxide sputtering
Oxide lift-off
Junction definition:
from 20 µm²
to 150 µm²
Bottom electrode
Oxide: Al2O3 150 nm
MTJ
Lithography
Metal sputtering
Metal lift-off
Top contact:
Al 300 / TiWN 15 nm

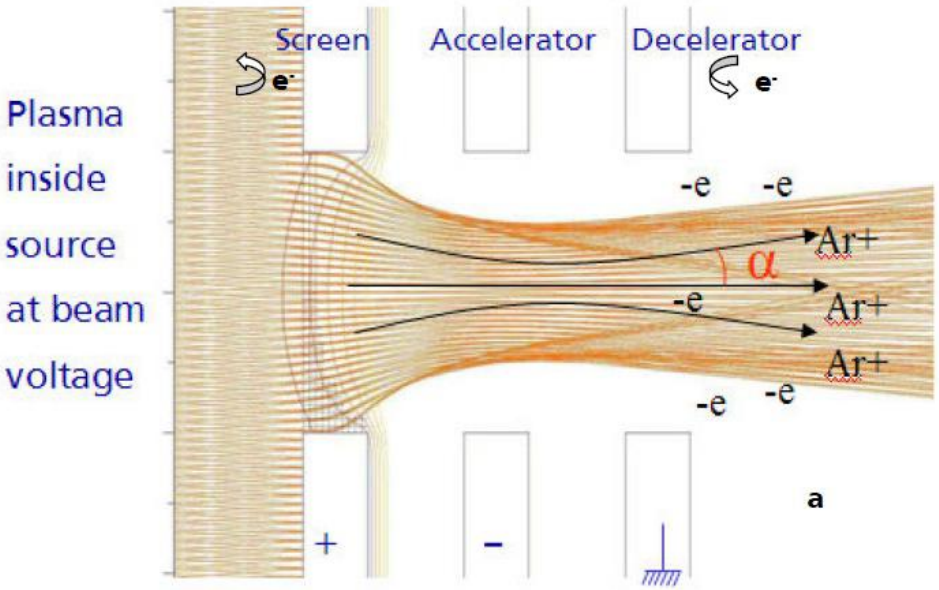
Plasma
inside
source
at beam
voltage
Screen
Accelerator
Decelerator
e-
e-
-e
-e
Ar+
α
-e
Ar+
Ar+
-e
-e
+
–
a

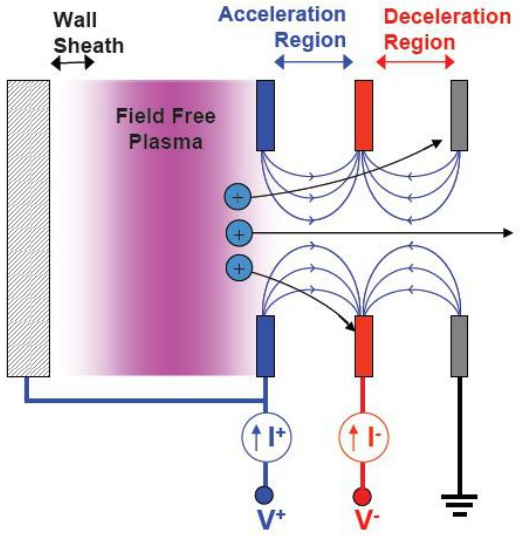
Wall
Sheath
Acceleration
Region
Deceleration
Region
Field Free
Plasma
I+
I-
V+
V-

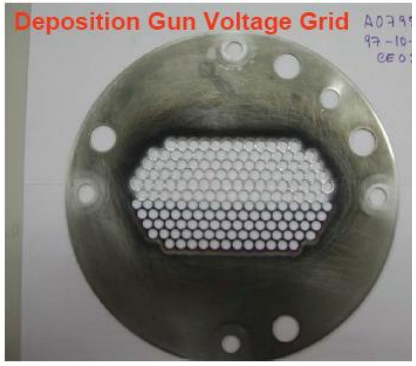
Deposition Gun Voltage Grid

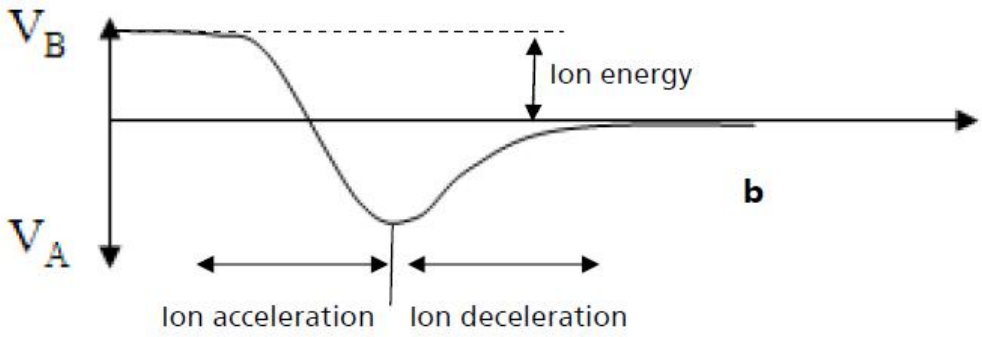
V_B
Ion energy
b
V_A
Ion acceleration
Ion deceleration

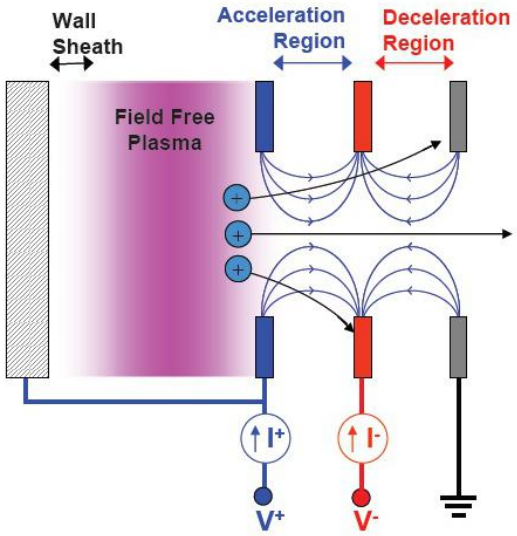
Wall Sheath
Acceleration Region
Deceleration Region
Field Free Plasma
I+
I-
V+
V-


Deposition Gun Voltage Grid

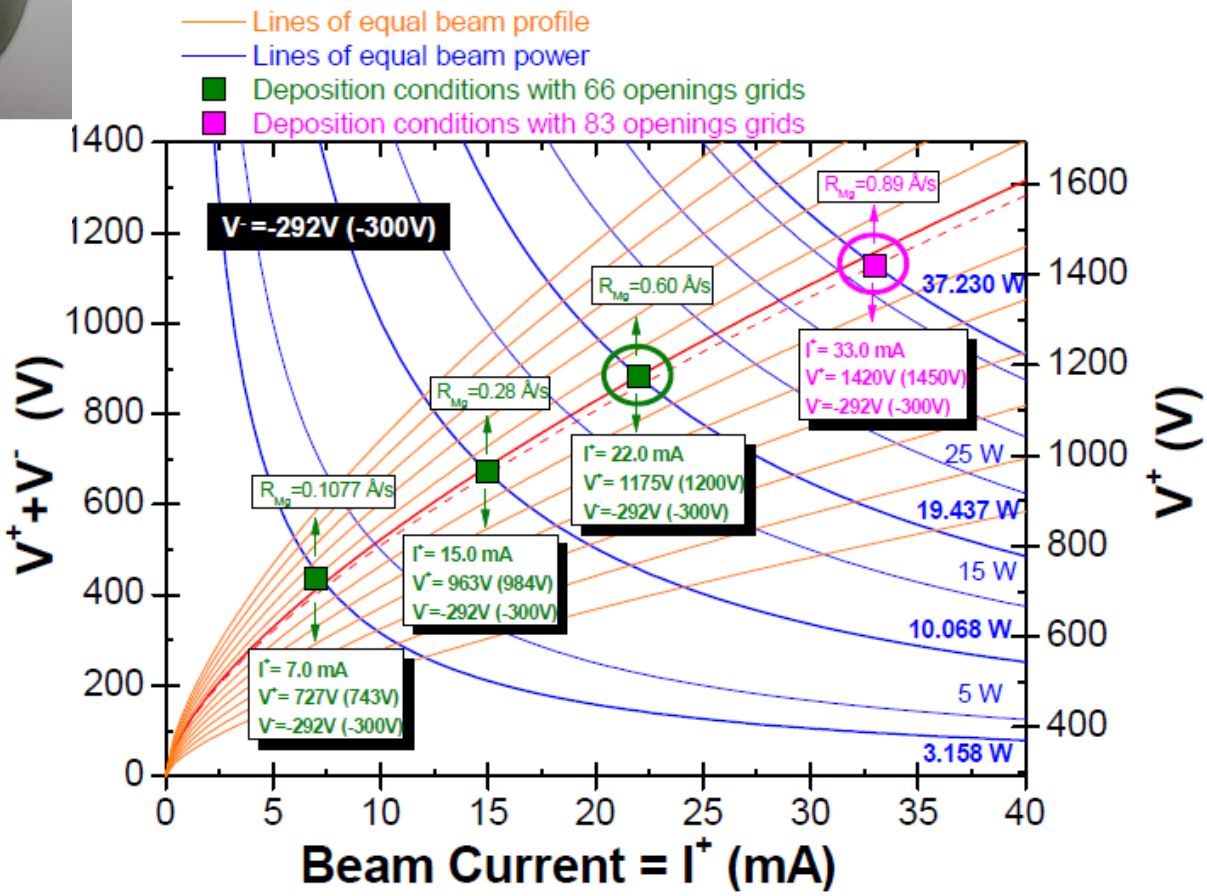
Lines of equal beam profile
Lines of equal beam power
Deposition conditions with 66 openings grids
Deposition conditions with 83 openings grids
V⁻ =-292V (-300V)
R_Mg=0.89 Å/s
37.230 W
R_Mg=0.60 Å/s
I⁺= 33.0 mA
V⁺= 1420V (1450V)
V⁻=-292V (-300V)
25 W
R_Mg=0.28 Å/s
I⁺= 22.0 mA
V⁺= 1175V (1200V)
V⁻=-292V (-300V)
19.437 W
R_Mg=0.1077 Å/s
I⁺= 15.0 mA
V⁺= 963V (984V)
V⁻=-292V (-300V)
15 W
10.068 W
I⁺= 7.0 mA
V⁺= 727V (743V)
V⁻=-292V (-300V)
5 W
3.158 W
V⁺+V⁻ (V)
V⁺ (V)
Beam Current = I⁺ (mA)
0
200
400
600
800
1000
1200
1400
1600
0
5
10
15
20
25
30
35
40

Effect of the profile on the sensor performance

INESC MN
Microsistemas & Nanotecnologias

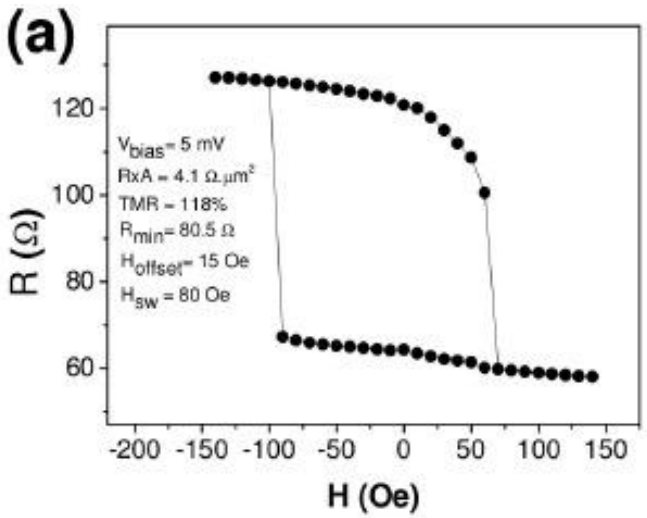

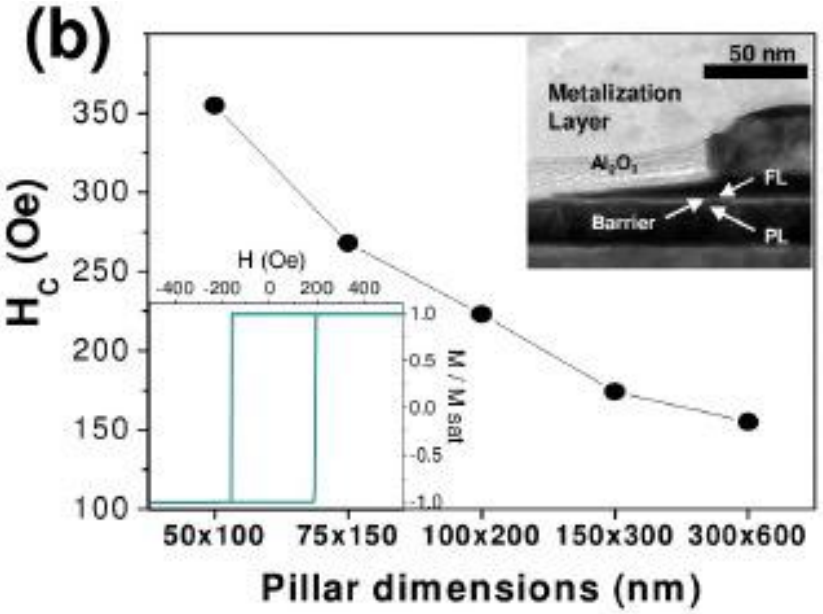

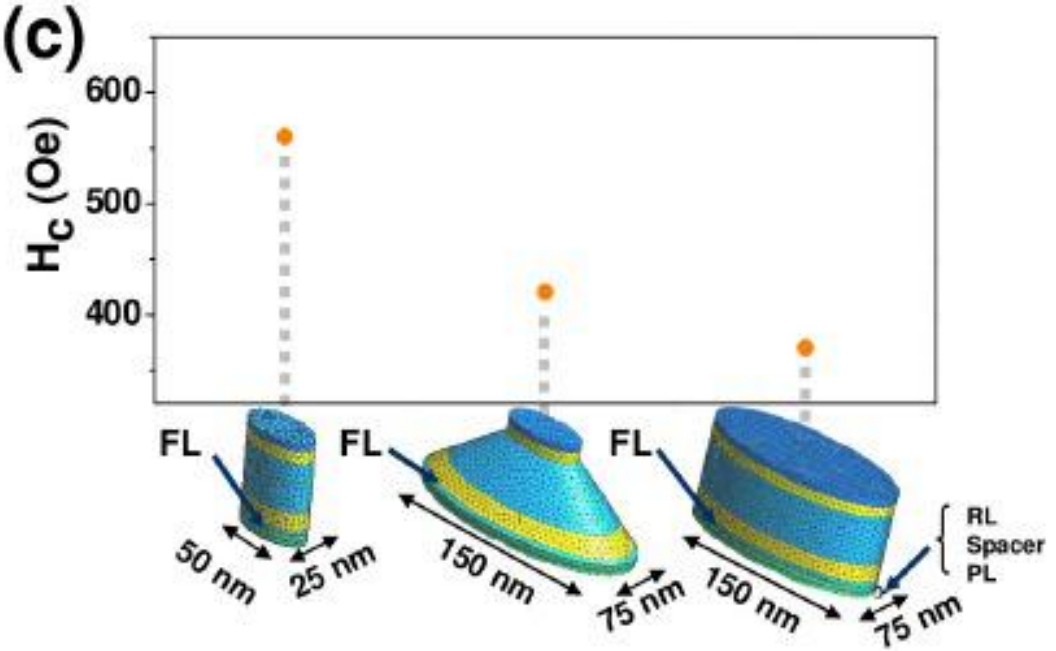

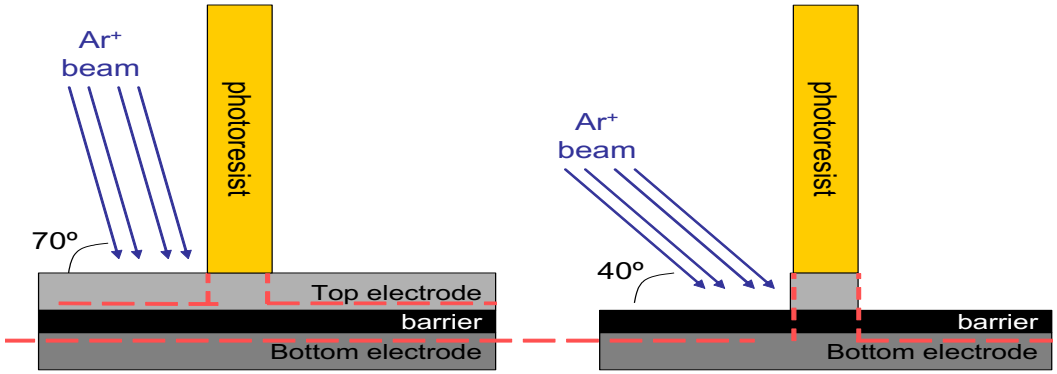

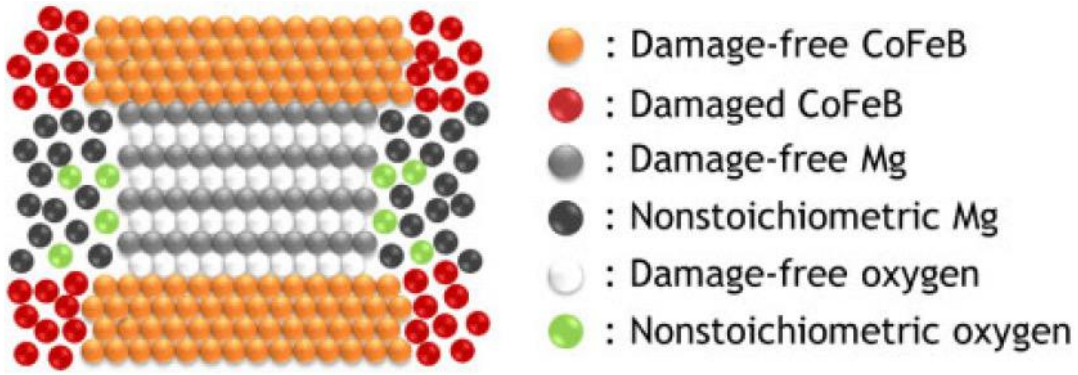

Fig. 5. (Color online) Substance distribution diagram of the patterned MTJs after the etching process.

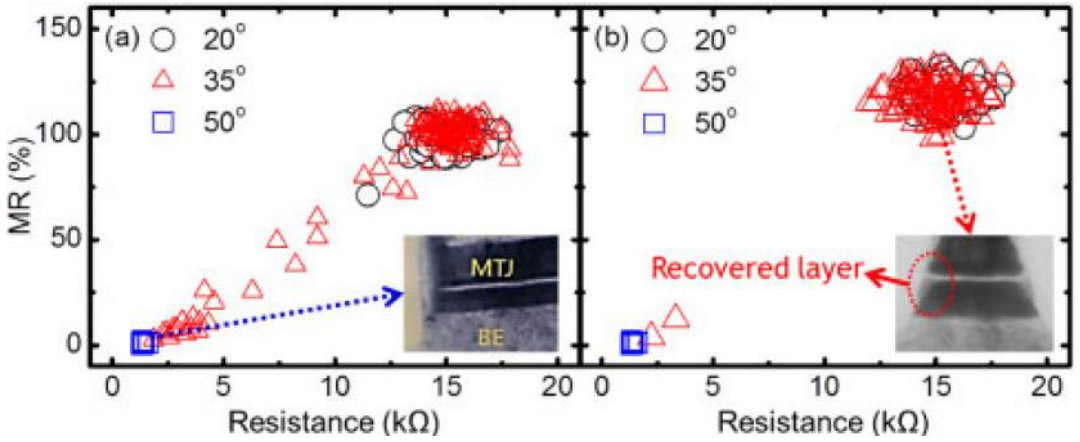

Japanese Journal of Applied Physics **56**, 04CE09 (2017)
https://doi.org/**10.7567/JJAP.56.04CE09**

Thin film stack for TMR sensors

INESC MN
Microsistemas & Nanotecnologias

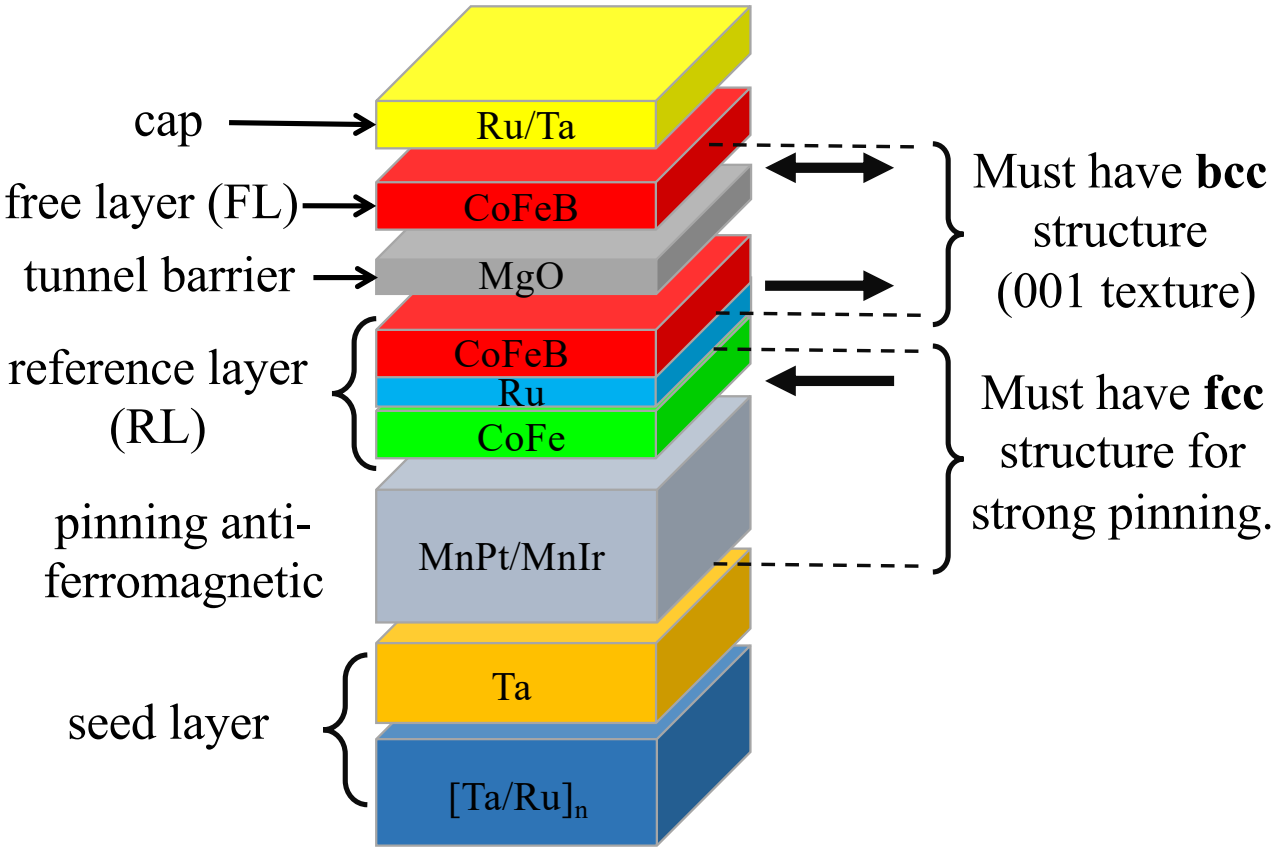

HRTEM image for CoFeB/MgO/CoFeB

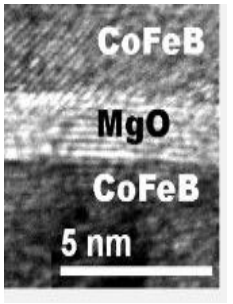

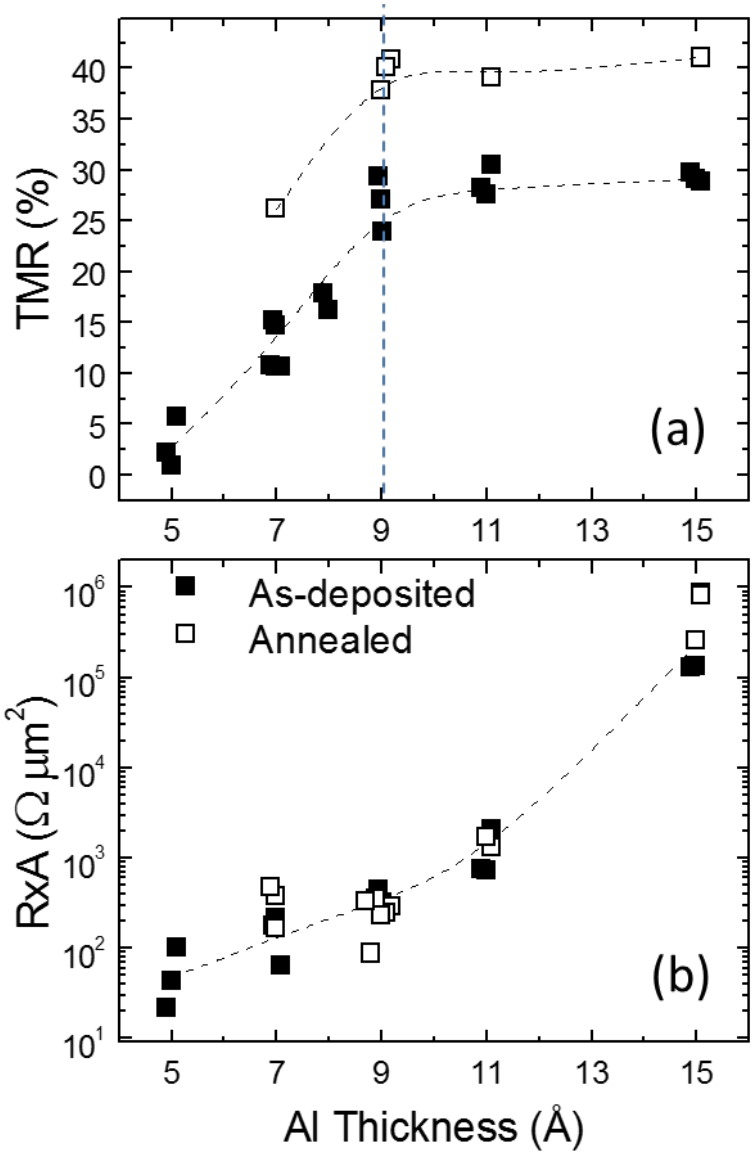

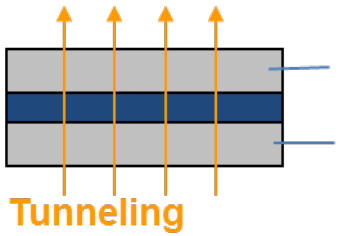

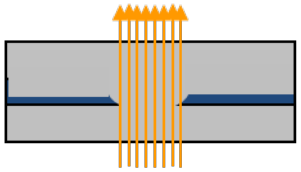

Discontinuous Barrier

Ta	30 Å
$Mn_{74}Ir_{16}$	250 Å
$CoFeB_{10}$	40 Å
Al (5- 9Å) + oxid.	
$CoFeB_{10}$	50 Å
$Ni_{80}Fe_{20}$	70 Å
Ta	30 Å
Al 600Å	

Accurate control of the thin film thickness

- impact on TMR
- impact on R

Ion Beam Assisted Deposition

Nordiko 3600 Ion Beam Deposition Tool

INESC MN
Microsistemas & Nanotecnologias

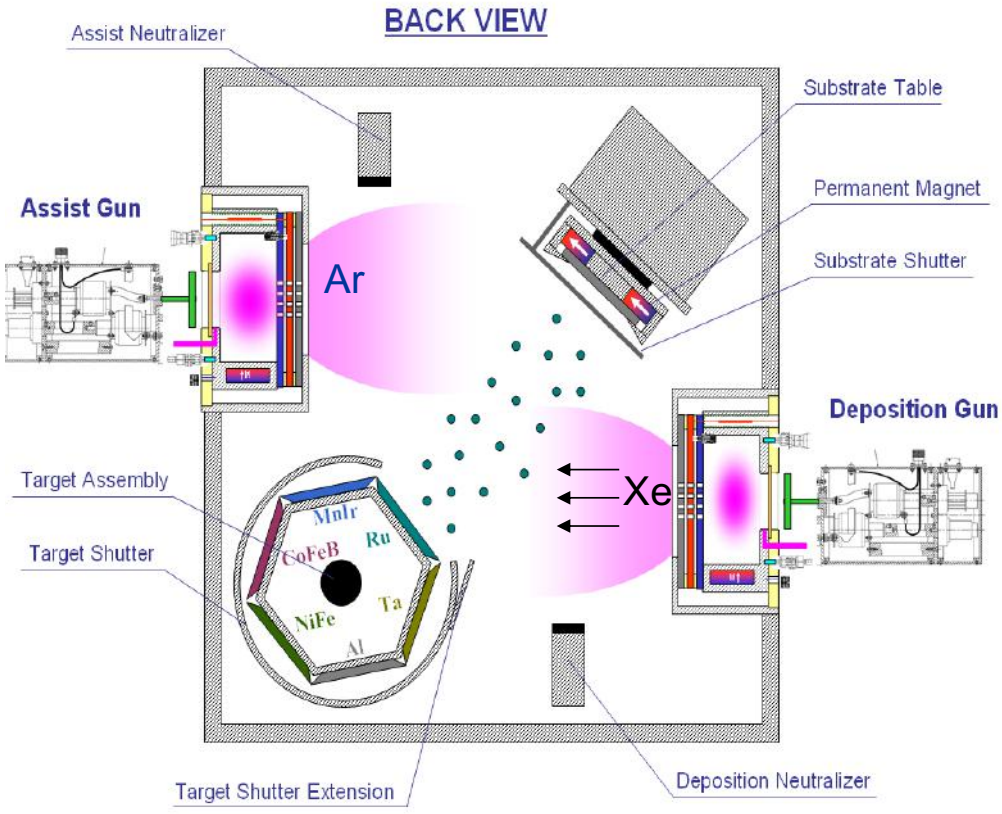

Ion Beam Assisted Deposition of MgO:

Ar ion beam, directed to the substrate
provides extra energy to the atoms as they are deposited

=> extra energy promote the crystalization of the MgO

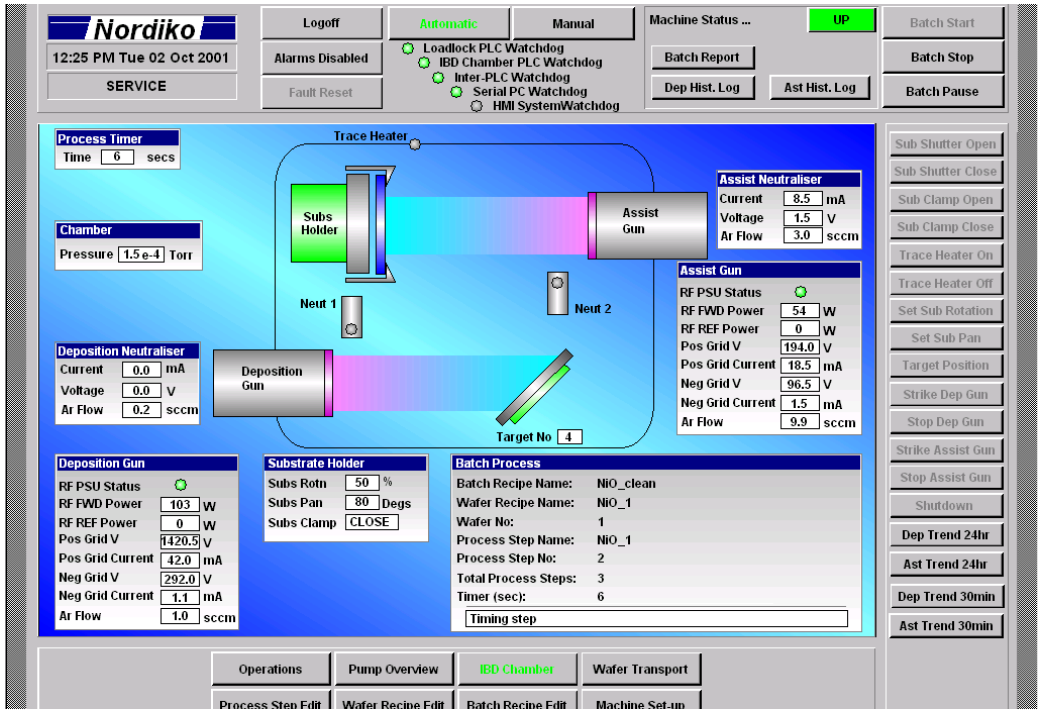

Ion Beam Assisted Deposition

Effect of Assist Gun Ion Energy (V^+)

Effective Deposition Rate = Deposition Rate – Etch Rate
Deposition Rate α Dep Gun Beam Power (I^+ V^+)
Etch Rate α Assist Gun Beam Power (I^+ V^+)

INESC MN
Microsistemas & Nanotecnologias

Assist V^+ <100V

Surface Effects

Assist beam ions enhance the mobility of surface atoms, without removing them.

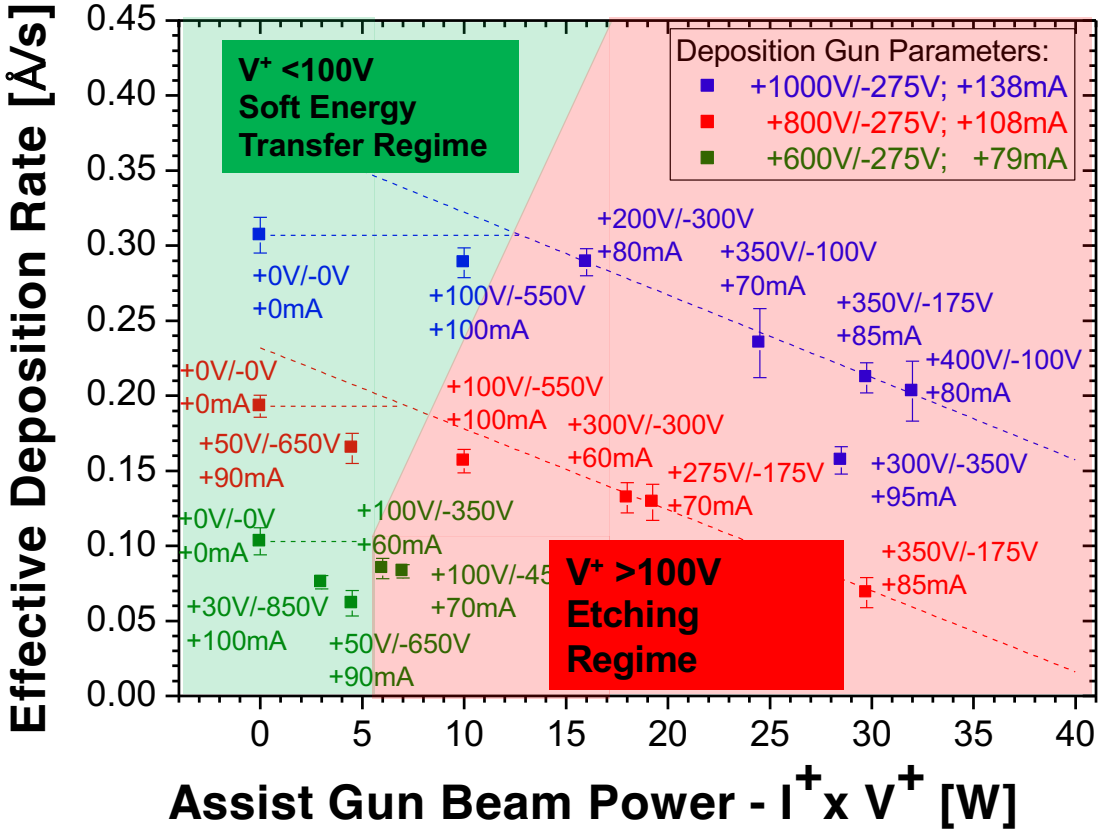

Assist V^+ >100V

Bulk Effects

Etch Rate :
0.0055 ±0.0002 (Å/s) / W

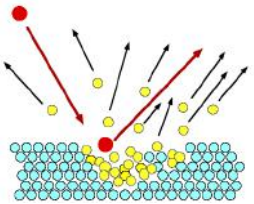

Ion Beam Assisted Deposition

Effect of Assist Gun Beam Current (I^+)

INESC MN
Microsistemas & Nanotecnologias

Soft Energy Transfer Regime
I^+ >=80mA is required

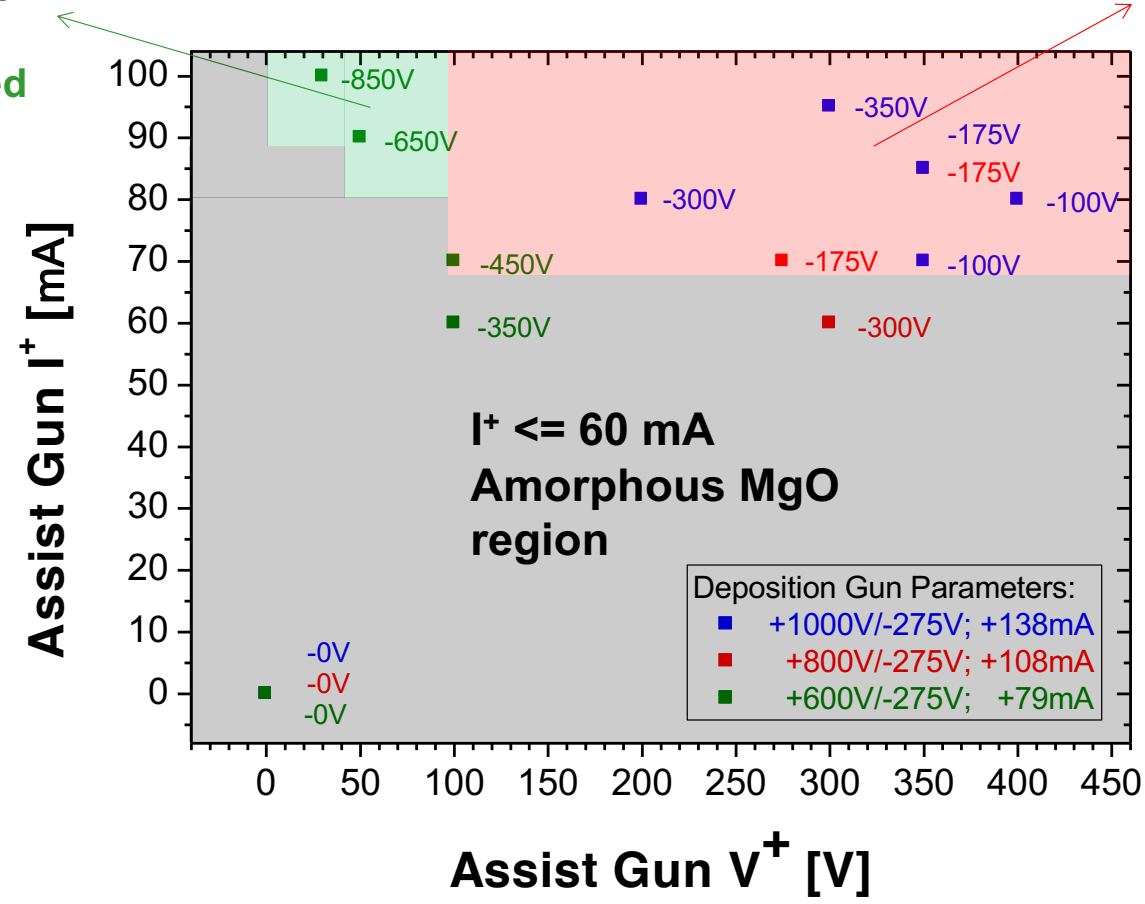

Etch Regime
I^+ >=70mA
Crystalline MgO

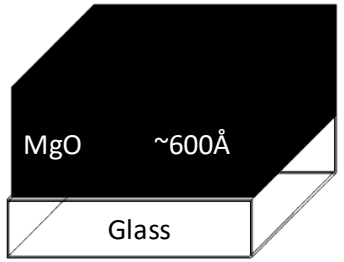

There is a minimum Assist Beam Current threshold under which MgO is always amorphous.

Assisted deposition (MgO)

INESC MN
Microsistemas & Nanotecnologias

X-rays difraction

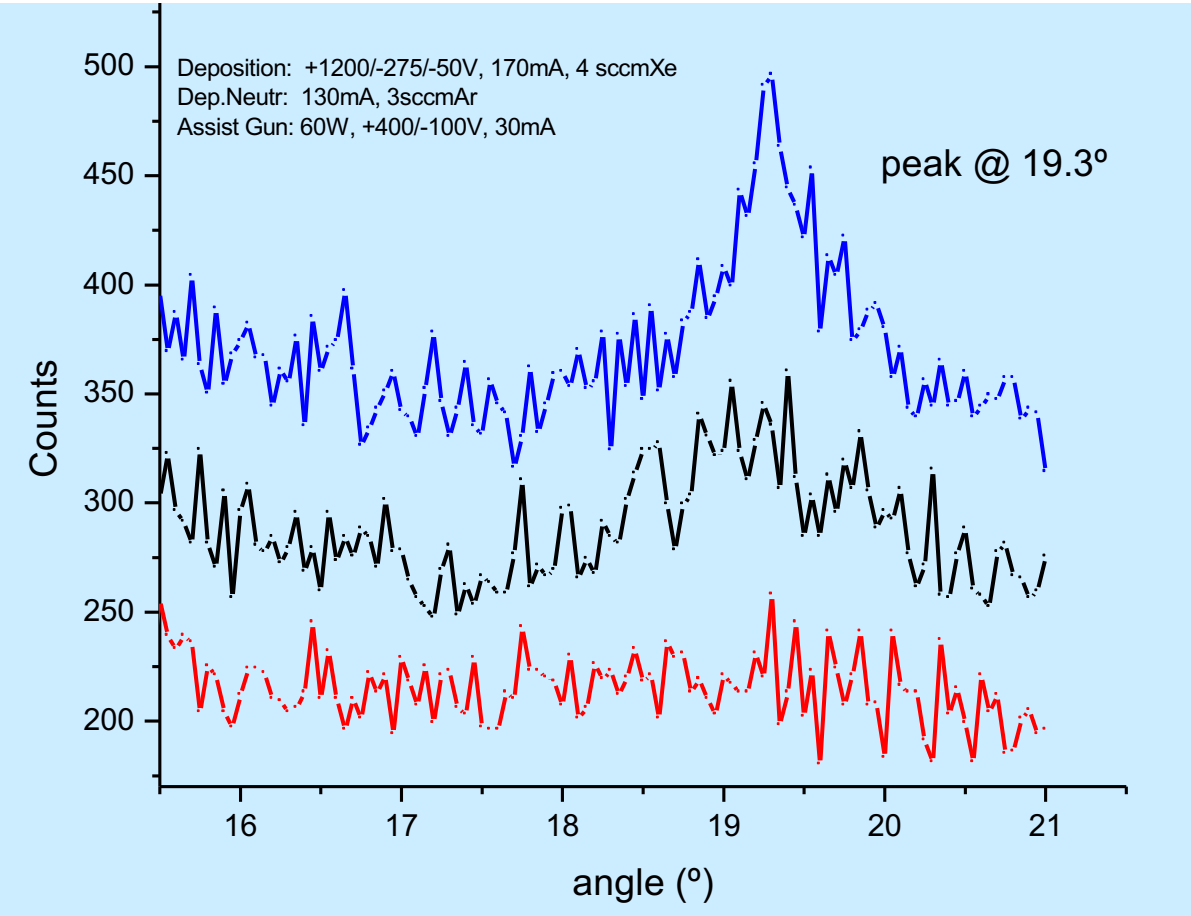

Cross section microscopy

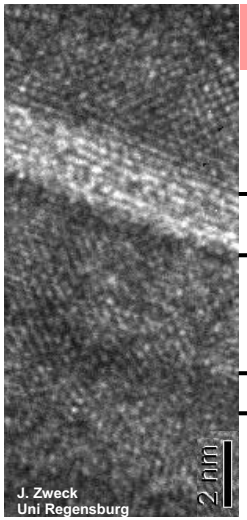

MgO crystalline barrier

CoFeB

MgO

CoFeB

Ru

CoFe

Assisted deposition (MgO): Impact of the beam-sample angle

INESC MN
Microsistemas & Nanotecnologias

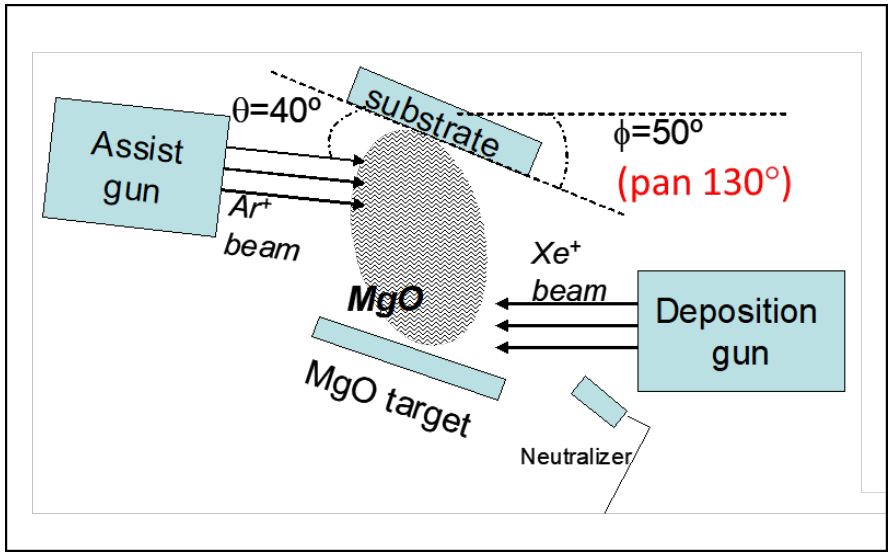

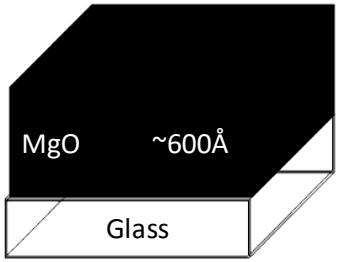

Sample	AG09	AG11	AG12	AG13	AG14
Pan	130º	110º	120º	140º	150º

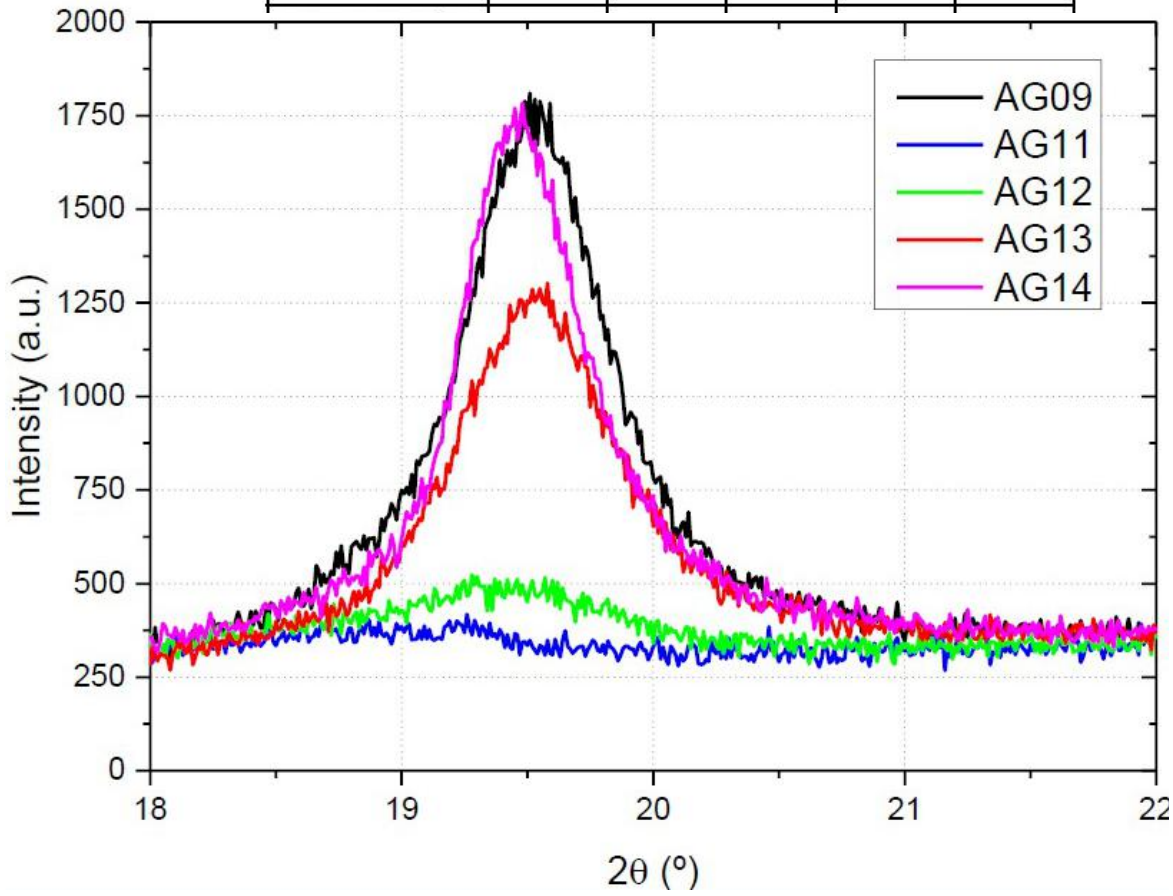

Accurate control of the thin film thickness

- impact on TMR
- impact on R

INESC MN
Microsistemas & Nanotecnologias

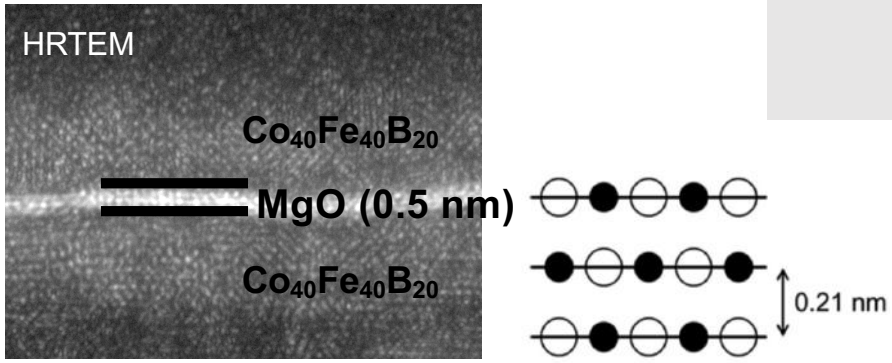

1 Å => 10x R

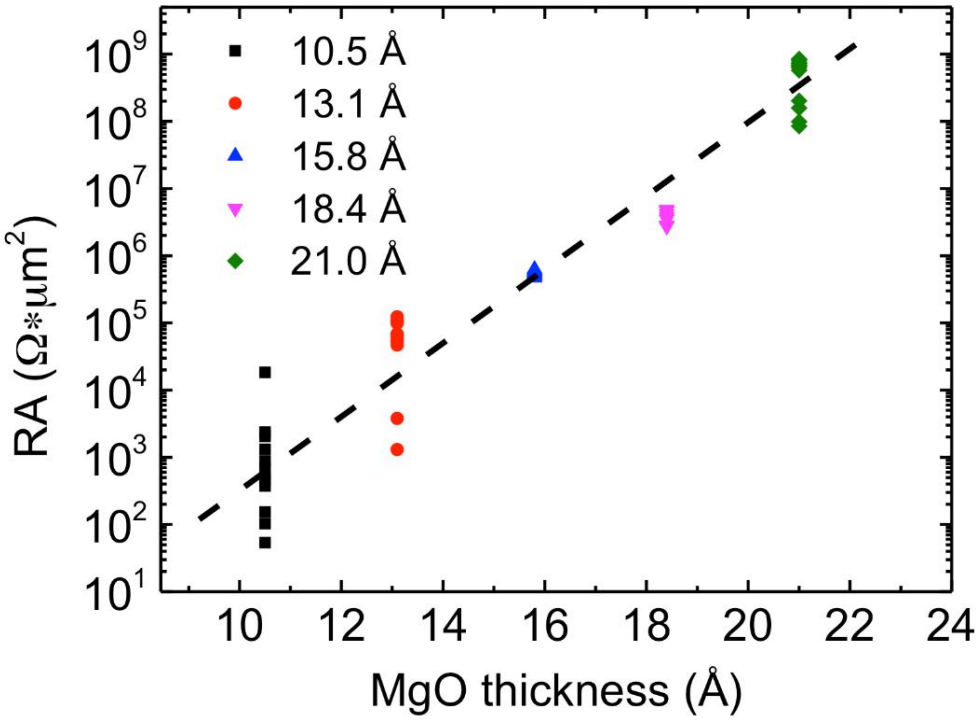

Interlayer magnetic coupling - Néel coupling

INESC MN
Microsistemas & Nanotecnologias

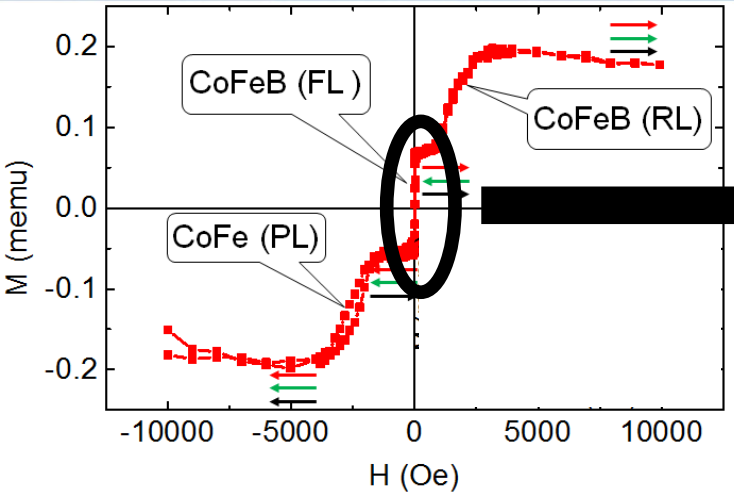

Looking near zero fields

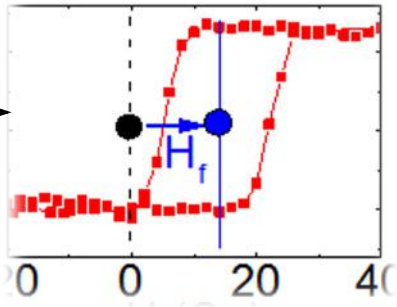

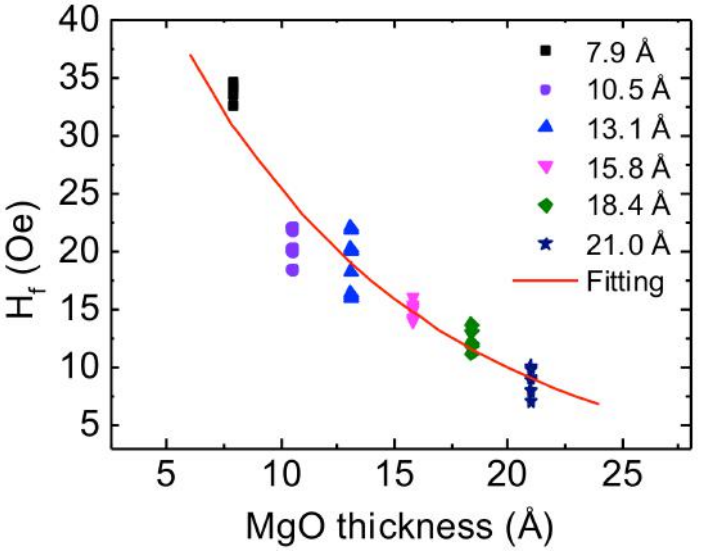

$$H_f = \frac{\pi^2 h^2 M_s}{\sqrt{2}\lambda t_{FL}} exp(-2\pi\frac{\sqrt{2}d}{\lambda}) \times [1 - exp(-2\pi\frac{\sqrt{2}t_{FL}}{\lambda})] \times [1 - exp(-2\pi\frac{\sqrt{2}t_{RL}}{\lambda})]$$

t_{FL} nm	t_{RL} nm	M_s emu/cc	λ nm	h nm
3	3	1466	9.47	0.13

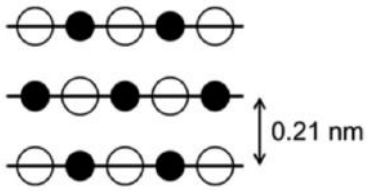

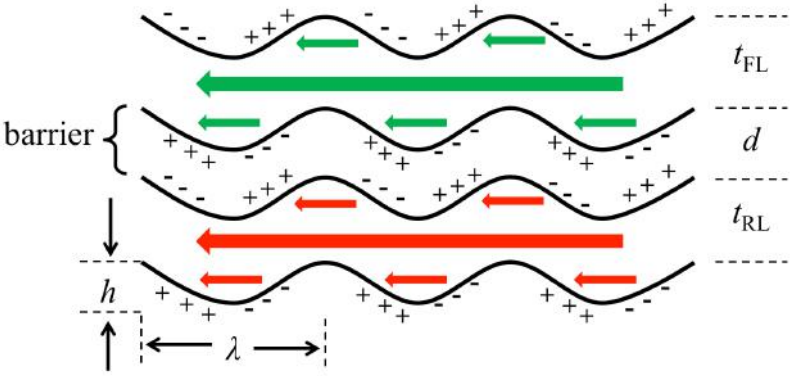

- A method to access the MgO roughness.

J. C. S. Kools, et.al., J. Appl. Phys. 85 , 4466 (1999).

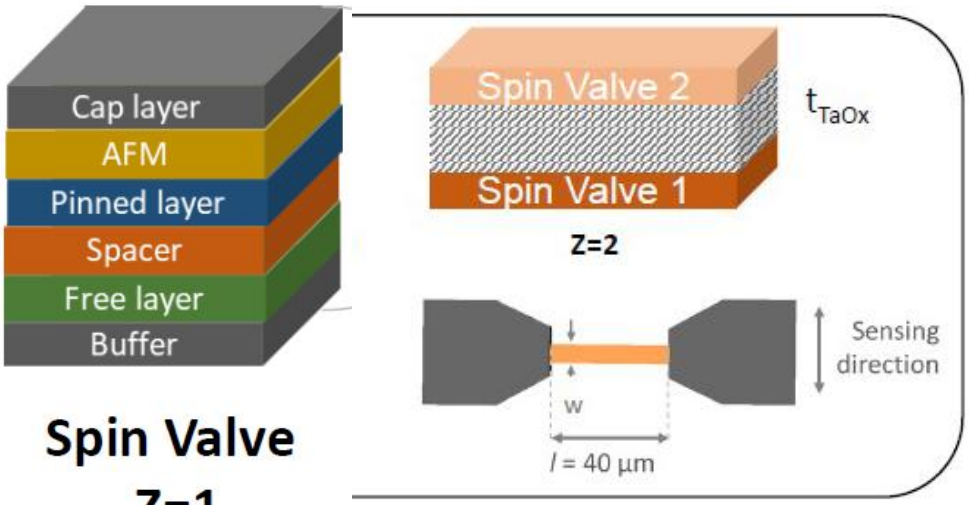

Spin Valve

Z=1

Atomic Force Microscopy

Z = 1

Ra = 2.1 Å

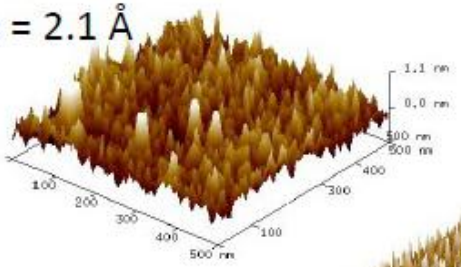

Z = 2

Ra = 2.4 Å

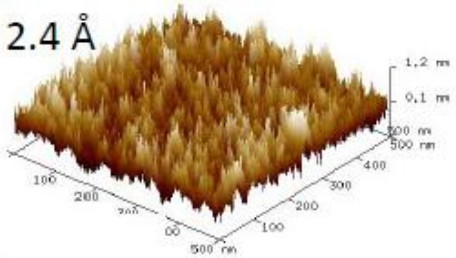

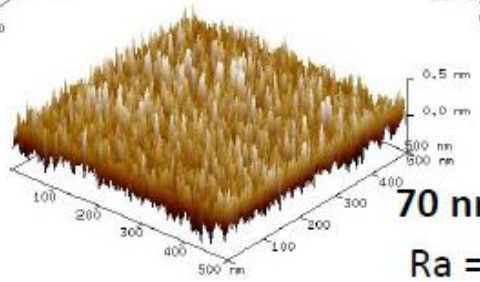

70 nm TaOx

Ra = 1.2 Å

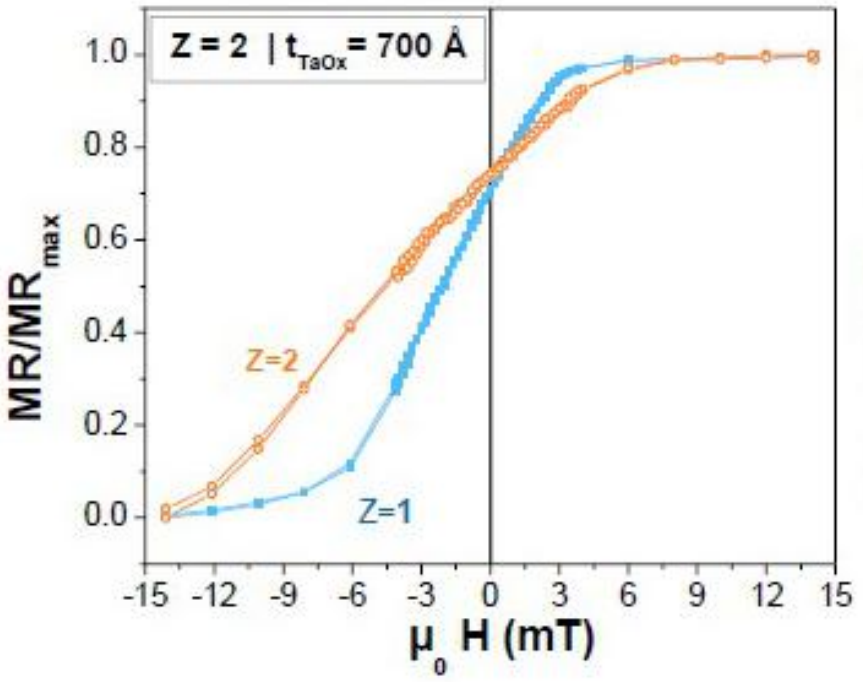

200mm backend GMR / TMR technology

INESC MN
Microsistemas & Nanotecnologias

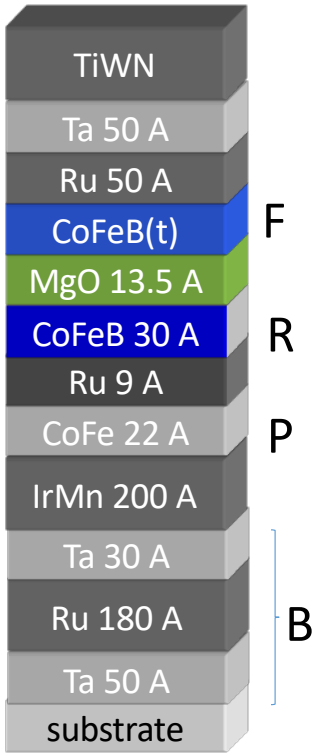

6 targets IBD (extra module 8 targets in PVD; 2019)
Dep pressure 2 x 10^{-5}Torr
Heated substrate
Assist gun,
Base Pressure 5x10^{-8} Torr

Nordiko
INNOVATION WITH RELIABILITY

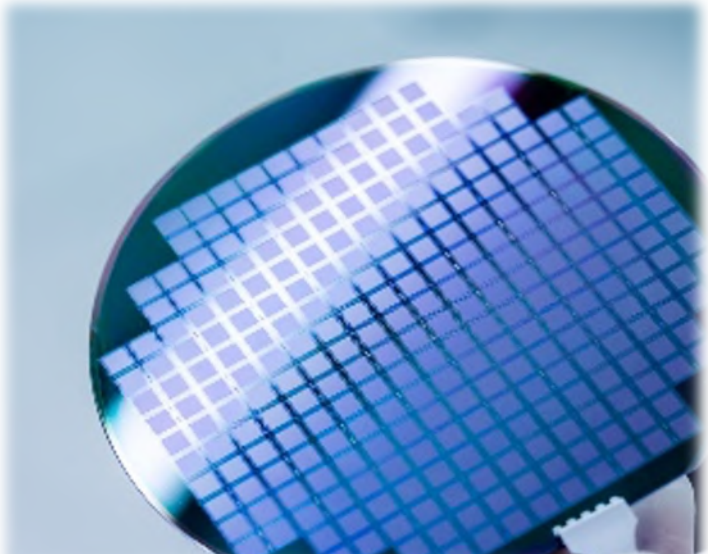

nffa.eu
nanoscience foundries & fine analysis

ACEINNA

BOSCH

MagIB

Inspectron
Track Trace Check Verify

LEOTECH

MASMA
SME Instrument

TUMAPOS
SME Instrument

Allegro MicroSystems, LLC
High-Performance Semiconductors

BOGEN

uniformity on Al2O3 thin film with different angle

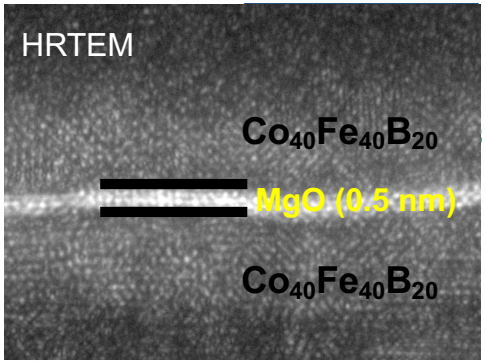

1 Å => 10x R

Al2O3 Etch Uniformity @ INL :
3.4% @130deg, 5.0%@165deg

Al2O3 Etch Uniformity @ INESC :
7.81% @60deg, 5.17%@15deg

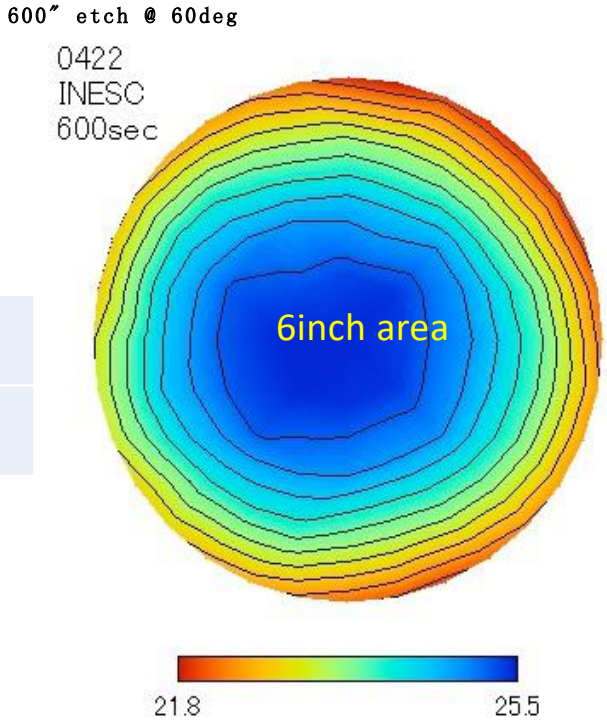

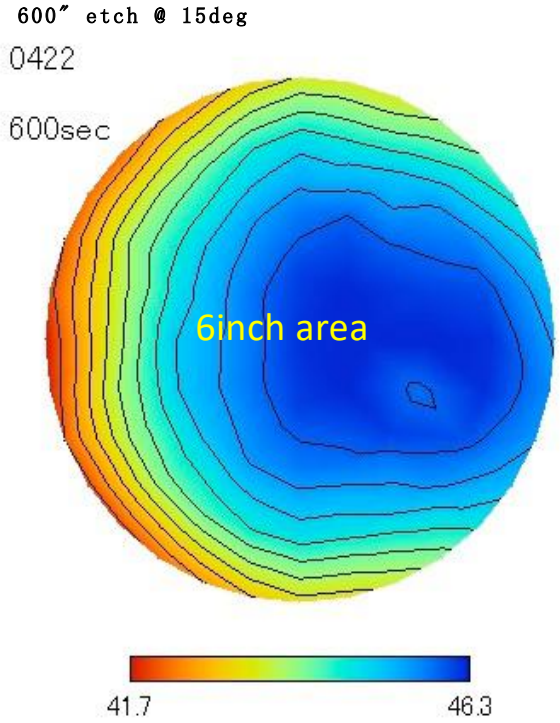

(nm/min)	0.59	0.74
Unif._(max-min)/(max+min)/2	3.91%	2.61%
Unif._Range./Mean/2)	7.81%	5.17%

Target erosion

INESC MN
Microsistemas & Nanotecnologias

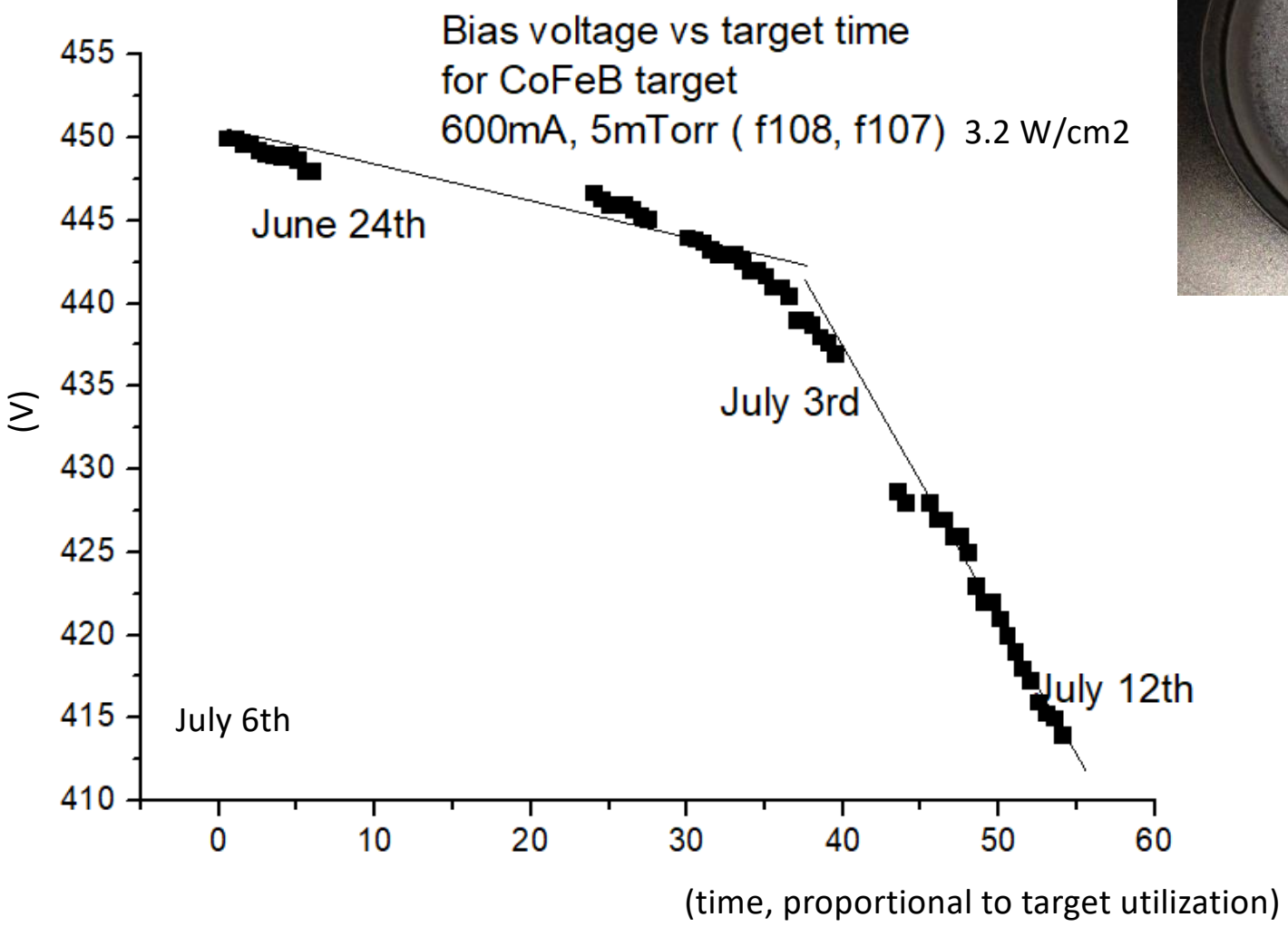

Magnetron configuration

INESC MN
Microsistemas & Nanotecnologias

Configuration 3

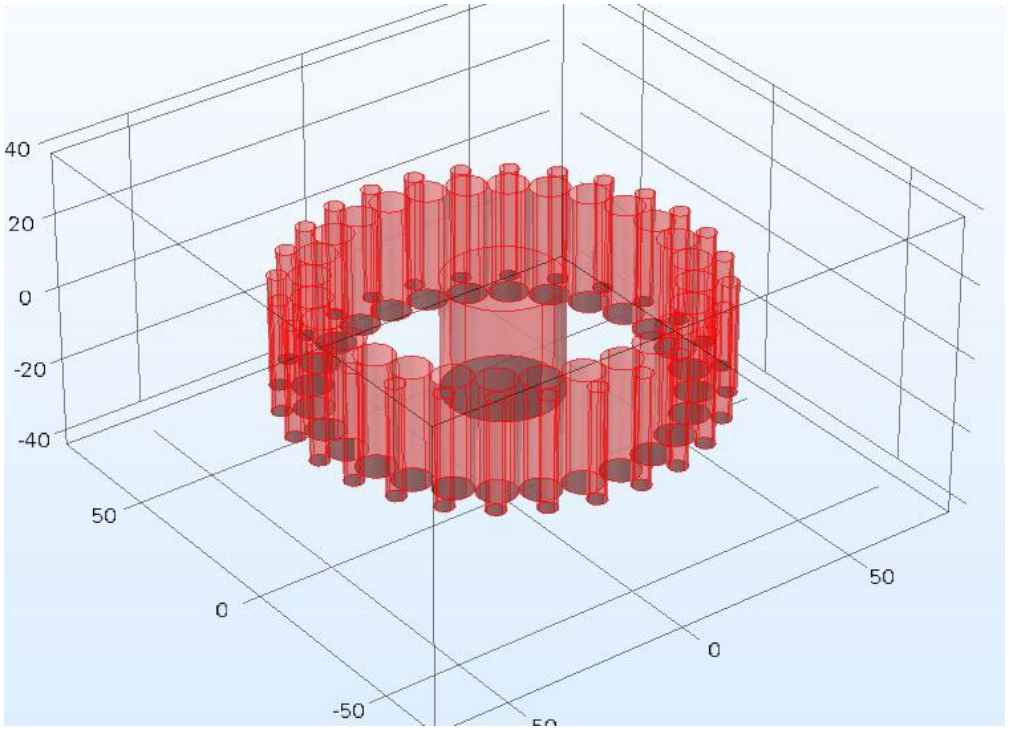

	Small outer magnets	Small inner magnets	Big magnet
Amount	28	28	1
μ_r	1.05		
B_r (T)	1.28		
Magnetization direction	+z	+z	-z
Radius (mm)	2.5	5	10
Height (mm)	30	30	30
Distance to magnetron centre (mm)	52.5	45	0

Configuration 3 (no target)

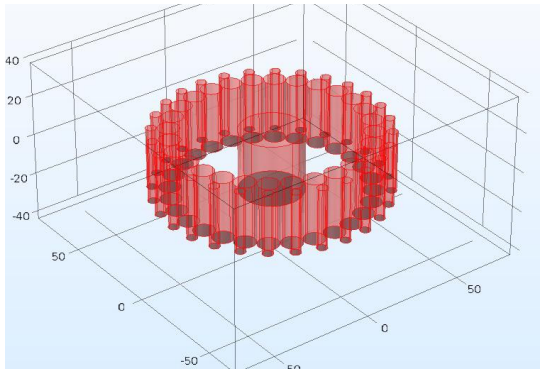

Magnetic flux density at target surface (4.5 mm above magnetron):

$|\vec{B}_{radial}|$

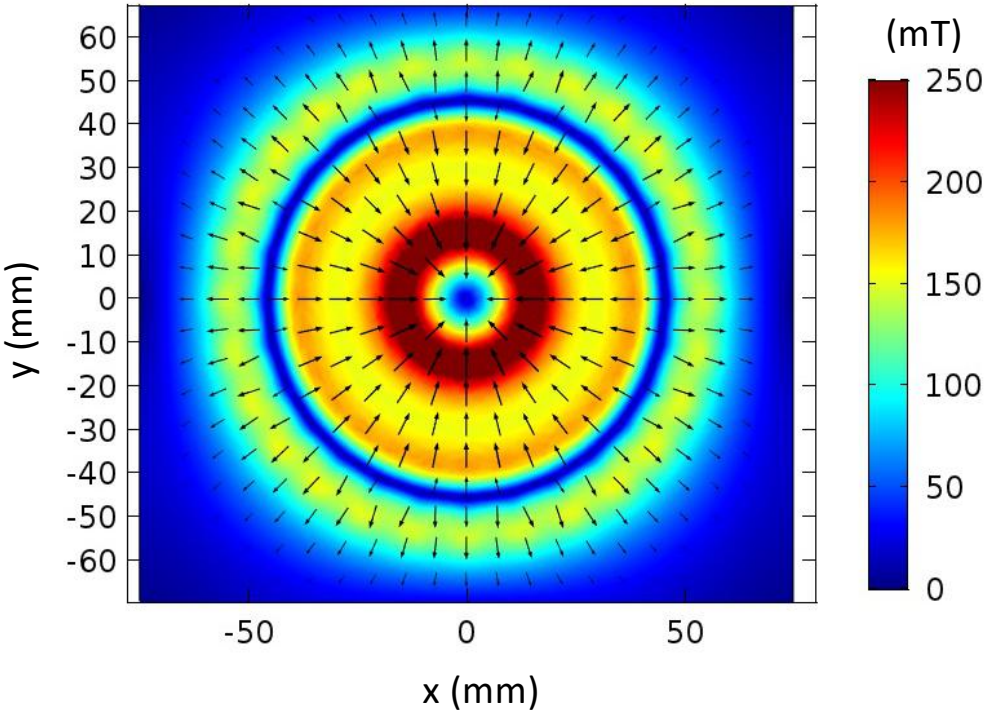

$\vec{B}_{vertical}$

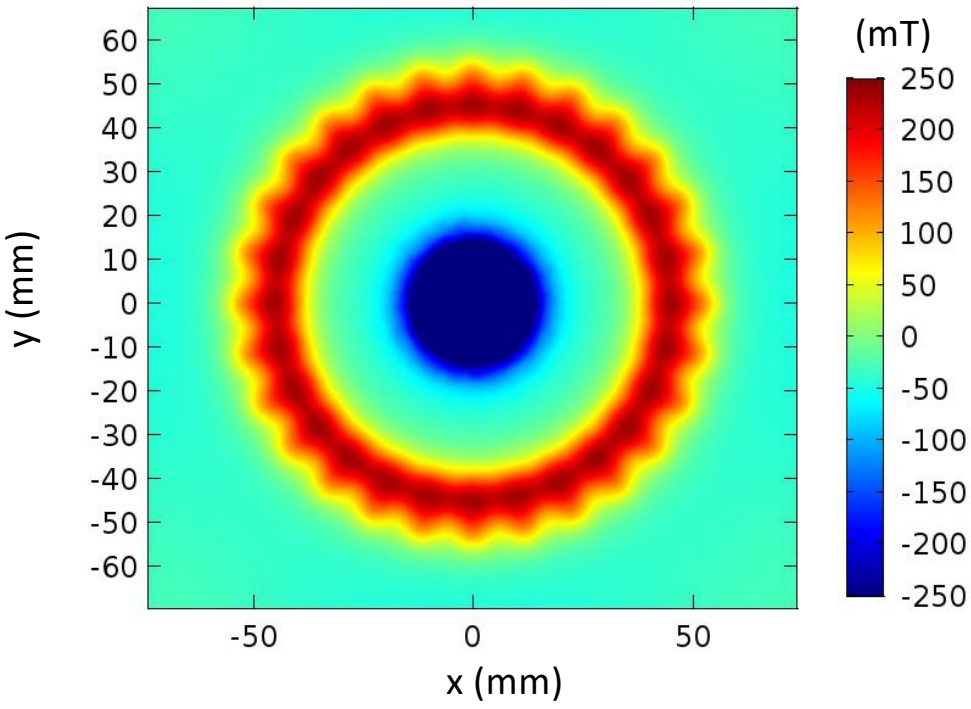

Magnetron Geometry (with target)

INESC MN
Microsistemas & Nanotecnologias

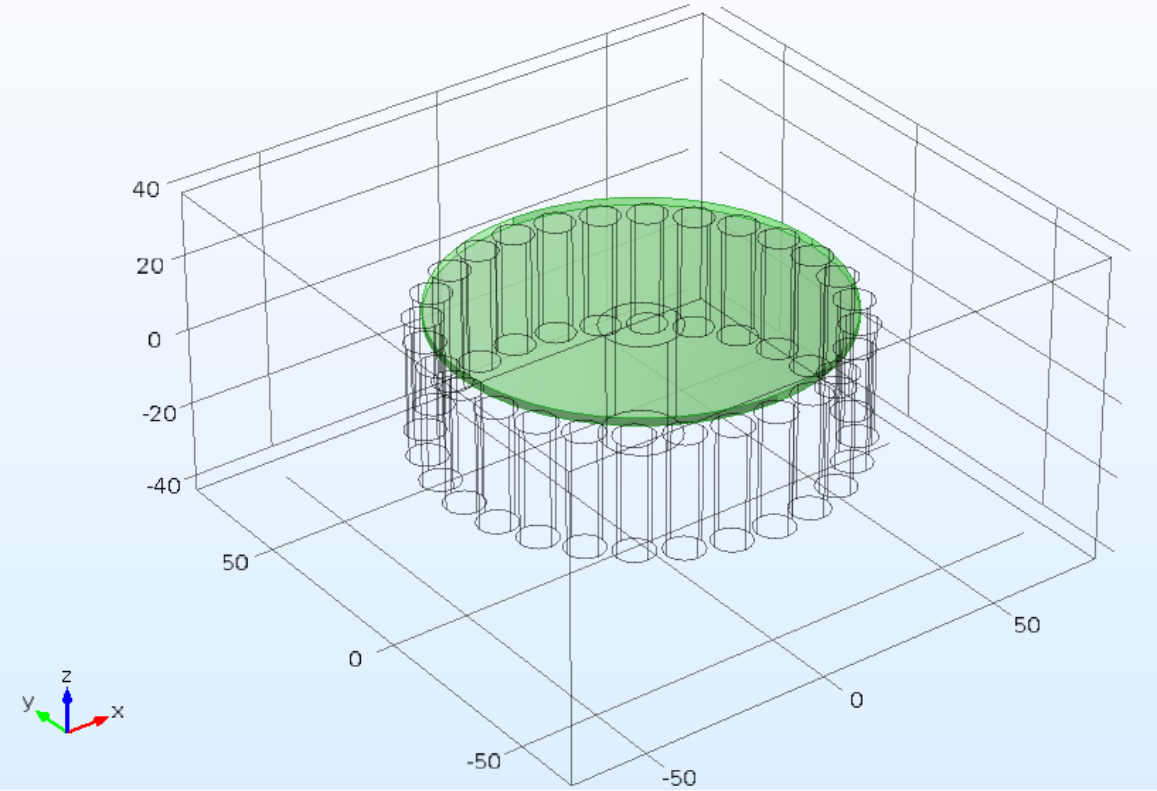

	Small magnets	Big magnet
Amount	28	1
μ_r	1.05	
B_r (T)	1.28	
Magnetization direction	+z	-z
Radius (mm)	5	10
Height (mm)	30	29

	$Co_{80}Fe_{20}$ Target
Radius (mm)	50
Height (mm)	2
μ_r	100[(1)]

[(1)] R. M. Bozorth, *Ferromagnetism,* 1993

Configuration 3 (CoFe target + b. plate)

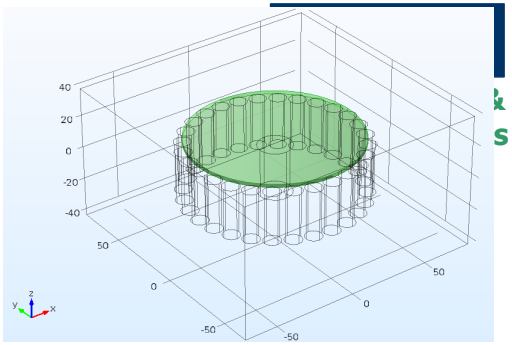

Magnetic flux density at target surface (6 mm above magnetron):

$|\vec{B}_{radial}|$

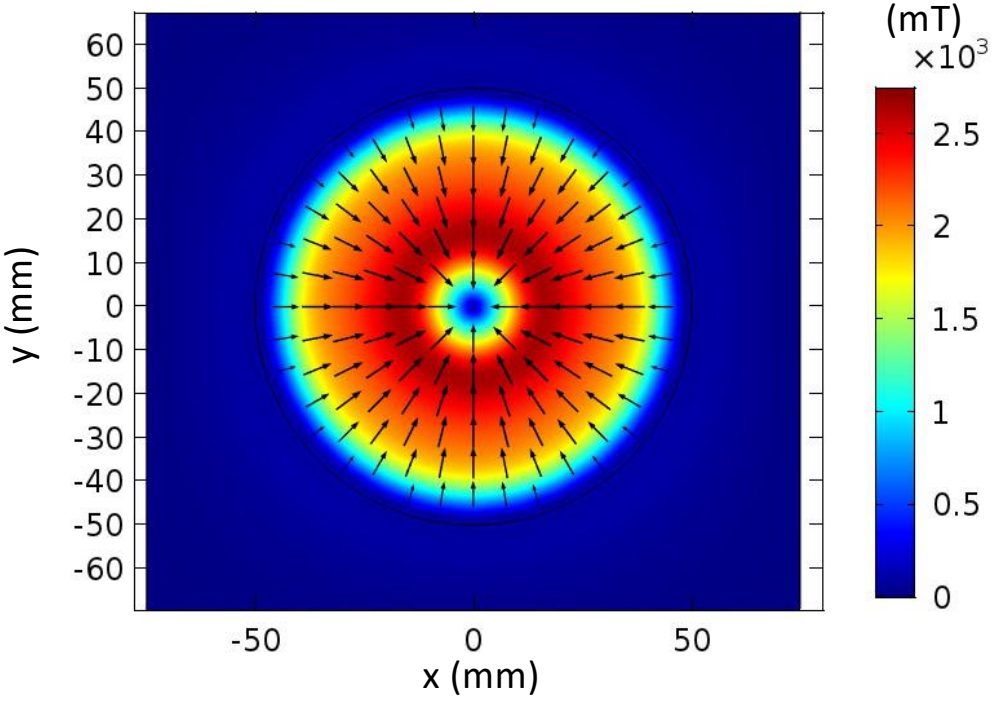

$\vec{B}_{vertical}$

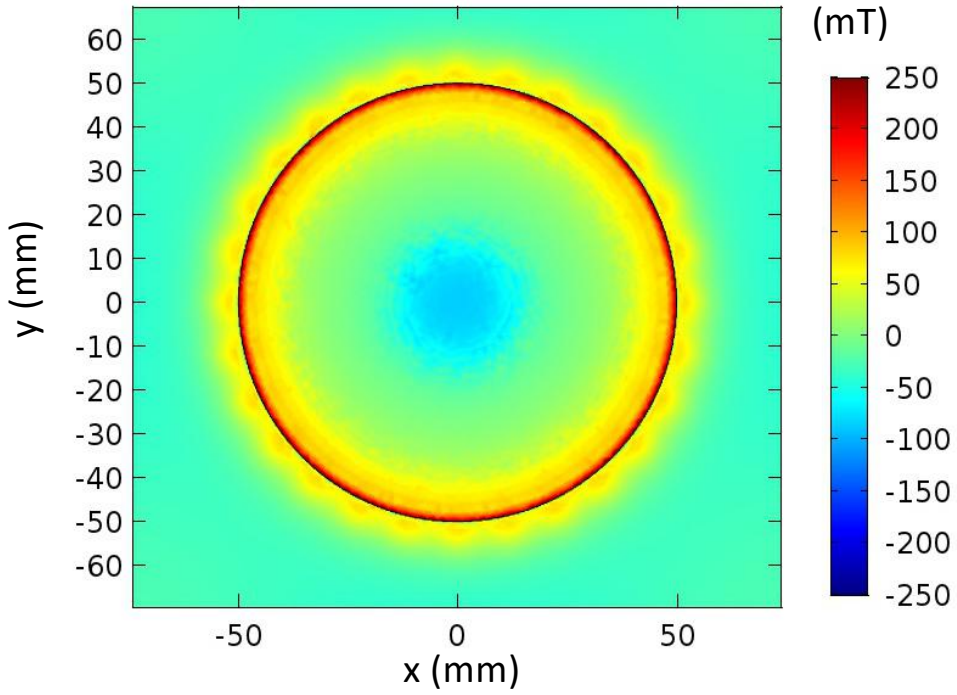

INESC MN
Microsistemas & Nanotecnologias

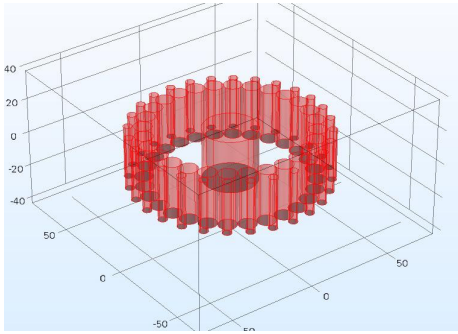

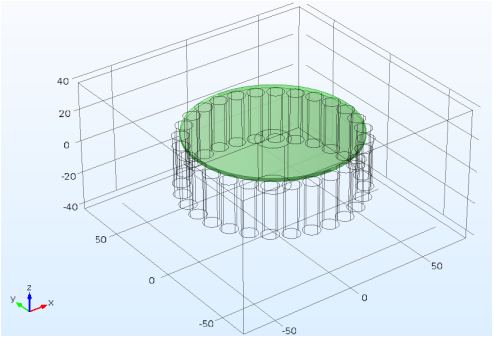

No target

Or

with a non-magnetic target

With a magnetic target

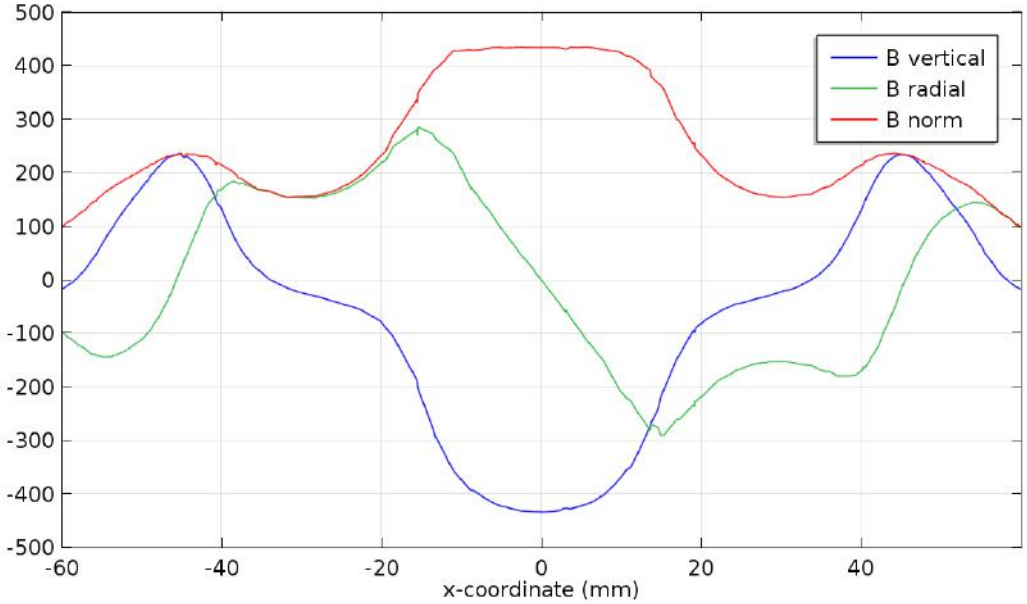

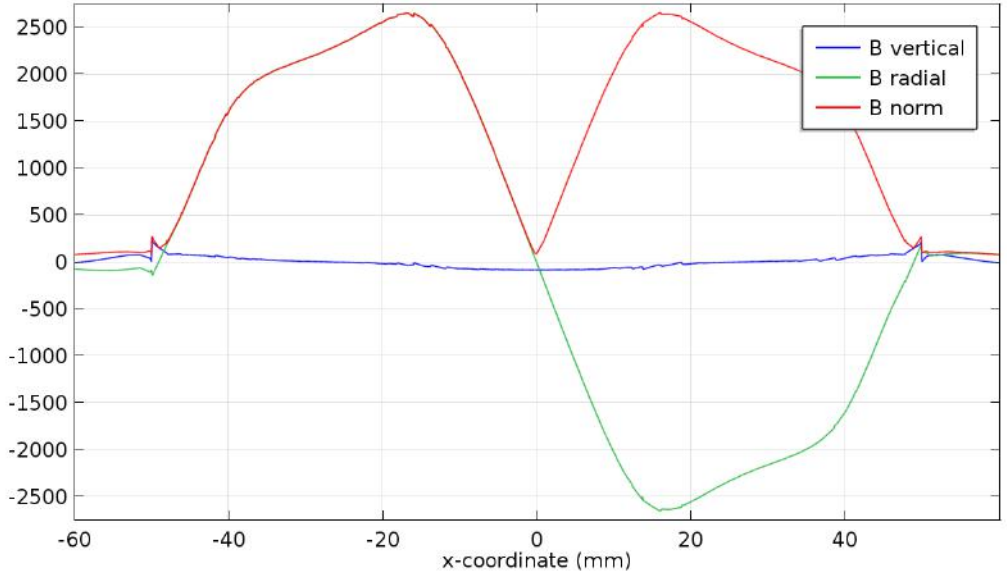

INESC MN
Microsistemas & Nanotecnologias

Configuration of magnet array:

- to increase the magnetic field for magnetic targets
- to use a maximum area of the target

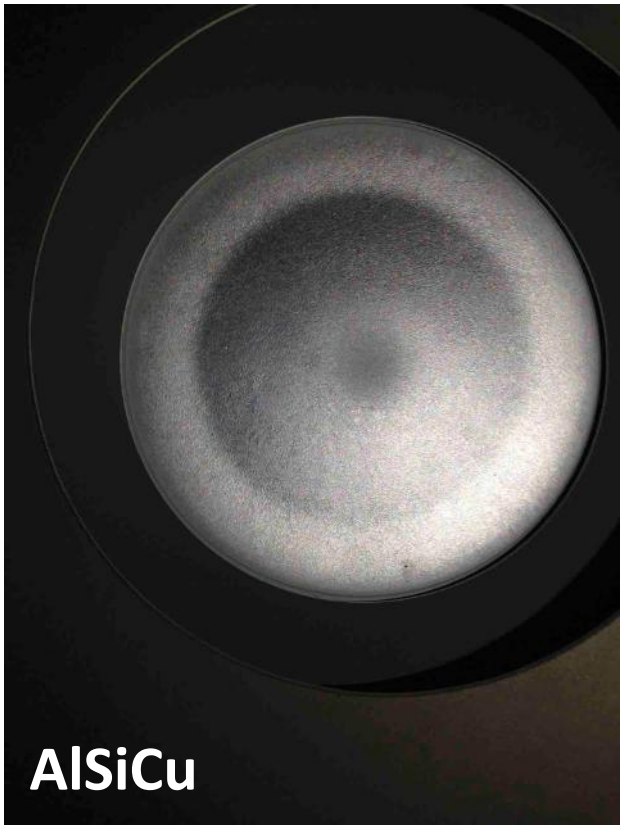

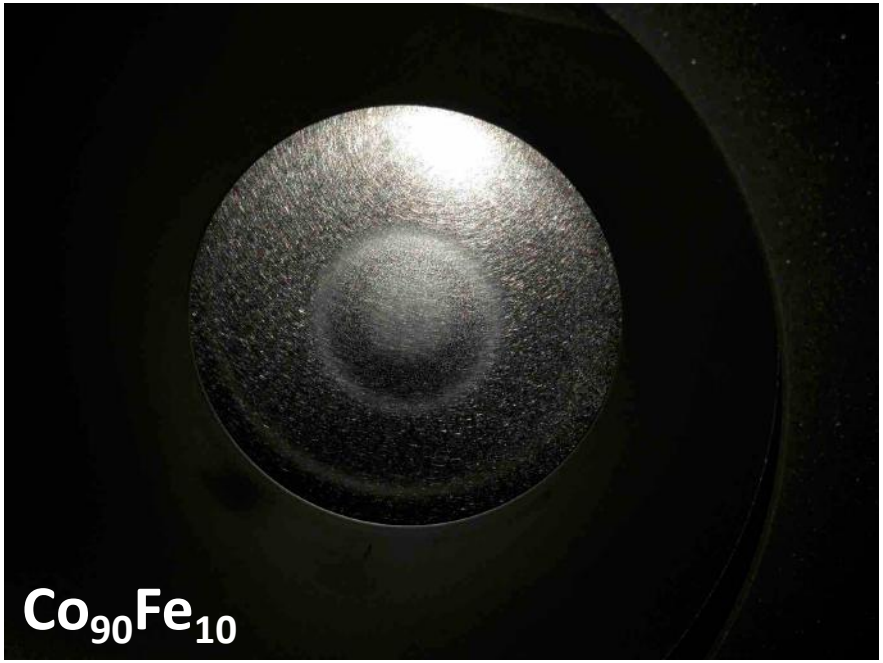

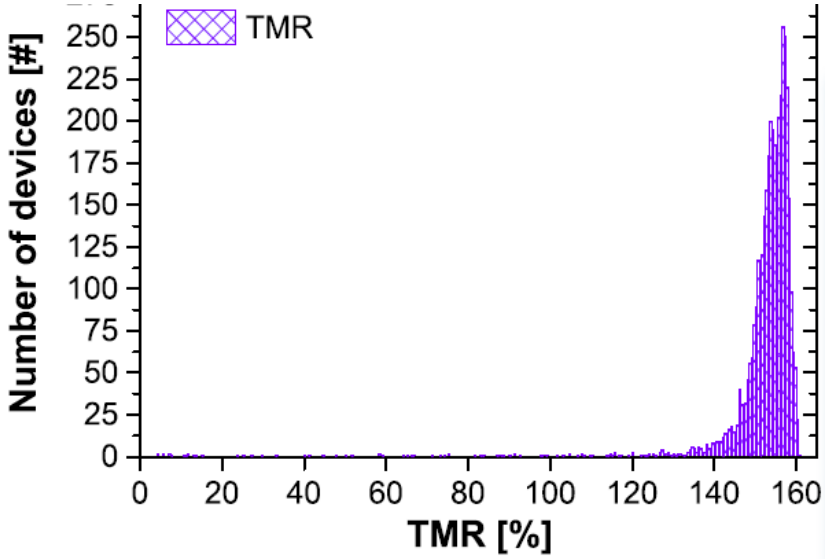

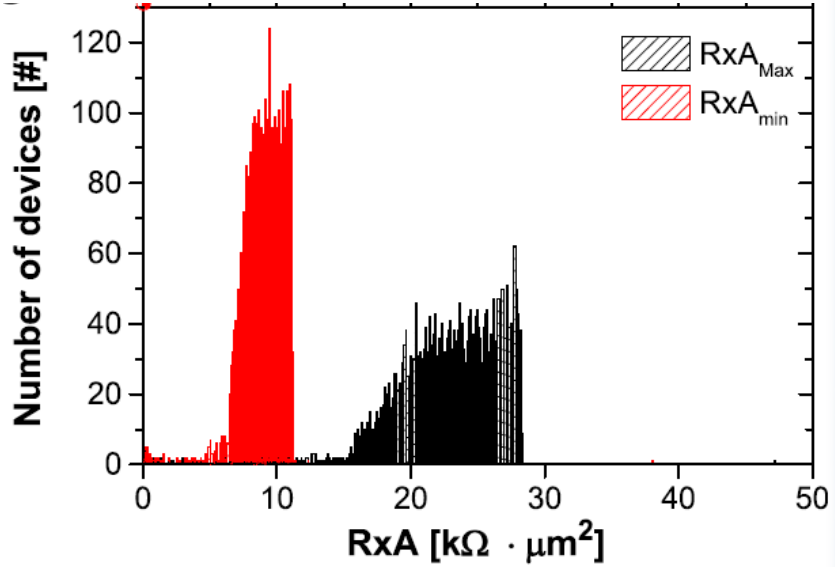

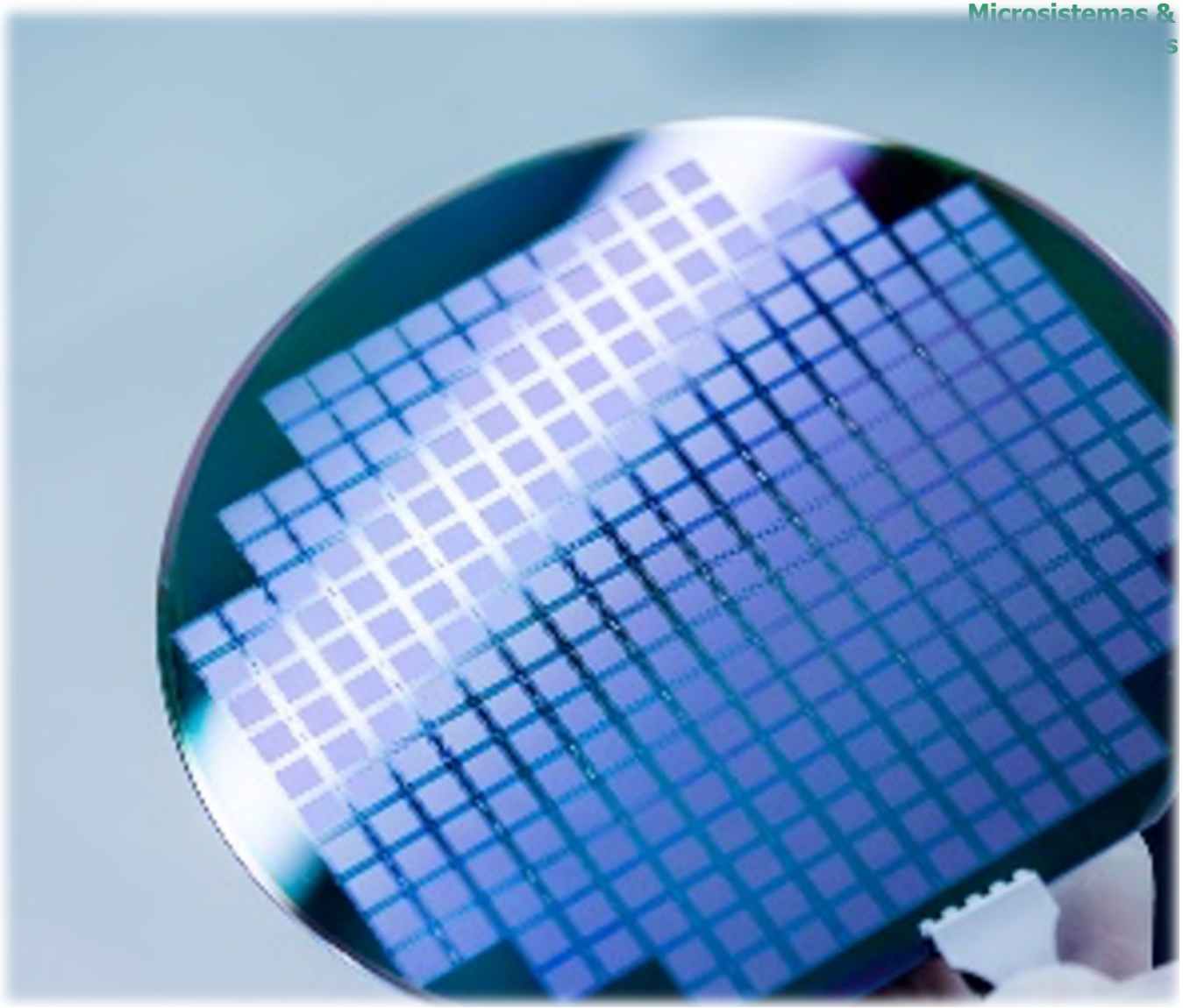

INESC MN
Microsistemas &
s

Proceedings of the IEEE, 104 (10), pp. 1894 (2016)

GMR biosensor qualification (6 inch wafers)

INESC MN
Microsistemas & Nanotecnologias

Magnetoresistance (%)
Mean = 6.26 %
Std = 0.97%

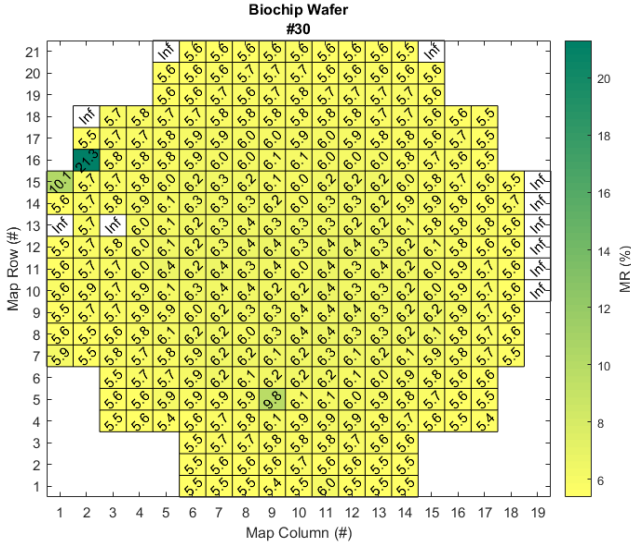

Minimum Resistance (Ω)
Mean = 743.1 Ω
Std = 38.2 Ω

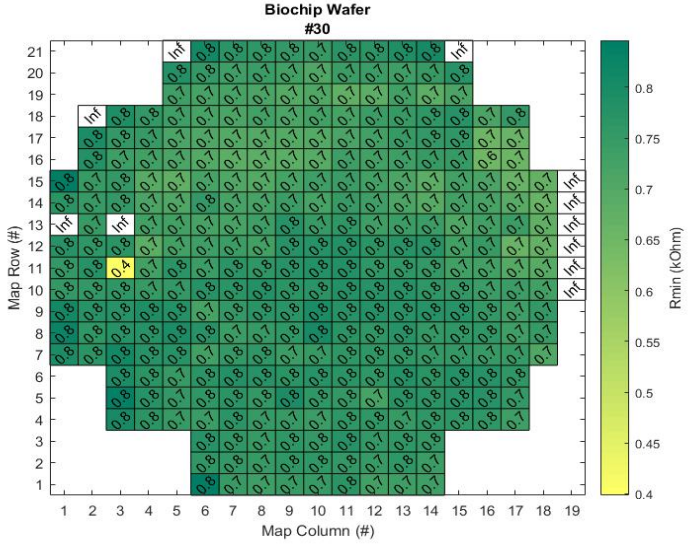

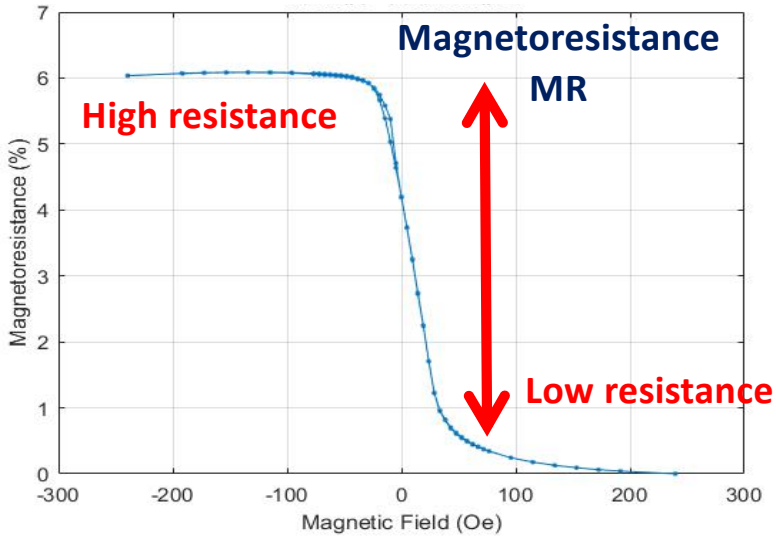

INESC MN
Microsistemas &
Nanotecnologias

Challenges from industry:

High thermal stability

(150°C under random, strong fields)

MR and R characterization during heating

INESC MN
Microsistemas & Nanotecnologias

N2000 - N2TJ1338- Single MTJ Square pillar: 7.5x7.5 µm^2

Ta(50) / [Ru(180) / Ta(30)]x3 / **MnPt(**213) / CoFe(18) / Ru(7.5) / CoFeB(16)/**MgO(14)** / CoFeB(20) /Ru(50) / Ta(100)
Annealing 390 ºC 0.5T 2h

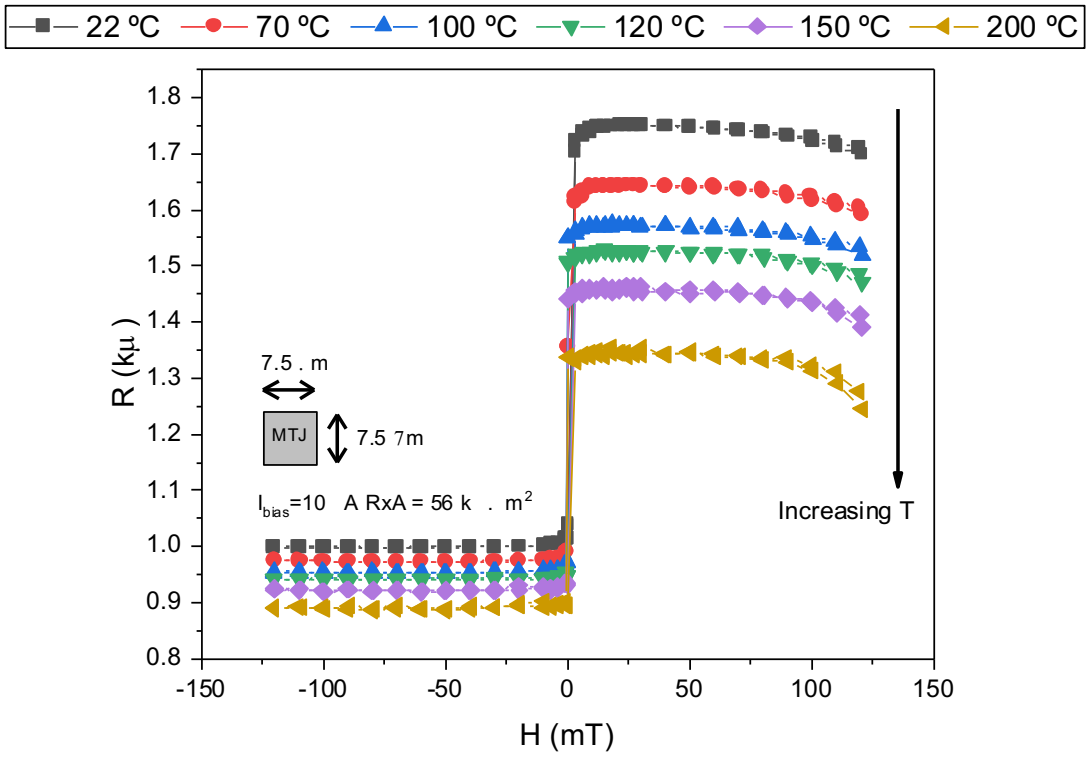

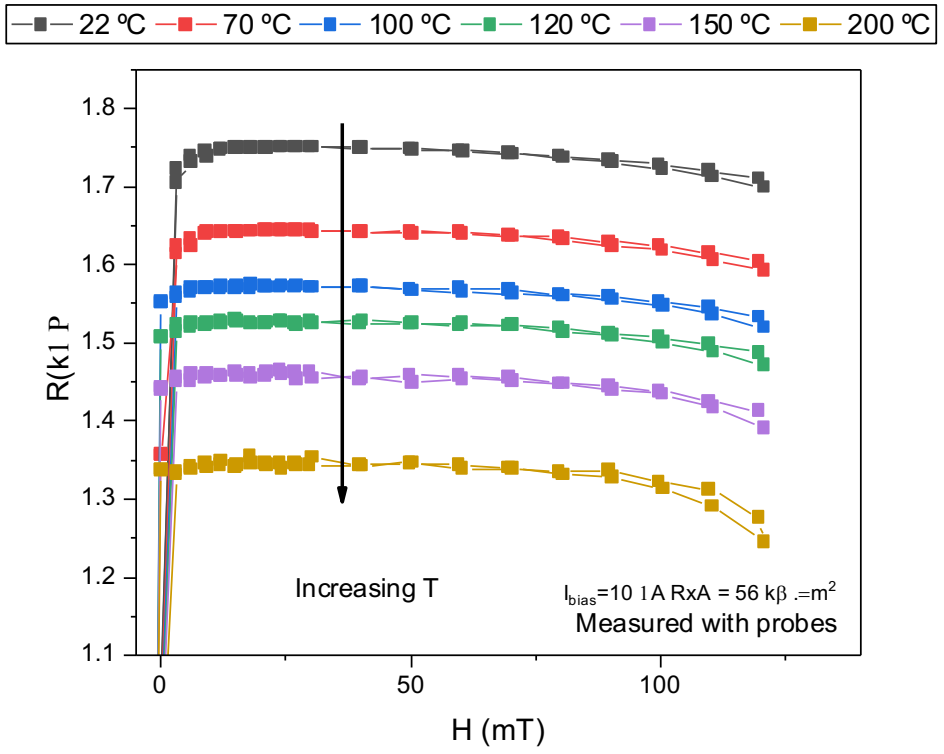

Optimization of the Spin-Flop:
=> flat plateau at larger fields to stabilize the reference layer

INESC MN
Microsistemas & Nanotecnologias

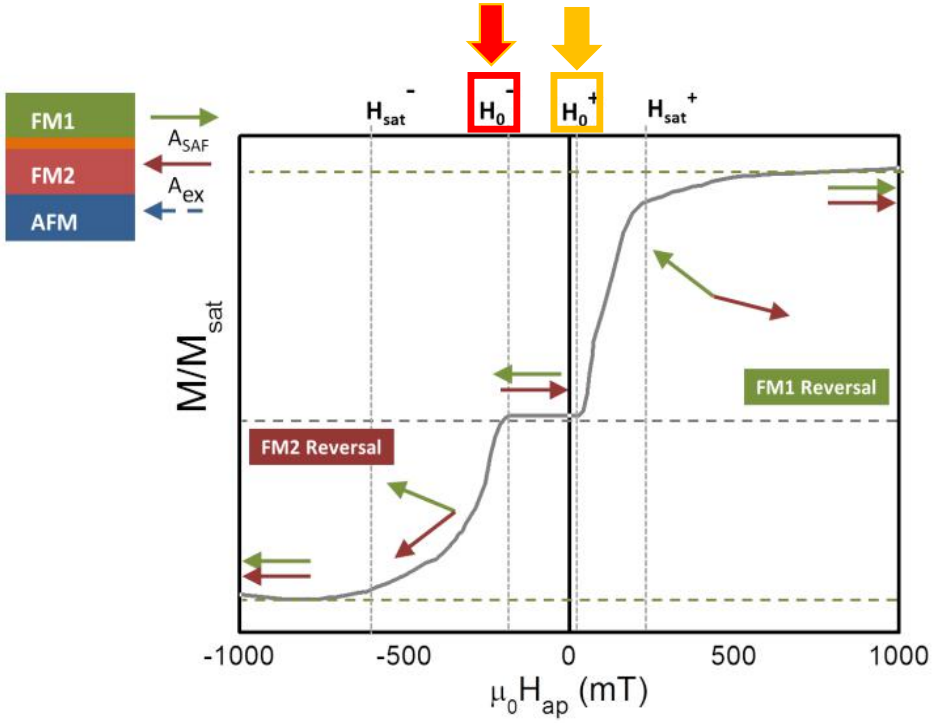

Figure 3.8: M(H) loop illustration of a SAF pinned layer.

Analytical formulation:

$$M_s^{(1)} = M_s^{(FM1)} t^{(\mathrm{FM1})} \text{ and } M_s^{(2)} = M_s^{(FM2)} t^{(\mathrm{FM2})}$$

$$\begin{cases} H_{sat}^{+} = \frac{1}{2}\left[\frac{\mathcal{A}_{\mathrm{SAF}}}{M_s^{(1)}} + \frac{\mathcal{A}_{\mathrm{SAF}}}{M_s^{(2)}} - \frac{\mathcal{A}_{ex}}{M_s^{(2)}} + \sqrt{\left(\frac{\mathcal{A}_{\mathrm{SAF}}}{M_s^{(1)}} + \frac{\mathcal{A}_{\mathrm{SAF}}}{M_s^{(2)}} - \frac{\mathcal{A}_{ex}}{M_s^{(2)}}\right)^2 + \frac{4\mathcal{A}_{\mathrm{SAF}}\mathcal{A}_{ex}}{M_s^{(1)} M_s^{(2)}}}\right] \\ H_{sat}^{-} = -\frac{1}{2}\left[\frac{\mathcal{A}_{\mathrm{SAF}}}{M_s^{(1)}} + \frac{\mathcal{A}_{\mathrm{SAF}}}{M_s^{(2)}} + \frac{\mathcal{A}_{ex}}{M_s^{(2)}} + \sqrt{\left(\frac{\mathcal{A}_{\mathrm{SAF}}}{M_s^{(1)}} + \frac{\mathcal{A}_{\mathrm{SAF}}}{M_s^{(2)}} + \frac{\mathcal{A}_{ex}}{M_s^{(2)}}\right)^2 - \frac{4\mathcal{A}_{\mathrm{SAF}}\mathcal{A}_{ex}}{M_s^{(1)} M_s^{(2)}}}\right] \end{cases}.$$

$$H_0^{+} = \frac{1}{2}\left[\frac{\mathcal{A}_{\mathrm{SAF}}}{M_s^{(1)}} - \frac{\mathcal{A}_{\mathrm{SAF}}}{M_s^{(2)}} - \frac{\mathcal{A}_{ex}}{M_s^{(2)}} + \sqrt{\left(-\frac{\mathcal{A}_{\mathrm{SAF}}}{M_s^{(1)}} + \frac{\mathcal{A}_{\mathrm{SAF}}}{M_s^{(2)}} + \frac{\mathcal{A}_{ex}}{M_s^{(2)}}\right)^2 + \frac{4\mathcal{A}_{\mathrm{SAF}}\mathcal{A}_{ex}}{M_s^{(1)} M_s^{(2)}}}\right]$$

$$H_0^{-} = -\frac{1}{2}\left[-\frac{\mathcal{A}_{\mathrm{SAF}}}{M_s^{(1)}} + \frac{\mathcal{A}_{\mathrm{SAF}}}{M_s^{(2)}} + \frac{\mathcal{A}_{ex}}{M_s^{(2)}} + \sqrt{\left(-\frac{\mathcal{A}_{\mathrm{SAF}}}{M_s^{(1)}} + \frac{\mathcal{A}_{\mathrm{SAF}}}{M_s^{(2)}} + \frac{\mathcal{A}_{ex}}{M_s^{(2)}}\right)^2 + \frac{4\mathcal{A}_{\mathrm{SAF}}\mathcal{A}_{ex}}{M_s^{(1)} M_s^{(2)}}}\right]$$

[1] B. Dieny, \Improvement in the pinning related to the use of synthetic pinned layer," in Magnetoelectronics (M. Johnson, ed.), ch. Spin Valves, pp. 105{113, Elsevier Inc., 2004

INESC MN
Microsistemas & Nanotecnologias

Degradation of TMR with T
Resistance variation with T

Tunnel barrier?

Reference/pinned layer materials ?

Antiferromagnetic material ?

Exchange Bias: $H_{ex}(T)$

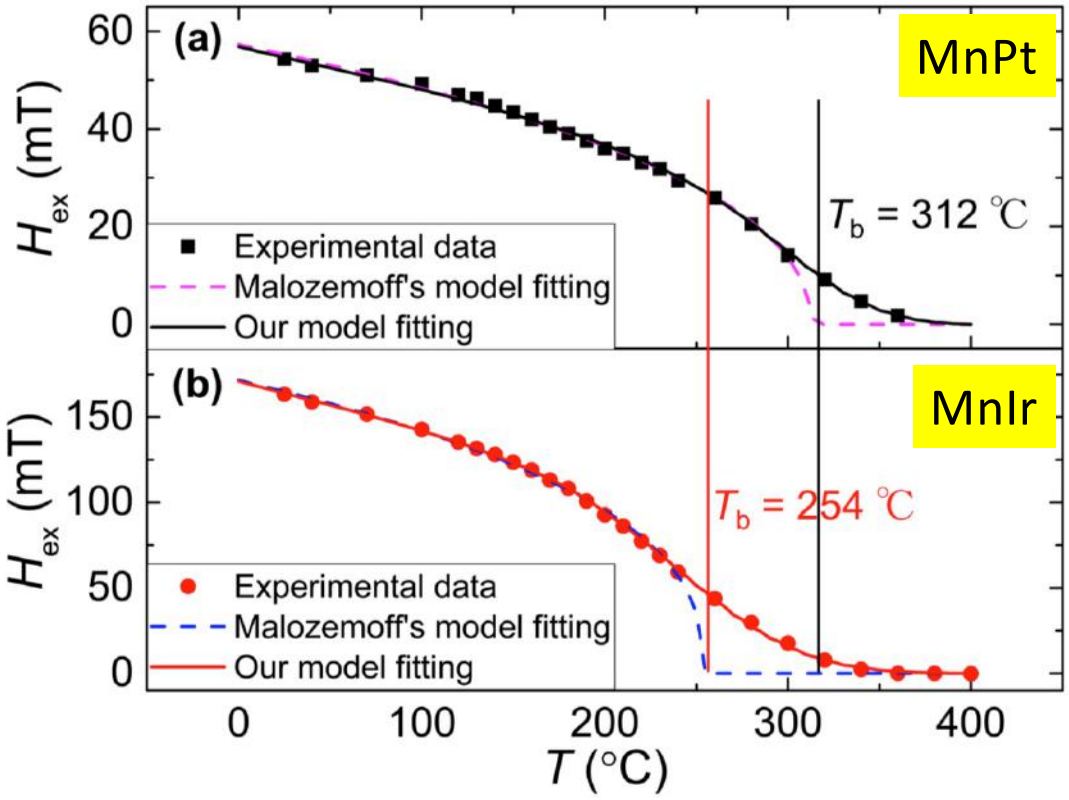

Thermal stability of H_{ex}

1. Interfacial coupling decrease;
2. T_b distribution, grain size;
3. Magnetization, T_c.

H_{ex} dependence on temperature

Malozemoff's Model:

$$H_{ex}(T) = \frac{J^0_{int}}{M_{FM}t_{FM}} j(T) = H^0_{ex} j(T)$$

$$j(T) = \begin{cases} \left(1 - \frac{T}{T_b}\right)^{\gamma} & : T < T_b \\ 0 & : T \geq T_b \end{cases}$$

Improved Model - T_b distribution :

$$H_{ex}(T) = \frac{H^0_{ex}}{1 - \left(\frac{T}{T_c}\right)^{3/2}} \sum_i f(T_{bi}) \begin{cases} \left(1 - \frac{T}{T_{bi}}\right)^{\gamma} & : T < T_{bi} \\ 0 & : T \geq T_{bi} \end{cases}$$

$$f(T_b^i) = \frac{1}{\Delta T_b \sqrt{2\pi}} exp\left[-\frac{\left(T_b^i - T_b^{center}\right)^2}{2\left(\Delta T_b\right)^2}\right]$$

H. Lv *et al., J Magn. Magn. Mater*. **477**, 68-175 (2019).

Bilayer: buffer/ AF(15)/ $Co_{70}Fe_{30}$ (2.7)

Coercivity vs Temperature

INESC MN
Microsystems and Nanotechnologies

H_c dependence on temperature

Bilayer: buffer/ AF(15)/ $Co_{70}Fe_{30}$ (2.7)

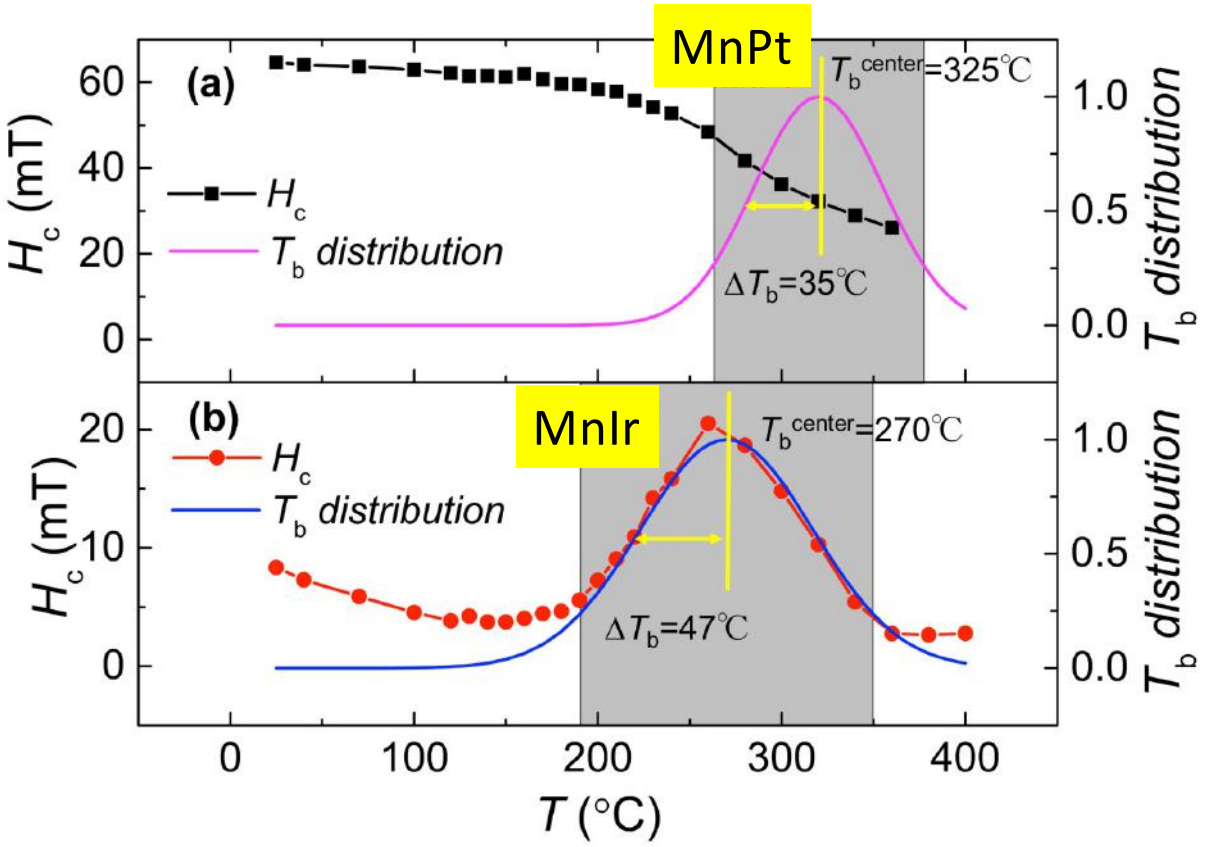

H_c Model: dependency on the grain size

$$H_{ex}(T_{ms}) \propto \int_{V_c(T_{mS})}^{V_{set}(T_{mS})} f(V)dV$$

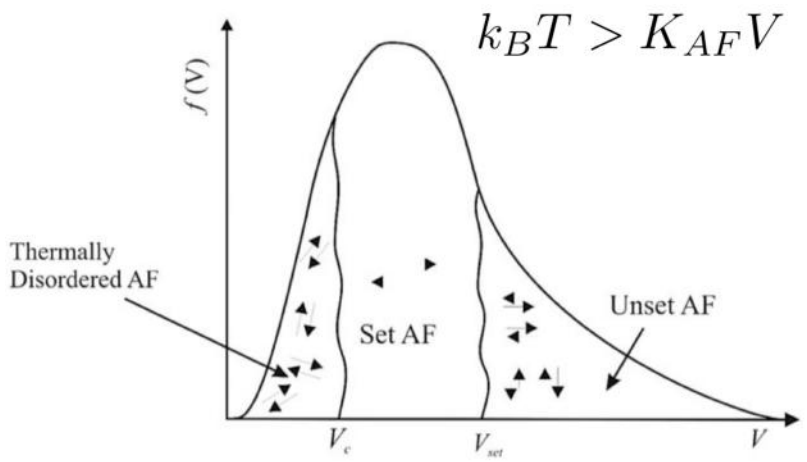

- H_c enhanced at high temperature;
- H_c enhancement is correlated with T_b distribution.

INESC MN
Microsistemas &
Nanotecnologias

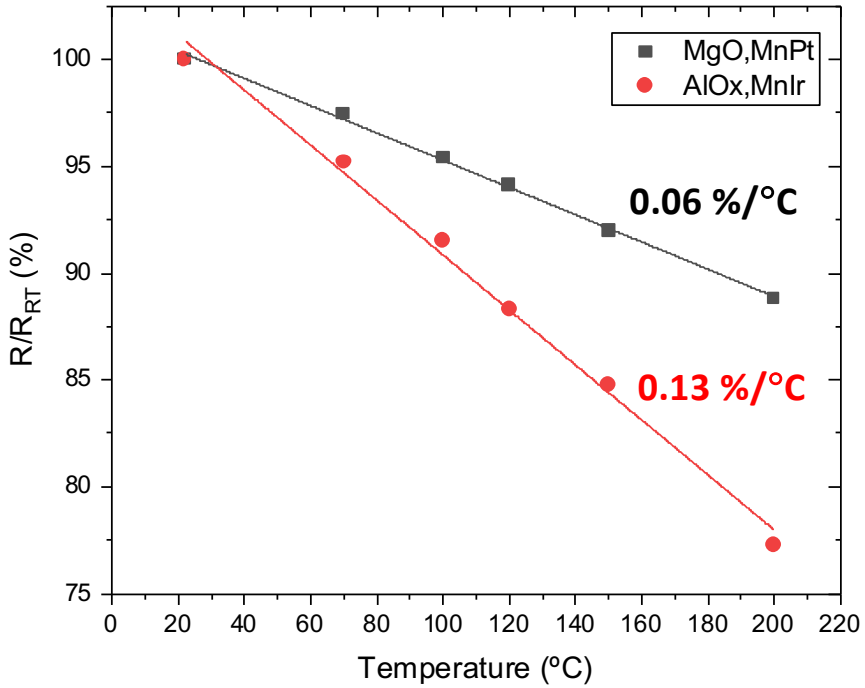

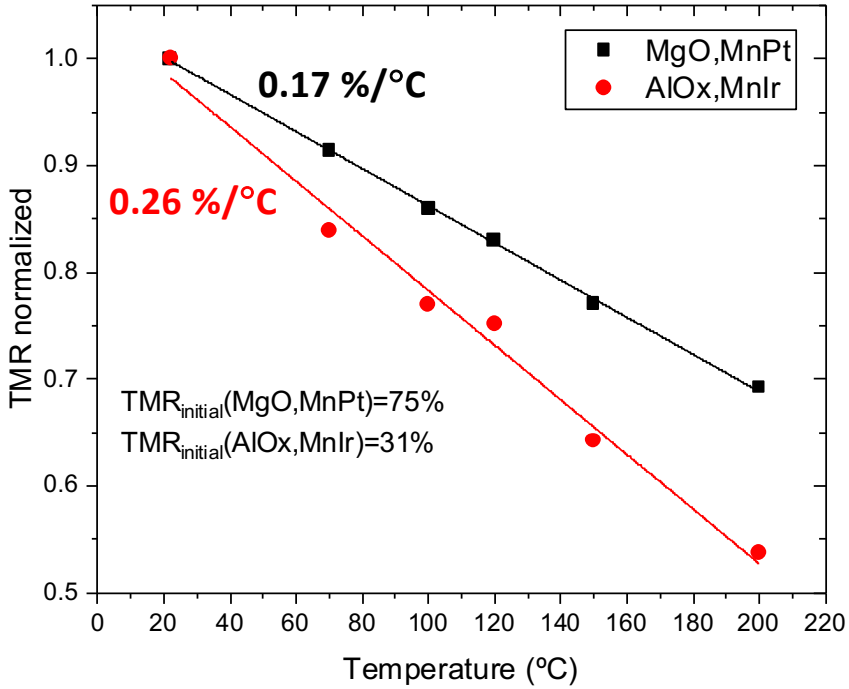

INESC MN
Microsistemas &
Nanotecnologias

Technological challenges:

- Noise
- Signal-to-noise ratio
- Minimum detectable field (detectability)

MRI
1 T

1 mT
Earth field

1 μT

1 nT
Heart
1 pT
Brain
1 fT

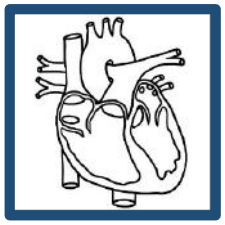

Amplitude:
few **pTesla** at chest surface
(below 100 Hz)

Amplitude:
few **fTesla** at skull surface
(below 100 Hz)

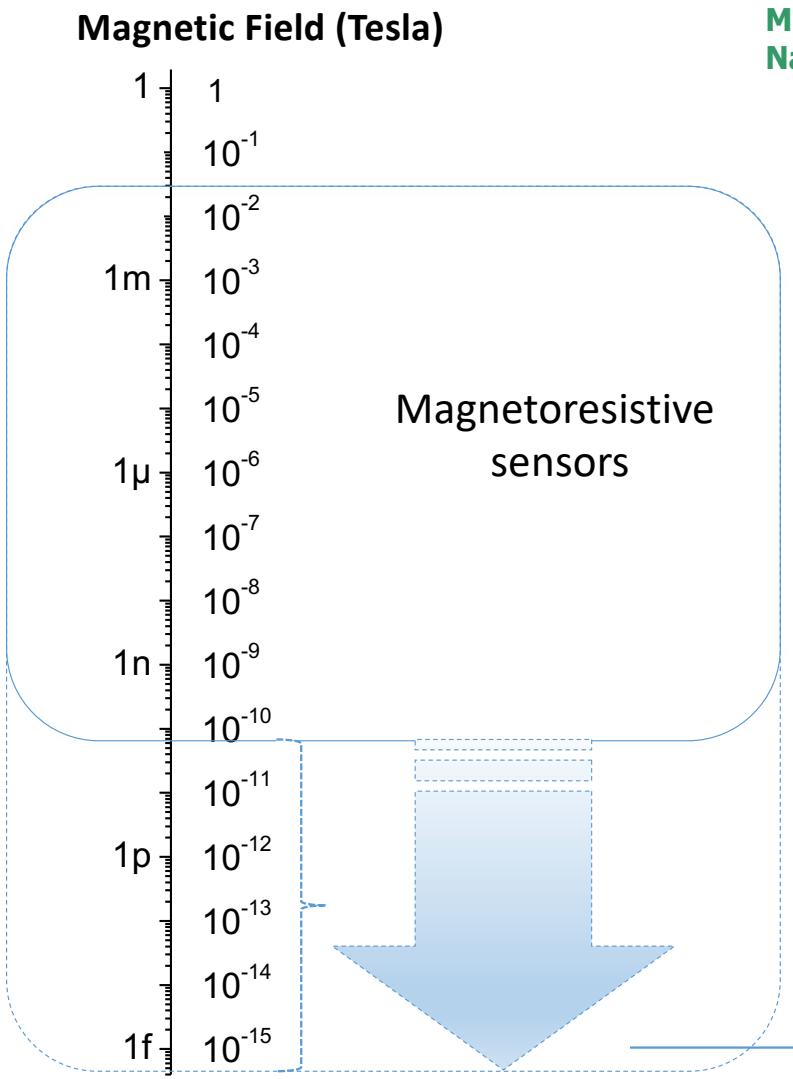

How to distinguish signal from noise ?

INESC MN
Microsistemas & Nanotecnologias

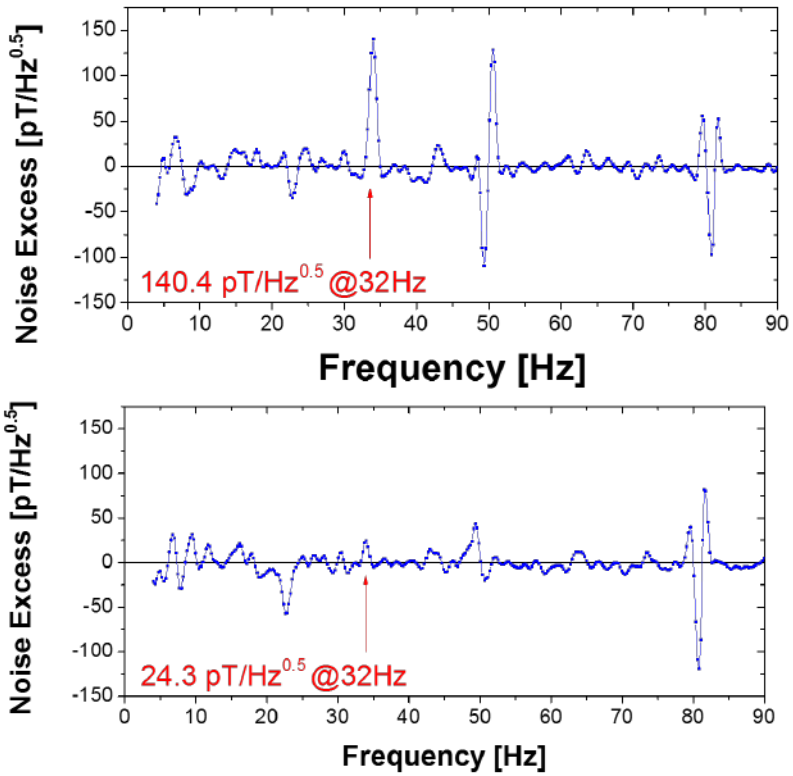

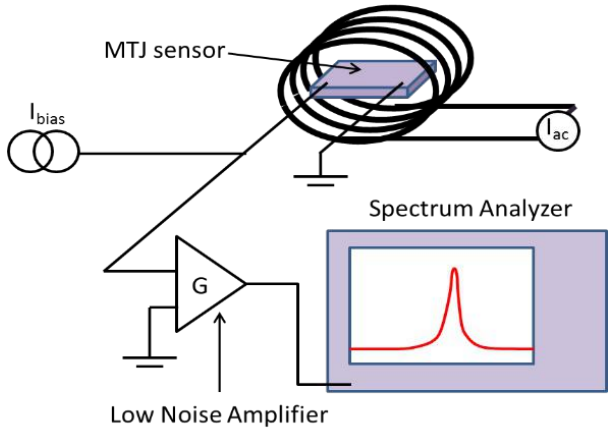

Detectivity limit:

SNR = 1
(Signal = Noise)

P.P.Freitas, R.Ferreira and S.Cardoso "Spintronic Sensors", P**roceedings of the IEEE**, 104, 1894 (2016)

E. Paz · S. Serrano-Guisan · R. Ferreira · P. P. Freitas – J. of Applied Physics; 115. 2014

Noise Spectrum of Magnetoresistive Sensors

Main noise contributions

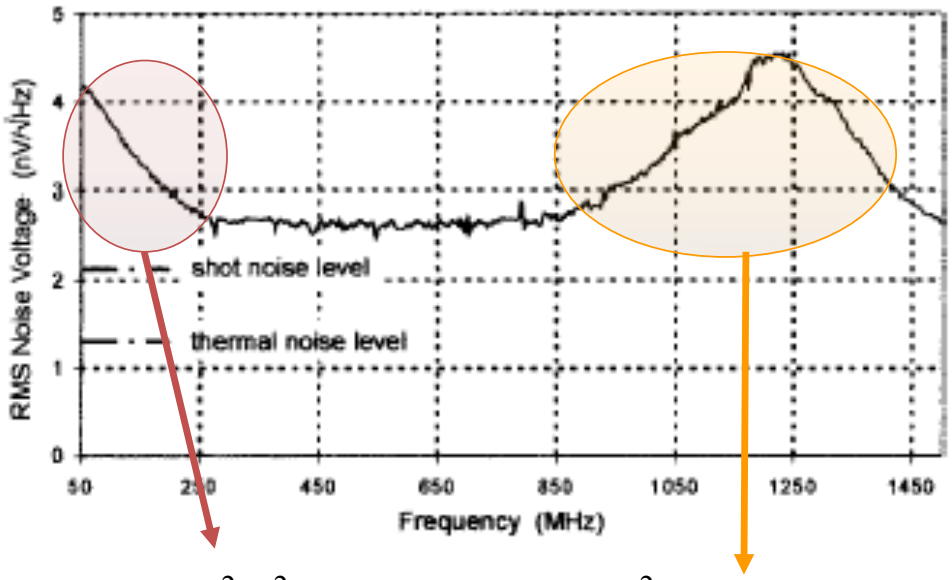

$$S_V(V^2/Hz) = \frac{\alpha_H I^2 R^2}{Af\ \Delta f} + \frac{4K_B TR}{\Delta f} + \frac{2eIR^2}{\Delta f} + FMR_{Noise}$$

1/f noise

Thermal Noise

Shot Noise

High-Frequency Noise

At low frequencies

Only the white noise sources contribute to the noise background

$$S_V(V^2/Hz) = \frac{\alpha_H I^2 R^2}{A\ f}$$

[noise, in Volt]

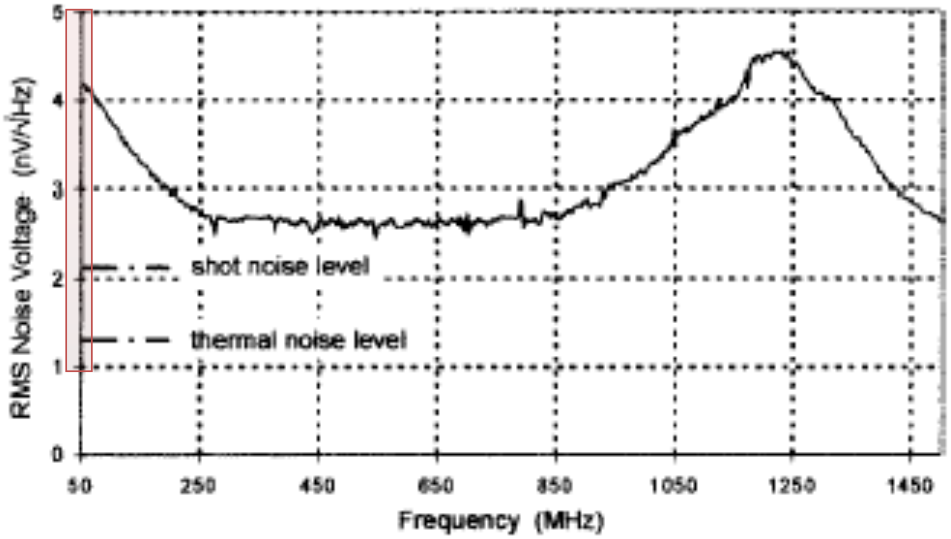

The noise level in the low-frequency range depends only on:

- **Magnetoresistance**, MR
- **linear range, ΔH**
- **Area, A**

No explicit dependence on device RxA and bias current.

Field detectivity (D)

INESC MN
Microsistemas & Nanotecnologias

Detectivity limit: **SNR = 1** (Signal = Noise)

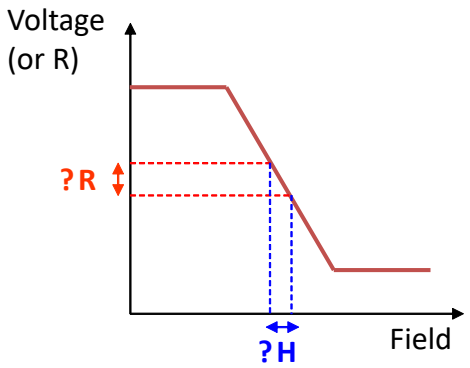

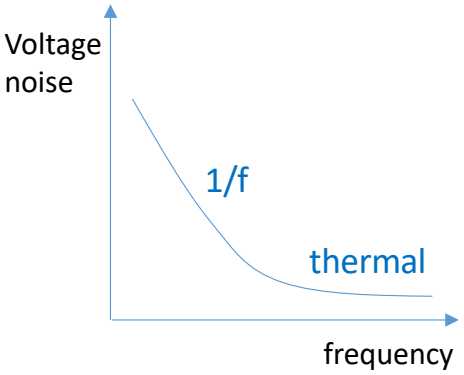

$$S_V\left(T/\sqrt{Hz}\right)=\frac{\sqrt{\frac{\alpha_H I^2 R^2}{A\,f}}}{I.\frac{\Delta R}{\Delta H}}=\frac{\Delta H}{MR}\sqrt{\frac{\alpha_H}{A\,f}}$$ *[in Tesla]*

(in 1/f regime)

Operate at high f
Increase MR
Increase A
Reduce linear range ΔH
Reduce Hooge value

S=TMR/ΔH
sensor sensitivity

α_H = Hooge's constant
A = MR area
f = operating frequency

Strategies to improve the minimum detectable field

Field modulation for high frequency

Increase MR

Increase A

Reduce linear range ΔH

Reduce Hooge value

Sensors, *18*(3), 790; (2018)
Micromachines, *7*(5), 88 (2016)
IEEE Trans. Magn. 48 (11), pp. 4115 (2012)
Journal of SPIN, Vol.1 (1), pp 71-91 (2011)
J.Appl.Phys. 103, 07E924 (2008)
Appl. Phys. Lett. 95, 023502 (2009)

magnetic MEMS

INESC MN
Microsistemas & Nanotecnologias

Modulate dc magnetic field at high frequency using MEMS resonators with incorporated magnetic flux guides

goal

shift the sensor operating frequency to the kHz region
where the noise can be 2 orders of magnitude lower then dc

spin valve noise spectrum

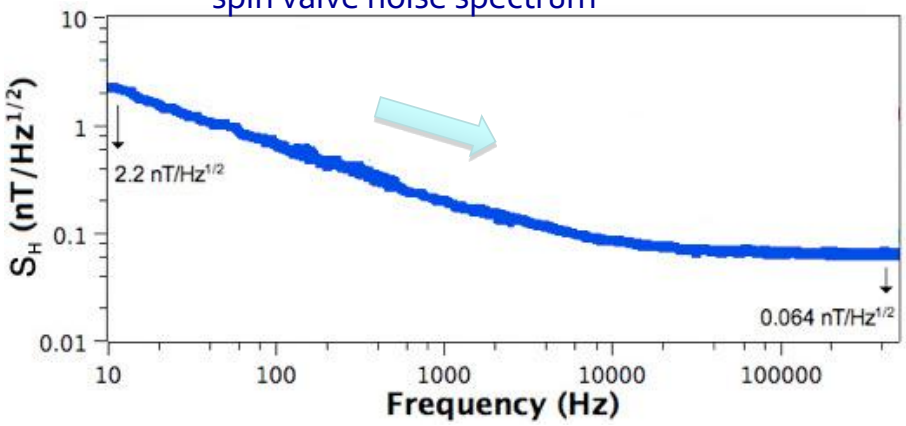

geometry

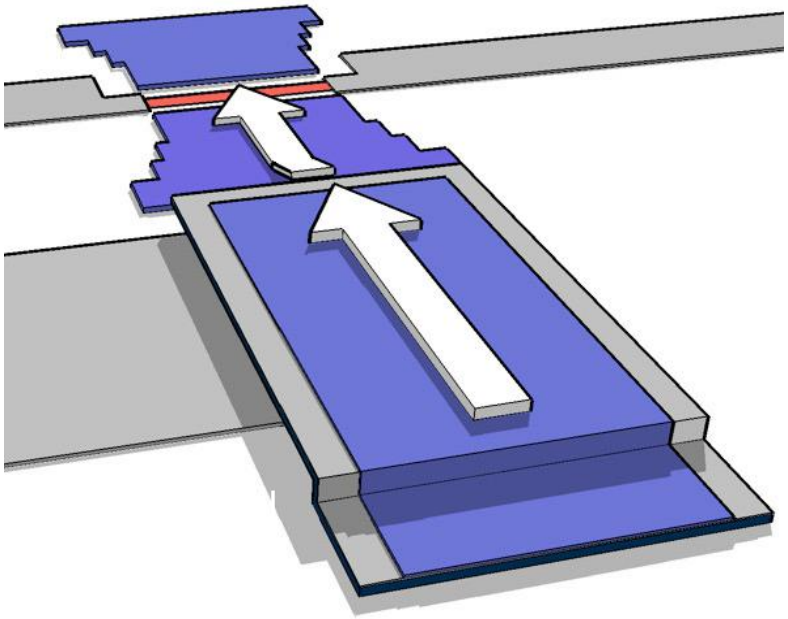

Appl. Phys. Lett. 95, 023502 (2009)

J.Appl.Phys. 103, 07E924 (2008)

Strategies to improve the minimum detectable field

Field modulation for high frequency

Increase MR

Increase A

Reduce linear range ΔH

Reduce Hooge value

Nat Mater, 2004, 3:862–867
J PhysD-Appl Phys, 2007, 40: R337
J. Physics: Cond.Matter, 19 (2007) 165221
Ann Rev Mater Res, 2009, 39: 277–296
J Appl Phys, 2007, 101: 09B501
J. Appl. Phys, 99, 08A907 2006

AlOx and MgO barriers

INESC MN
Microsistemas & Nanotecnologias

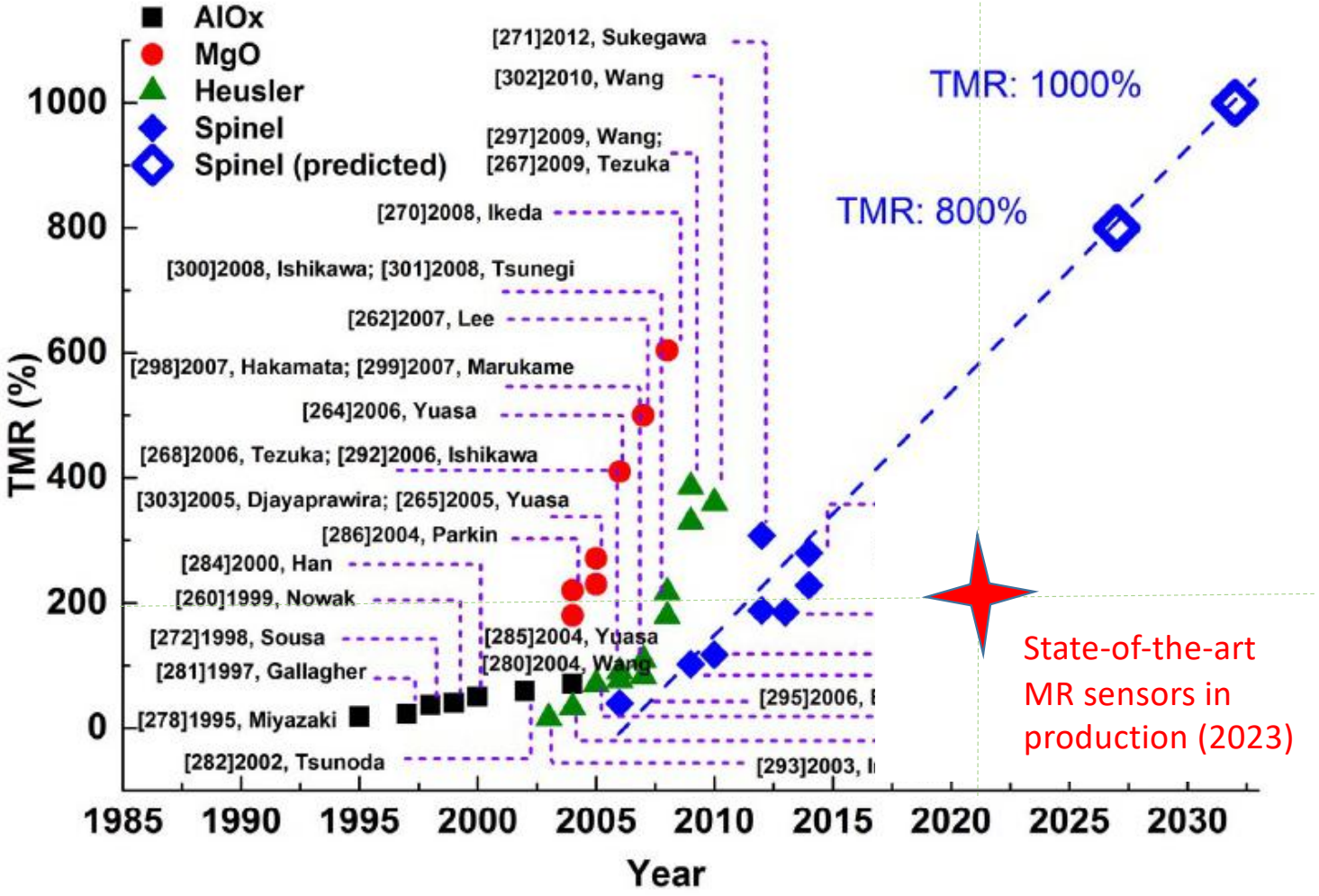

State-of-the-art MR sensors in production (2023)

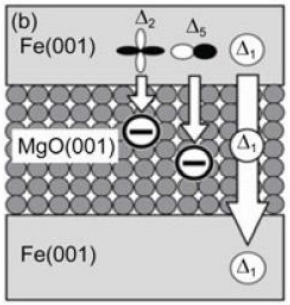

Crystalline barrier

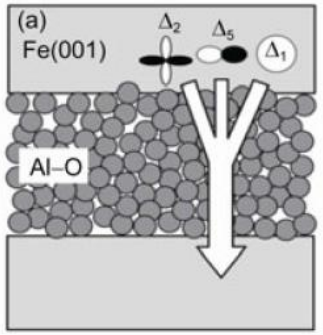

Amorphous barrier

"Magnetoresistive Sensor Development Roadmap (Non-Recording Applications)"
IEEE Trans.Magn. (2019)

Strategies to improve the minimum detectable field

Field modulation for high frequency

Increase TMR

Increase A

Reduce linear range ΔH

Reduce Hooge value

R.Chaves, et.al , Appl. Phys.Lett, 91, 102504 (2017)

E. Paz et.al – J. Applied Physics; 115. 2014

Linearization strategies for MgO

INESC MN
Microsistemas & Nanotecnologias

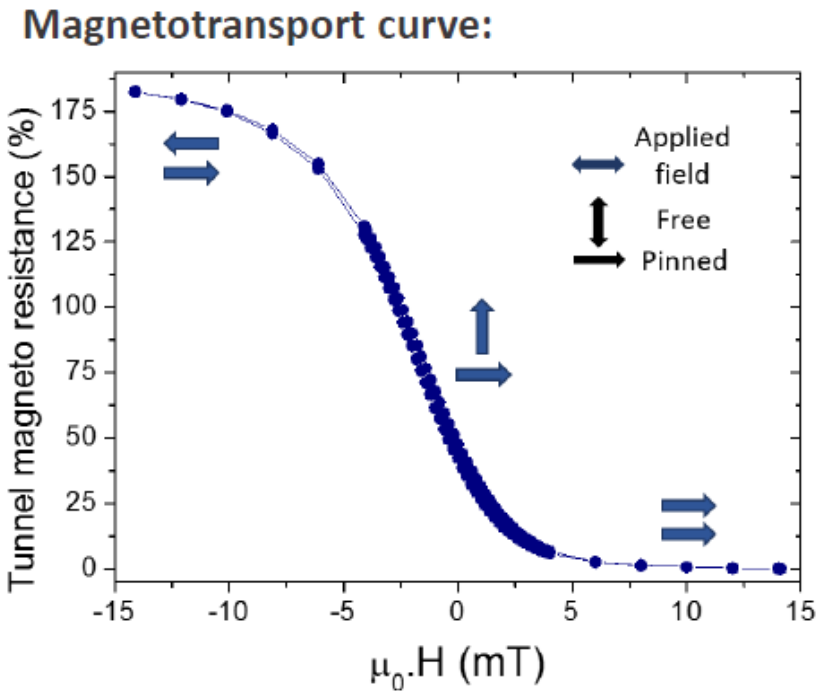

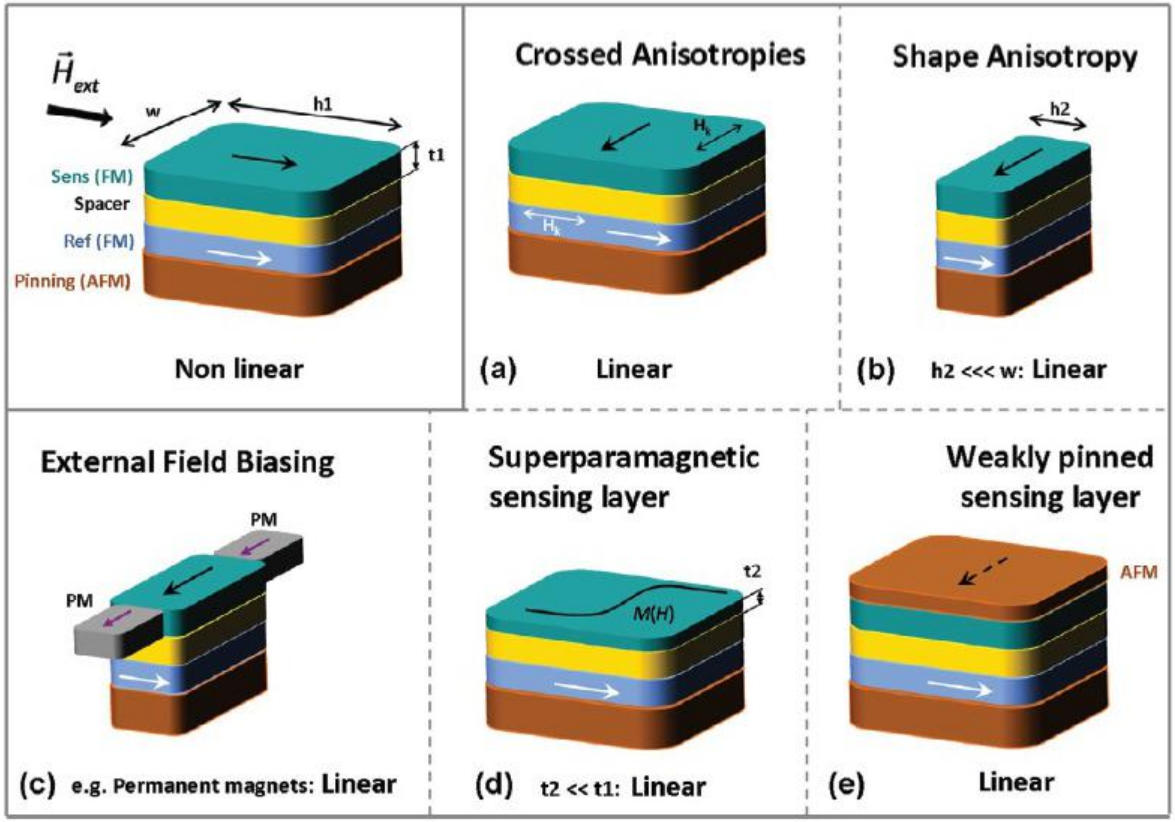

Fig. 12. Summary of linearization strategies for MR sensors.

Journal of SPIN, Vol.1 (1), pp 71-91 (2011)
J.Appl.Phys. 103, 07A910 (2008)
Sensors and Actuators , 202, pp. 64– 68 (2013);

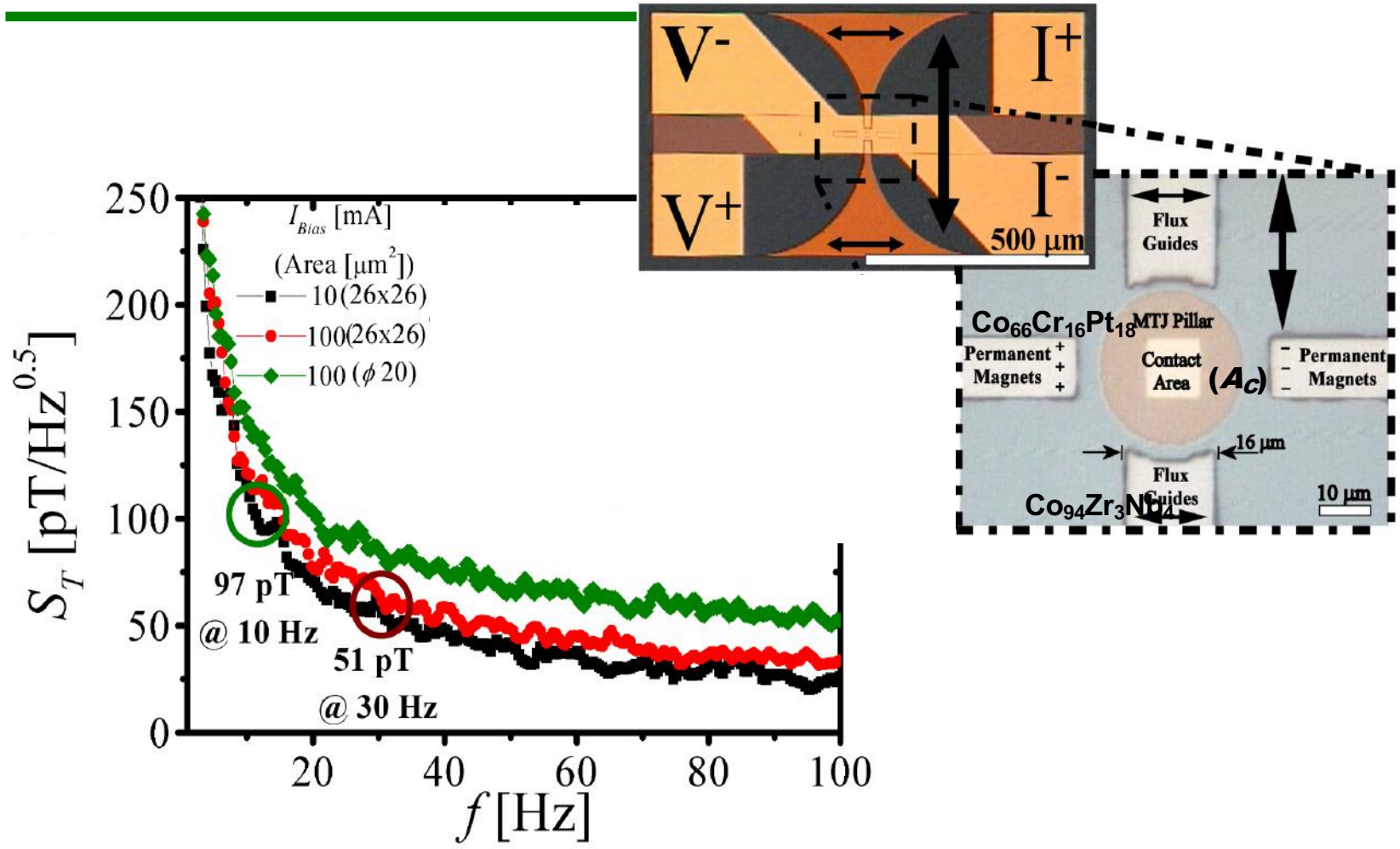

R.Chaves, et.al , Appl. Phys.Lett, 91, 102504 (2017)

INESC MN
Microsistemas & Nanotecnologias

Large Series
1102 TMR elements with
A= 100x100 μm² each.

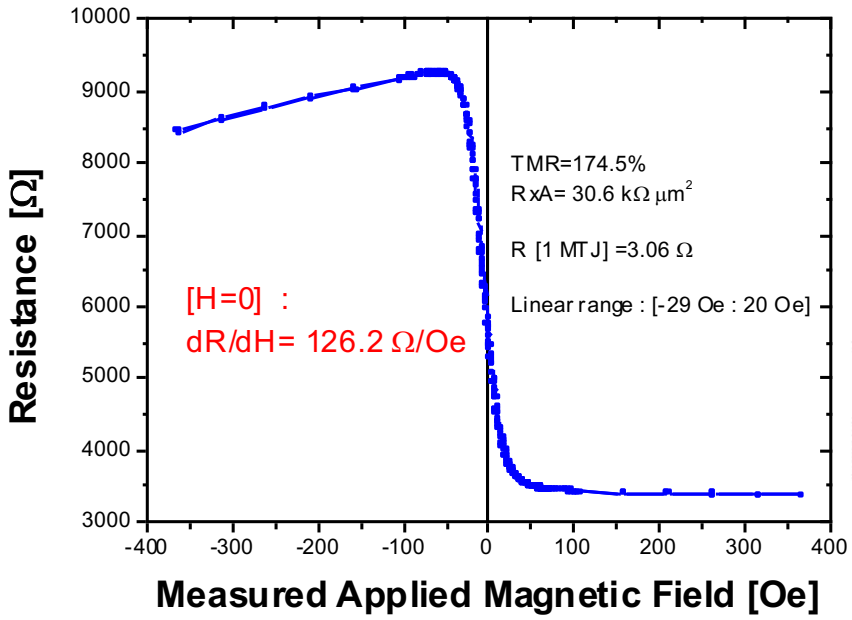

INL
INTERNATIONAL IBERIAN NANOTECHNOLOGY LABORATORY

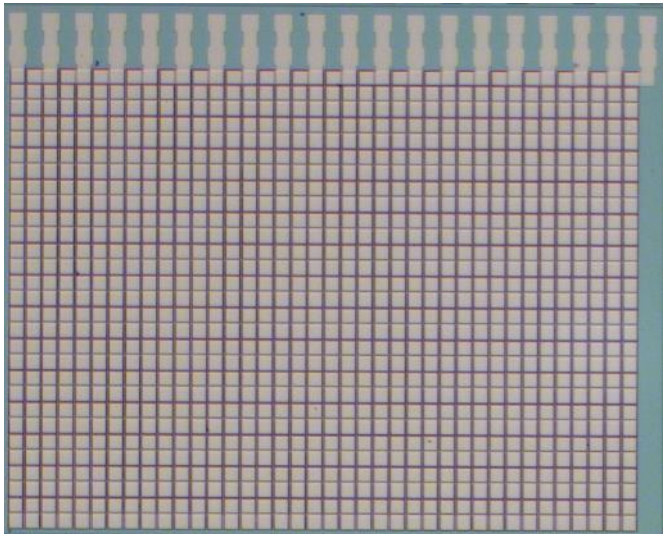

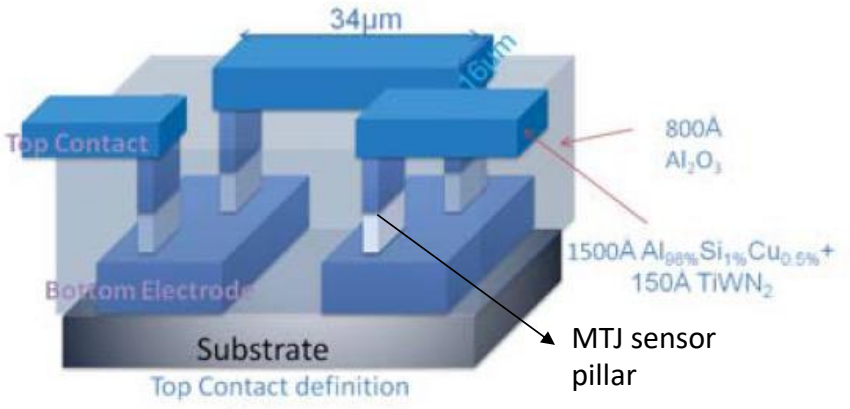

E. Paz · S. Serrano-Guisan · R. Ferreira · P. P. Freitas - Journal of Applied Physics; 115. 2014

Saving space: GMR sensors packed

INESC MN
Microsistemas & Nanotecnologias

Single sensor

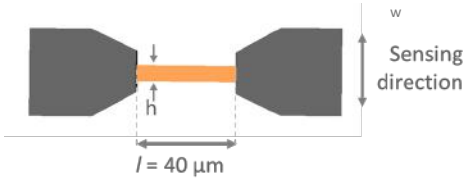

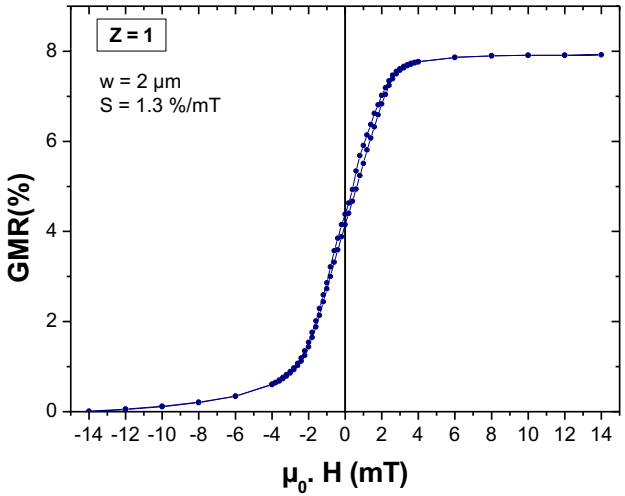

Packed sensors

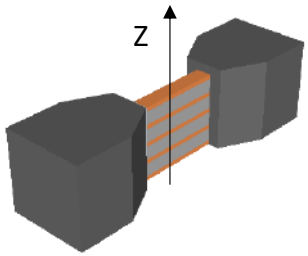

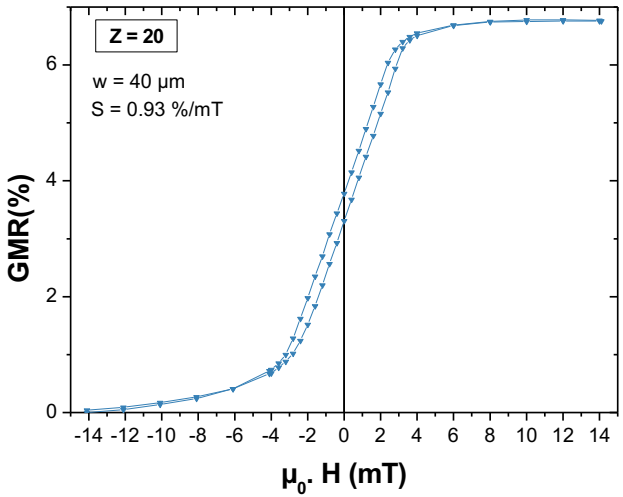

Packed arrays of sensors

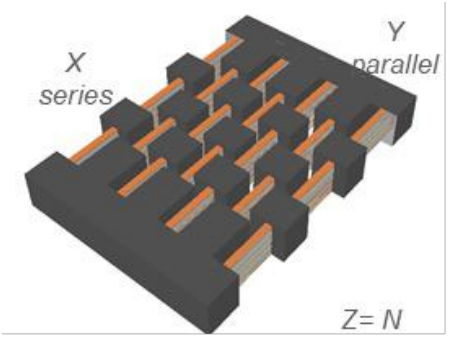

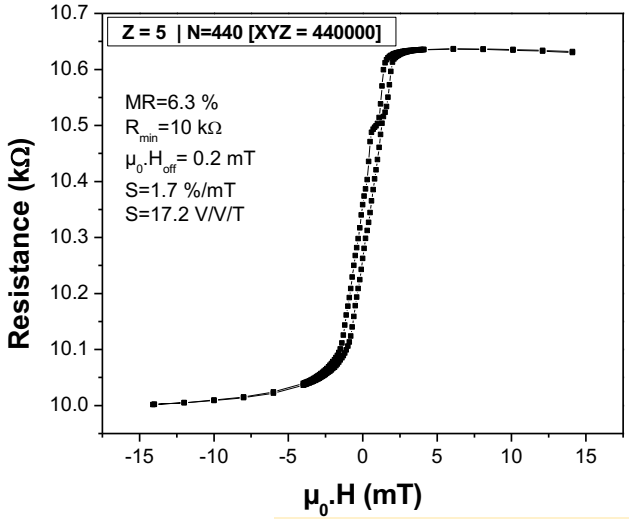

AIP Advances 8(5):056644 (2018)
Scientific Reports , 11, 215 (2021)

INESC MN
Microsistemas & Nanotecnologias

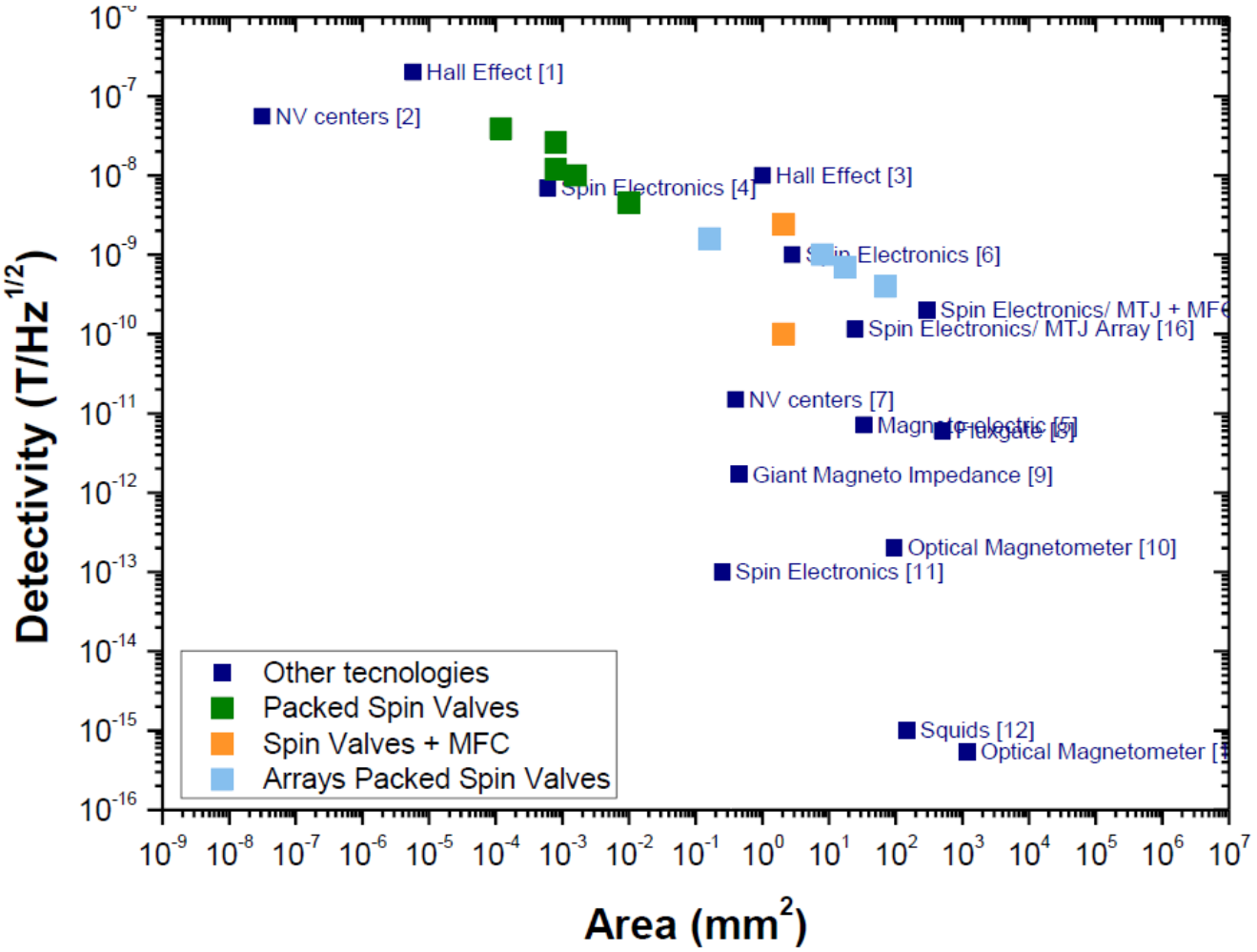

AIP Advances 8(5):056644 (2018)
Scientific Reports , 11, 215 (2021)

[1] E. Paz et al., *J. Appl. Phys.*, vol. 115,2014.
[2] tdk.com, "TDK biomagnetic sensor", 2019
[3] S. H. Liou *et al.*, *Proc. IEEE Sensors*, 2009

[1] P. Besse *et al* Appl. Phys. Lett. **80**, 4199 (2002)
[2] P. Maletinsky et al Nature Nanotechnology 7, 320-324 (2012)
[3] F. Montaigne et al Sensors and Actuators A: Physical 81, 324-327 (2000)
[4] L. Caruso et al Neuron 95, 1283-1291 (2017)
[5] R. Jahns et al Sensors and Actuators A: Physical 183, 16-21 (2012)
[6] F. Barbieri et al Scientific Reports 6, 39330 (2016)
[7] J. Barry et al PNAS 113, 14133-14138 (2016)
[8] Bartington Instruments, Mag-03 Three-axis
[9] S. Yabukami et al JMMM 290, 1318-1321 (2005)
[10] T. Sander et al Biomedical Optics Express 3, 981-990 (2012)
[11] M. Pannetier et al Science 304, 1648-1650 (2004)
[12] J. Gallop Supercond. Sci. Technol. 16, 1575 (2003)
[13] I. Kominis et al Nature 422, 596-599 (2003)
[14] E. Paz et al., *J. Appl. Phys.*, vol. 115,2014.
[15] tdk.com, "TDK biomagnetic sensor", 2019
[16] S. H. Liou *et al.*, *Proc. IEEE Sensors*, 2009

INESC MN
Microsistemas & Nanotecnologias

Strategies to improve the minimum detectable field

Field modulation for high frequency

Increase TMR

Increase A

Reduce linear range ΔH

Reduce Hooge value

Spin Valve sensor with vertical tapered profile Magnetic Flux Concentrators (MFCs)

INESC MN
Microsistemas & Nanotecnologias

SV835: Ta 20/ NiFe 30/ CoFe 22/ Cu 21/ CoFe 25/ MnIr 65/ Ta 100 [A]

- Sensor active area: 40 x 2 μm²
- Pole dimension: 40 μm
- MFC entrance dimension: 500 – 2000 μm
- Gap distance: 6 μm

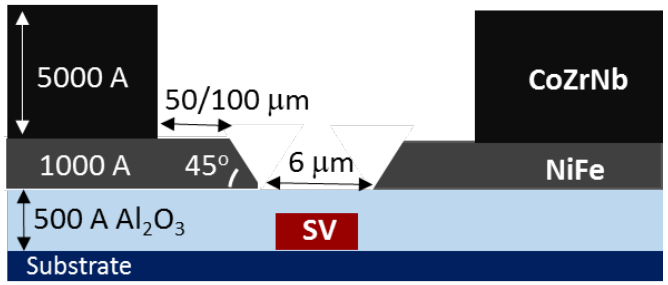

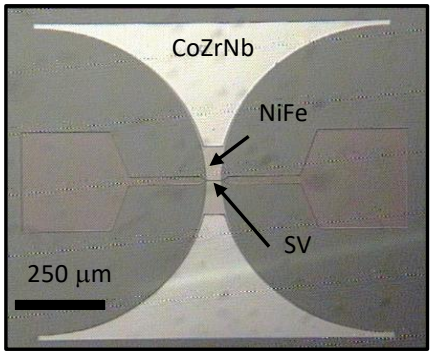

Magnetotransport curve (Spin Valve sensor)

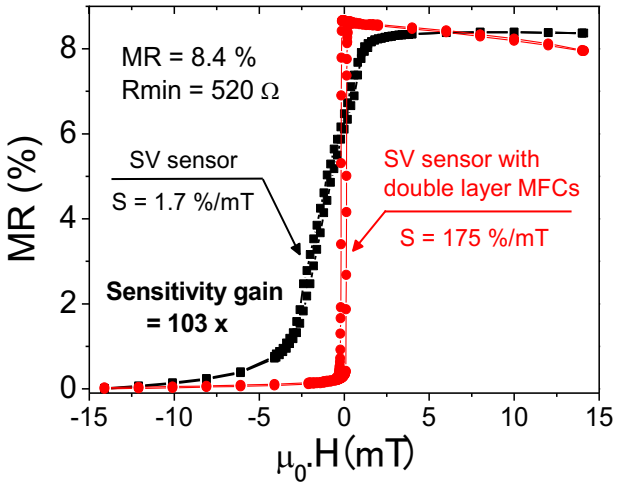

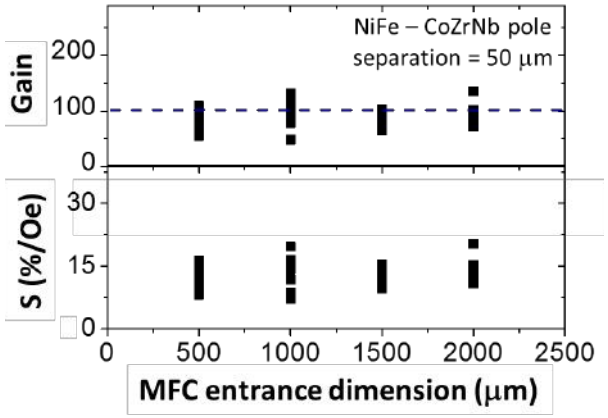

Sensitivity gains ~ 100 x

(~ one order of magnitude higher than with single layer MFCs)

High yield in the fabrication process

INESC MN
Microsistemas & Nanotecnologias

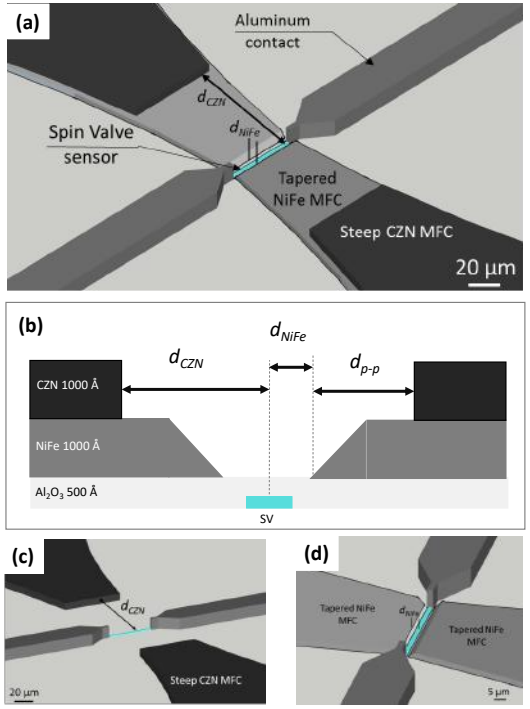

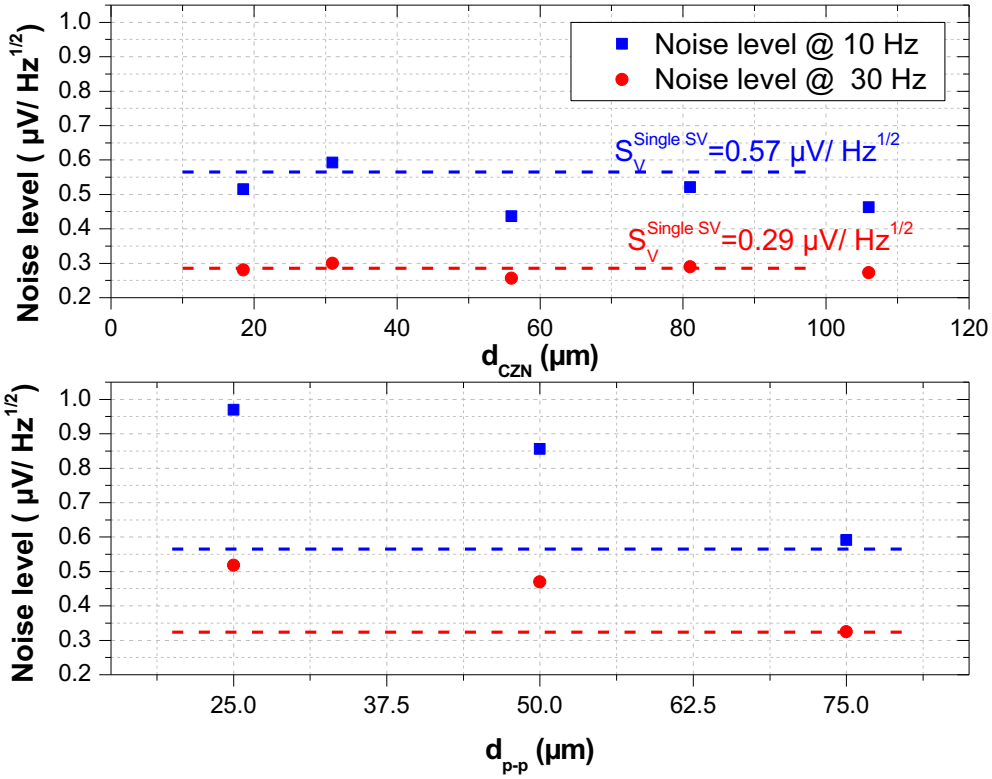

M. Silva, et.al
IEEE Trans Magn. (2019)
; DOI: 10.1109/TMAG.2019.2899808

detectivities of 322 pT/Hz$^{1/2}$ (for d_{p-p} = 100 µm) were obtained at 10 Hz

INESC MN
Microsistemas & Nanotecnologias

Strategies to improve the minimum detectable field

Field modulation for high frequency

Increase TMR

Increase A

Reduce linear range ΔH

Reduce Hooge value

J.P. Valadeiro, *et al.,* IEEE Trans. Magn. **51**, 1 (2015)
D.C. Leitao, *et al.*, IEEE Trans. Magn. **50**, 1 (2014)
J.Y. Chen, *et al.*, Appl. Phys. Lett. **100**, 142407 (2012)
S.H. Liao, *et al.*, IEEE Trans. Magn. **29**, 3873 (1993)
S. Cardoso, *et al.*, Microsys. Technol. **20**, 793 (2014)
R.J. Janeiro, *et al.*, IEEE Trans. Magn. **48**, 4111 (2012)
R.C. Chaves, *et al.*, Appl. Phys. Lett. **91**, 102504 (2007)
E. Paz, *et al.*, J. Appl. Phys. **115**, 17E501 (2014)
L. Jiang, *et al.*, Phys. Rev. B **69**, 054407 (2004)
E.R. Nowak, *et al.*, Thin Solid Films **377–378**, 699 (2000)
Y. Aoki, *et al.*, J. Magn. Magn. Mater. **240**, 134 (2002)
J. Schmalhorst, G. Reiss, Phys. Rev. B **68**, 224437 (2003)
Y.M. Lee, J. Hayakawa, S. Ikeda, F. Matsukura, H. Ohno, Appl. Phys. Lett. **90**, 212507 (2007)
W. Zhang, Q. Hao, G. Xiao, Phys. Rev. B **84**, 094446 (2011)
D.W. Guo, *et al.*, J. Appl. Phys. **115**, 17E513 (2014)

Noise performance (1/f region)
Hooge parameter

$$S^{1/f} = \sqrt{\frac{\alpha_H . V^2}{f . A . N}}$$

INESC MN
Microsistemas & Nanotecnologias

MgO vs AlOx barriers

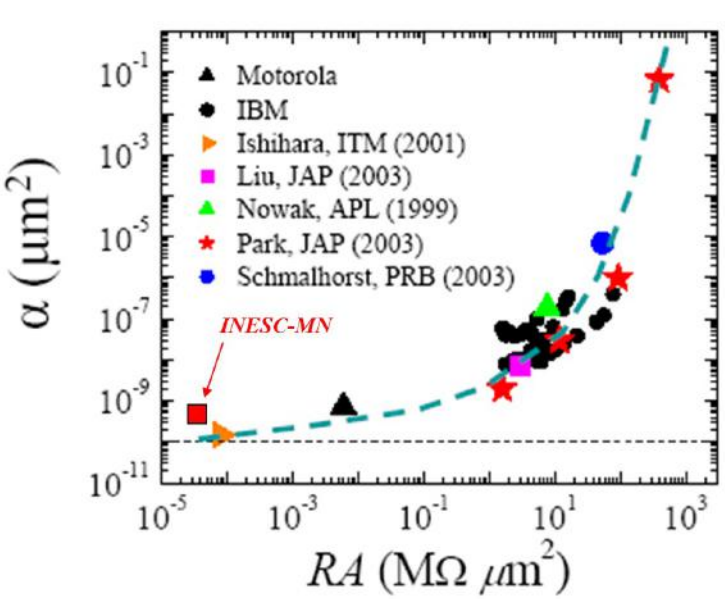

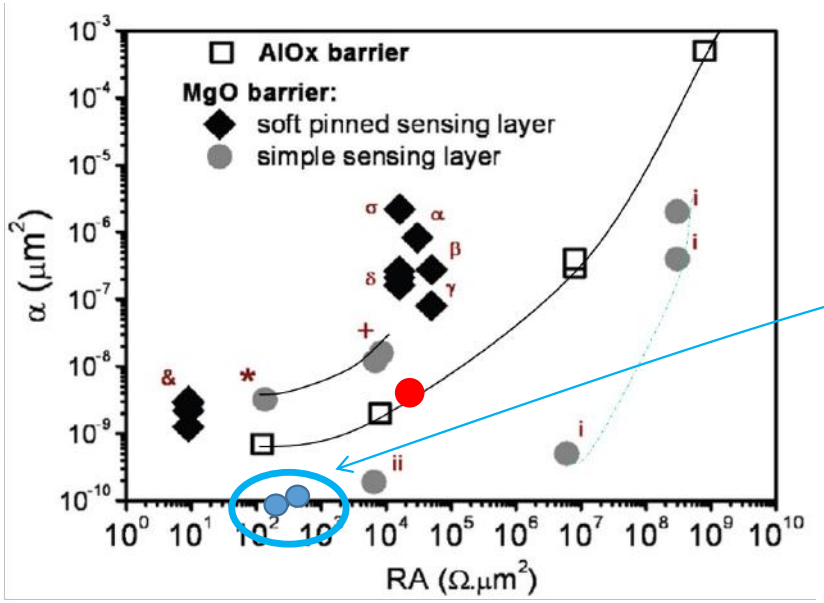

A.Silva, S.Cardoso, et.al.
Eur. Phys. J. Appl. Phys. (2015)
DOI: 10.1051/epjap/2015150214

Amorphous CoFeBSi, CoFeBTa

AIP-Advances, 13, 025108 (2023);

AlOx-MTJ data obtained with devices at saturation from references [119–122]. CoFeB/MgO/CoFeB-MTJ data obtained at operation point.

Data marked with **i** from references [119,123,124] and **ii** is unpublished data from INESCMN; * from reference [90]; + from reference [85]; & from reference [42]; ***α*** from reference [118]; ***β*** from reference [125]; ***δ*** is unpublished data from INESC-MN; ***σ*** from reference [41];***γ*** from reference [83].

Neuronal probes with MR sensors

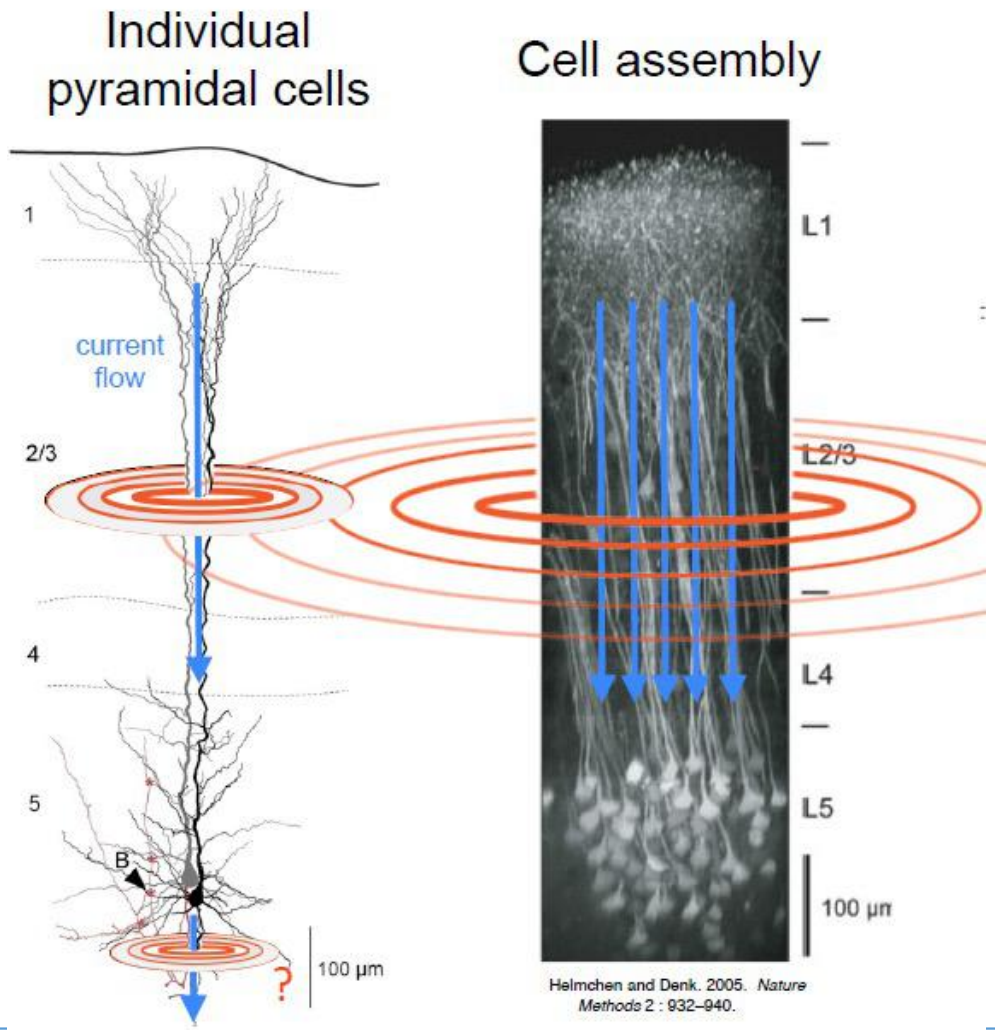

Estimation of the magnetic field:

- **MagnetoEncephaloGraphy :**
  SQUID - signal distance = 3 cm
  Field = 1 fT (Field decay : $1/(r^2)$
- **Magnetrodes:**
  MR - signal distance = 10-100 µm
  Field ≈ 100 pT – 1nT

Estimated fields ~pT - nT

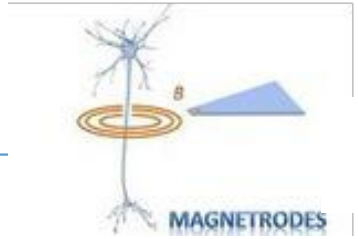

FET-EU project
Magnetrodes

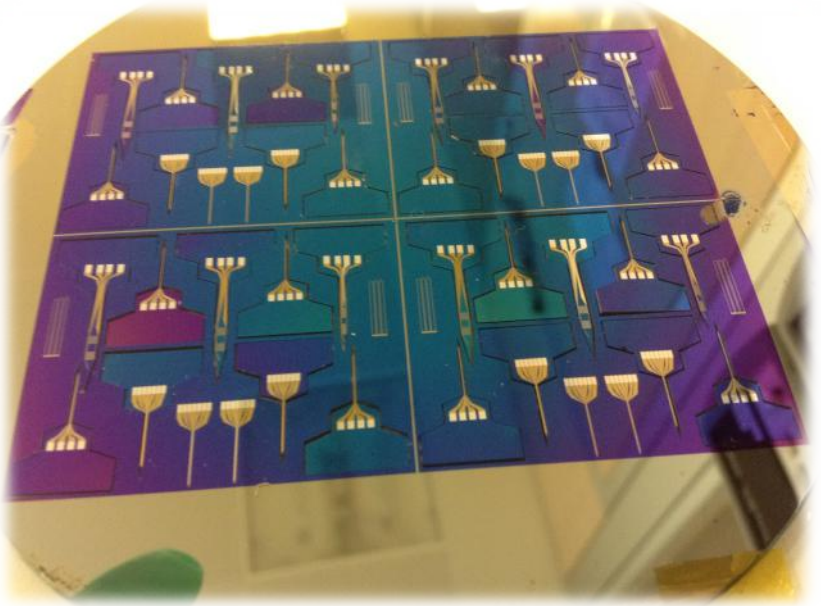

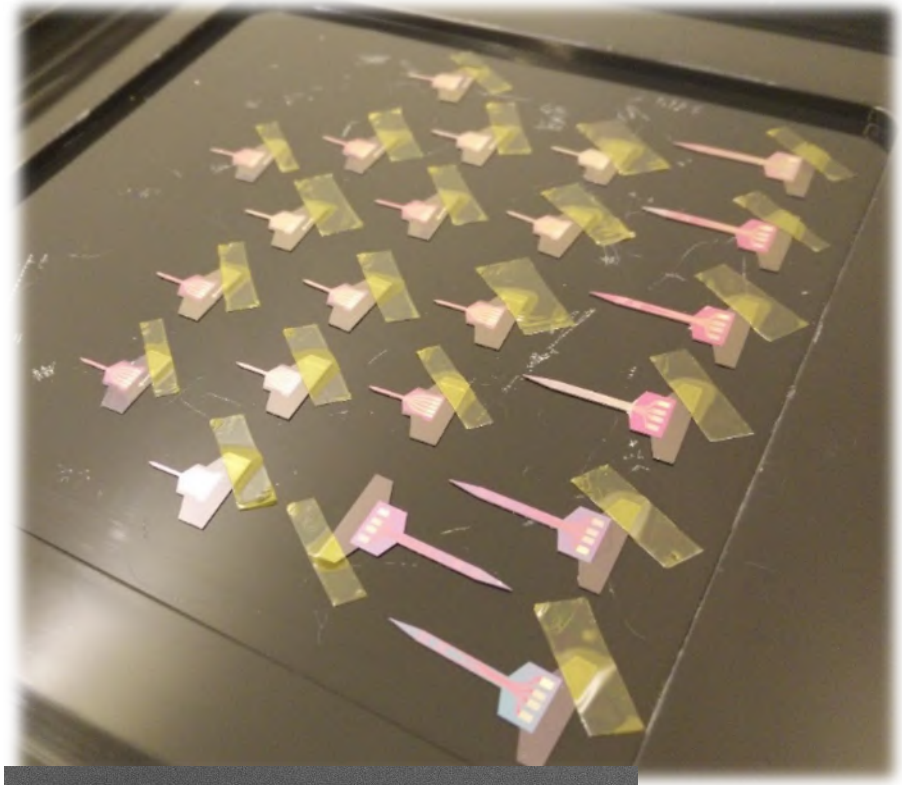

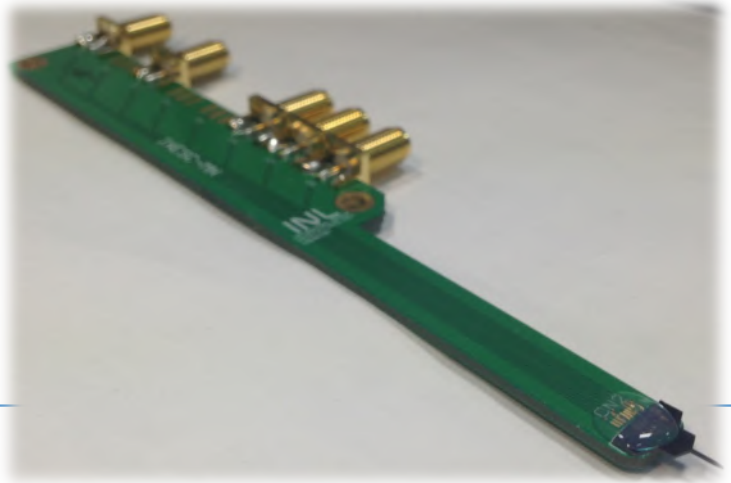

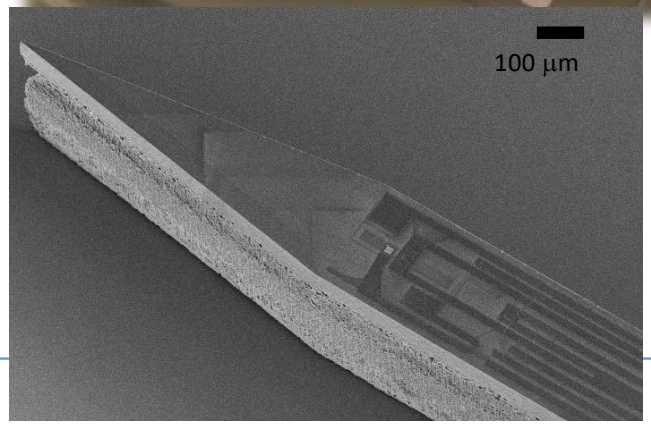

INESC MN
Microsistemas &
Nanotecnologias

INL
INTERNATIONAL IBERIAN
NANOTECHNOLOGY
LABORATORY

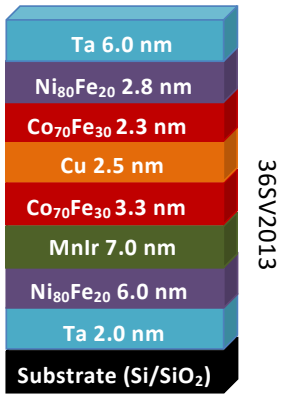

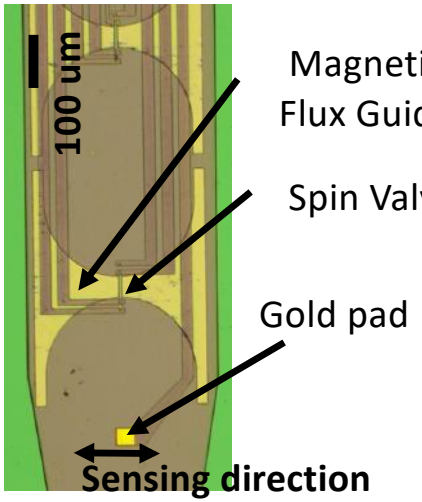

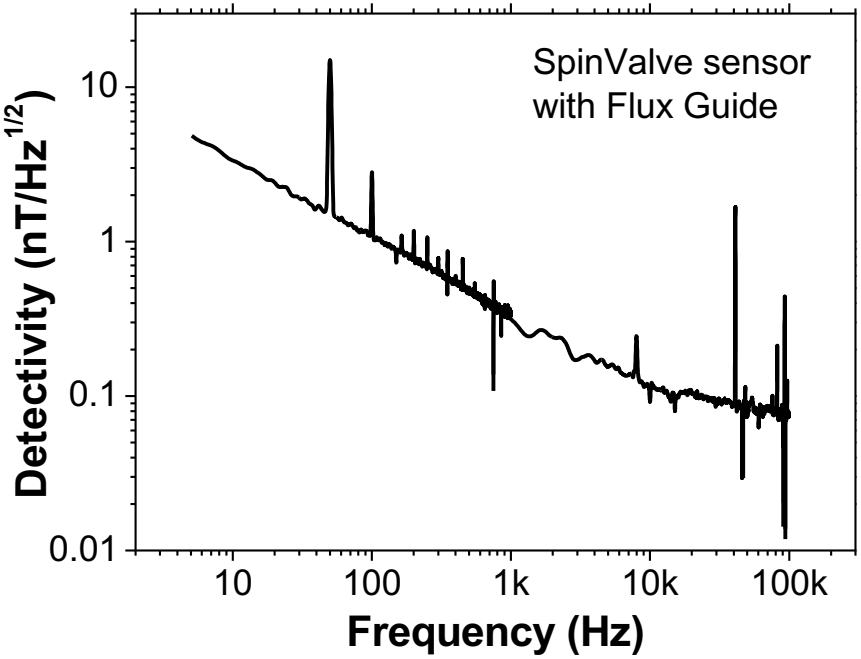

Detectivity values:

3.3 nT/Hz$^{1/2}$ @ 10 Hz
1.9 nT/Hz$^{1/2}$ @ 30 Hz
310 pT/Hz$^{1/2}$ @ 1 kHz

INESC MN
Microsistemas & Nanotecnologias

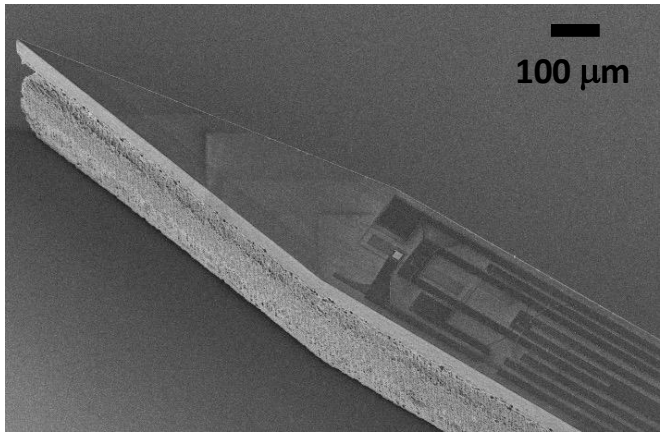

SEM image: sharp tip (*in-vivo*)

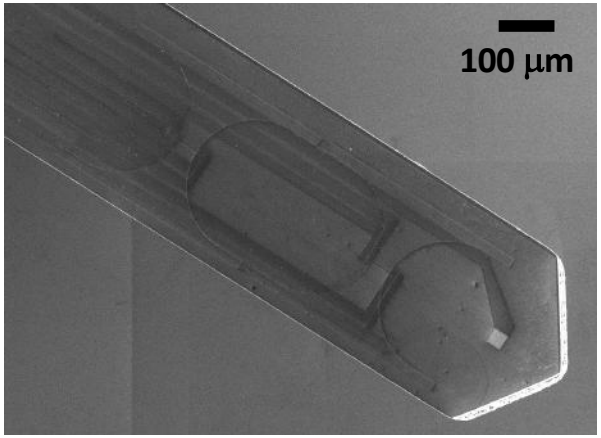

SEM image: flat tip (*in-vitro*)

When penetrating the tissues:

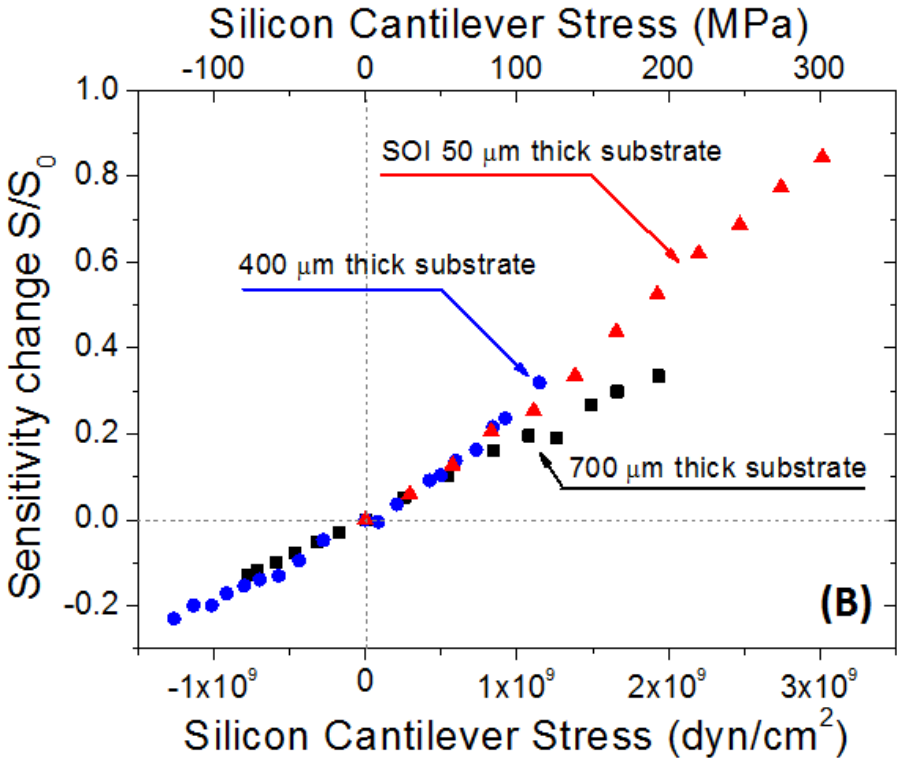

- axial force along the tip longitudinal direction;
- slight bending of the probe, **force perpendicular to the longest direction.**

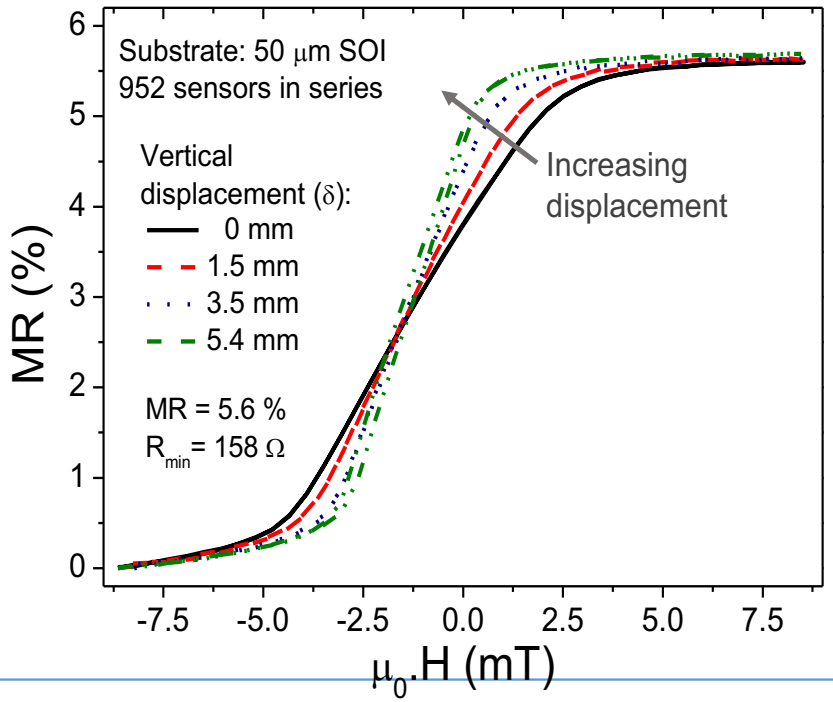

Sensor output: remains linear, non-hysteretic and without discontinuities

Valadeiro et al IEEE Trans Mag 51 (2015) 4401104

In Vivo validation of MR sensor probes

INESC MN
Microsistemas & Nanotecnologias

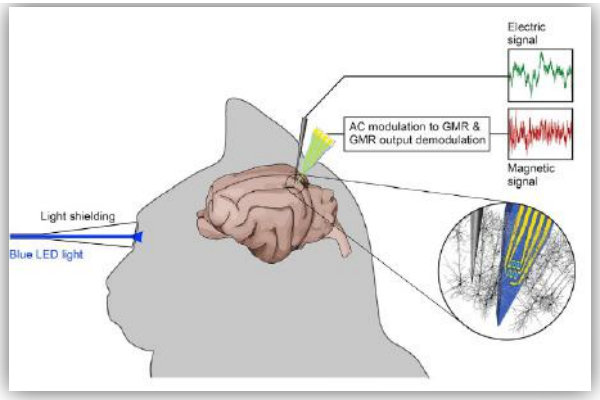

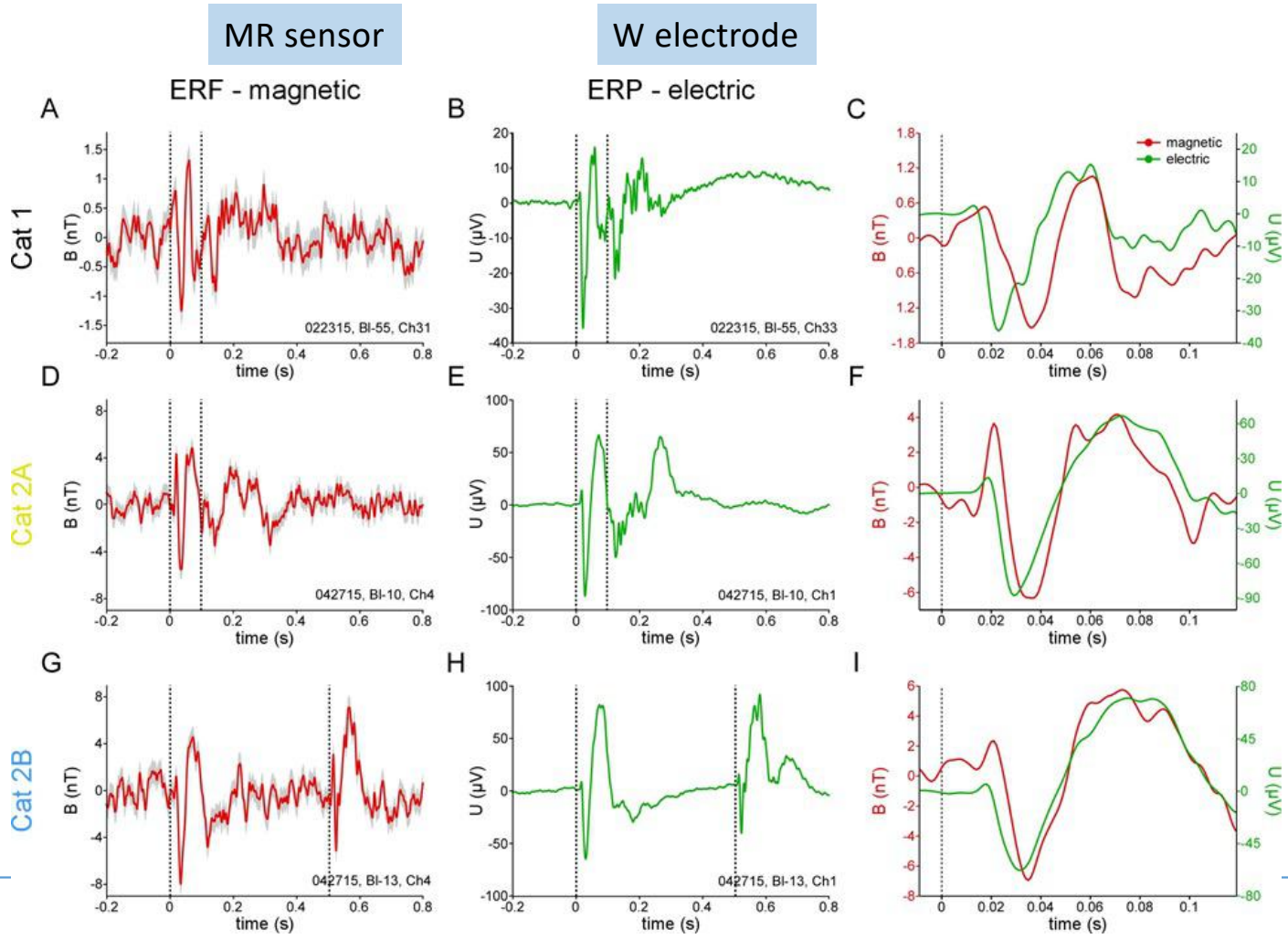

L.Caruso, S.Cardoso, P.P Freitas, P.Fries, M. Lecoeur, et.al
"In vivo magnetic recording of neuronal activity",
***Neuron,** 95, 1–9 (2017)*

Detectivity (D) - **minimum detectable field**

SNR =1

INESC MN
Microsistemas & Nanotecnologias

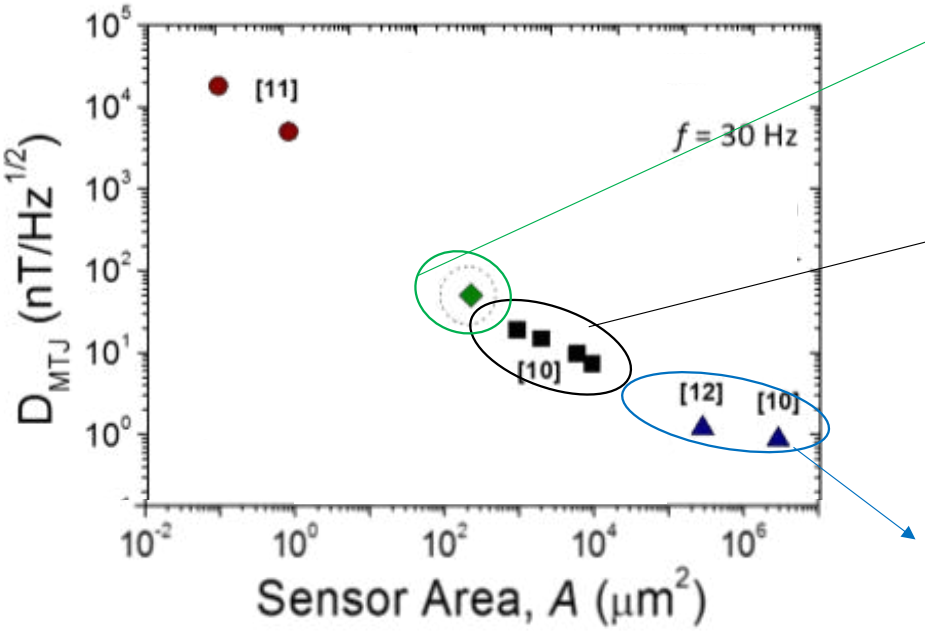

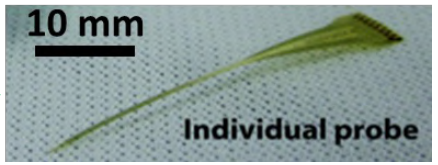

flexible probe - polyimide

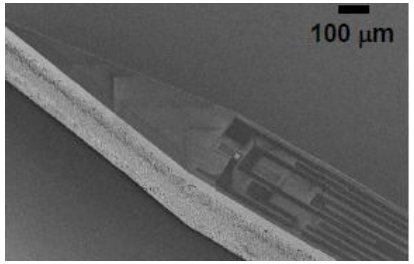

Si probe (single MR)

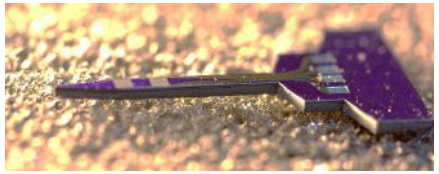

Si probe (arrays MR)

IEEE Trans Magn. vol. 51 (11) 4401104 (2015)
J.Gaspar et.al, IEEE Trans Magn. Vol.53 (4), 5300204 (2017

Applications

If no time:
move to

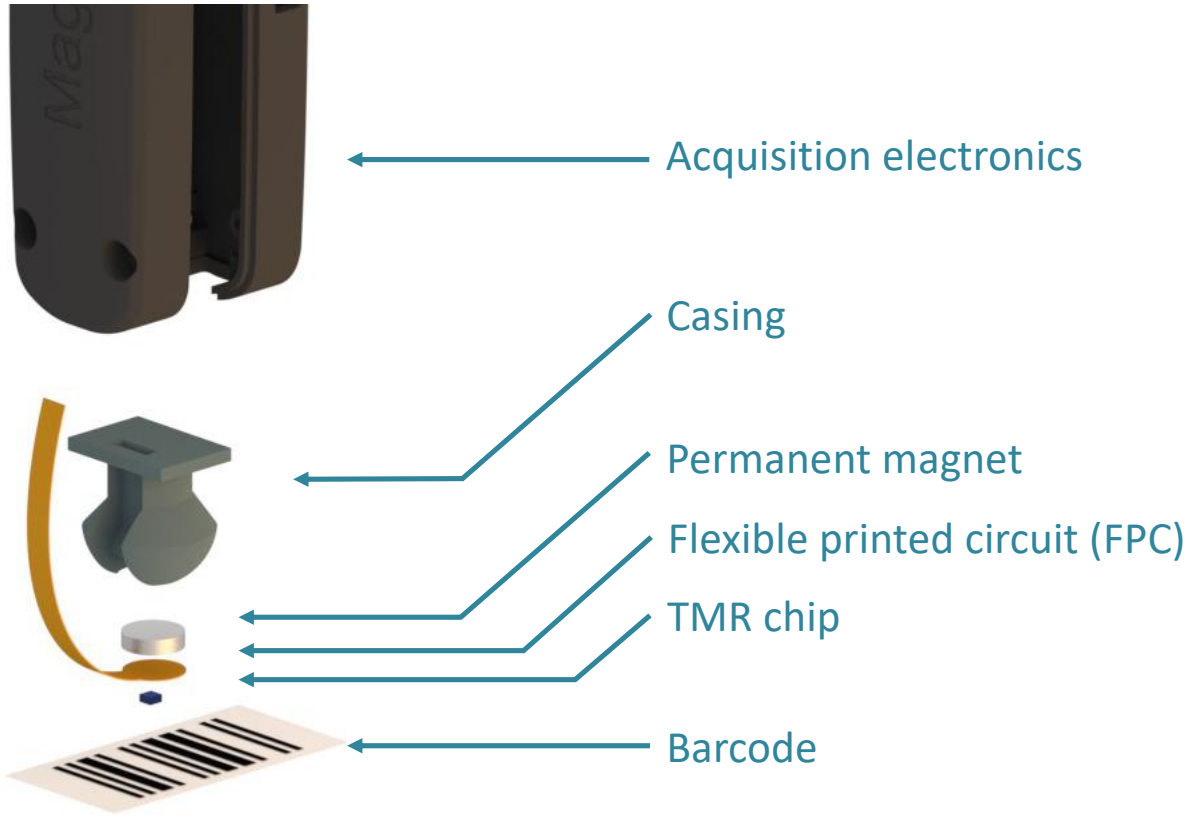
Acquisition electronics
Casing
Permanent magnet
Flexible printed circuit (FPC)
TMR chip
Barcode

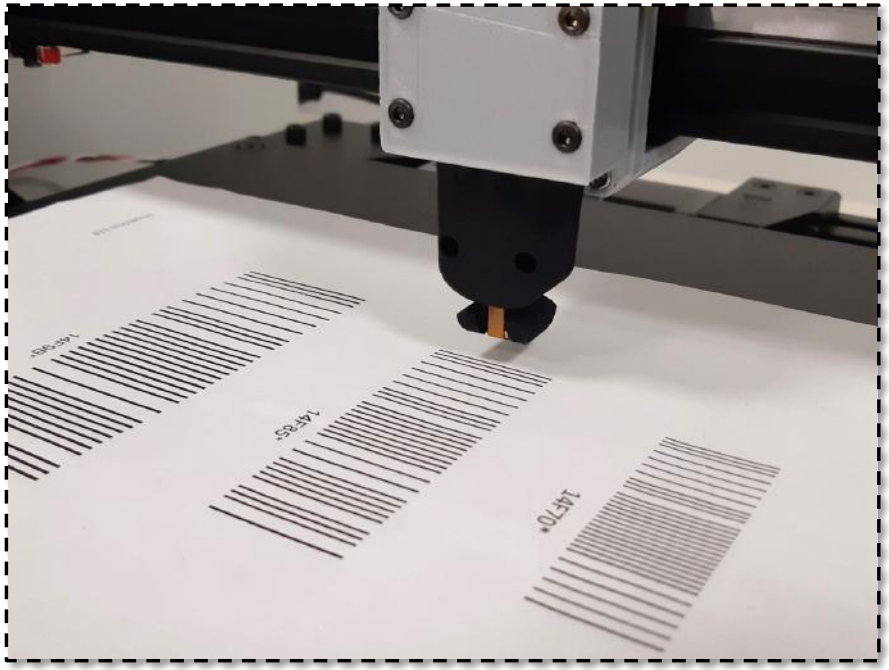

Alignment

Disc magnet provides a limited region where B < 1 mT (±170 µm) → **requires good accuracy from the alignment procedure**

No magnet

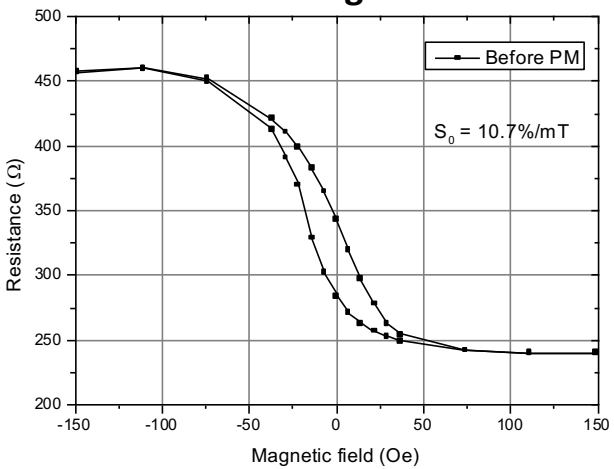

Poor alignment

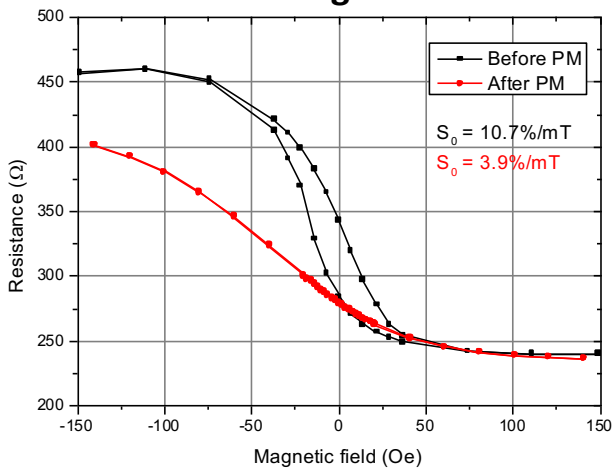

Good alignment

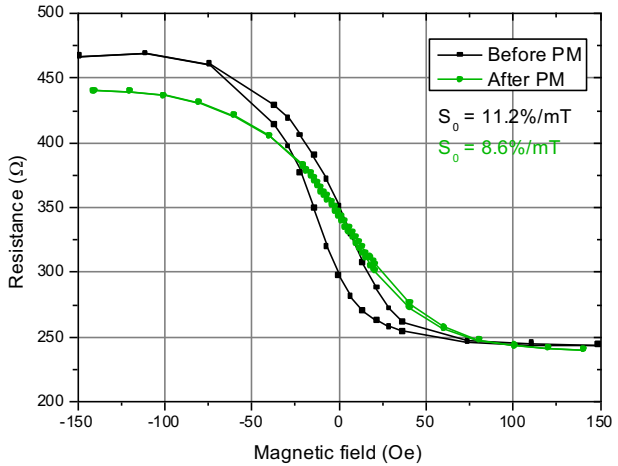

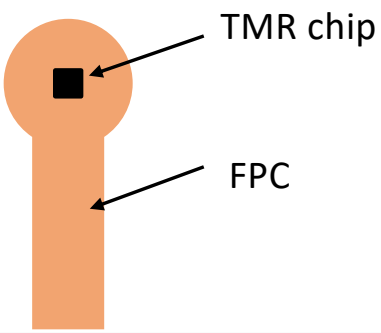

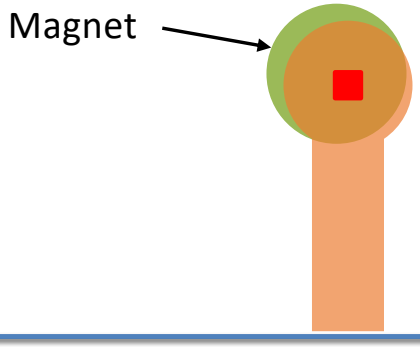

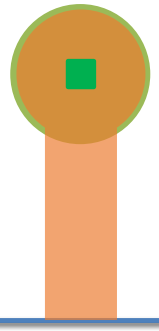

S.Abrunhosa. S.Cardoso, et.al
IEEE Trans. Magn. 58 (8), 4002304 (2022)

Swipe reader: assembly

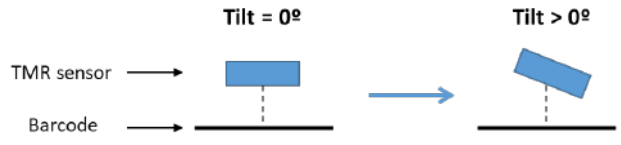

Purpose:

- Hold reader components
- Protect sensor chip
- Limit sensor tilt
- Minimise sensor-barcode distance

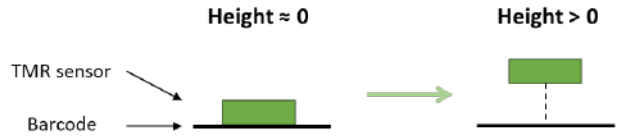

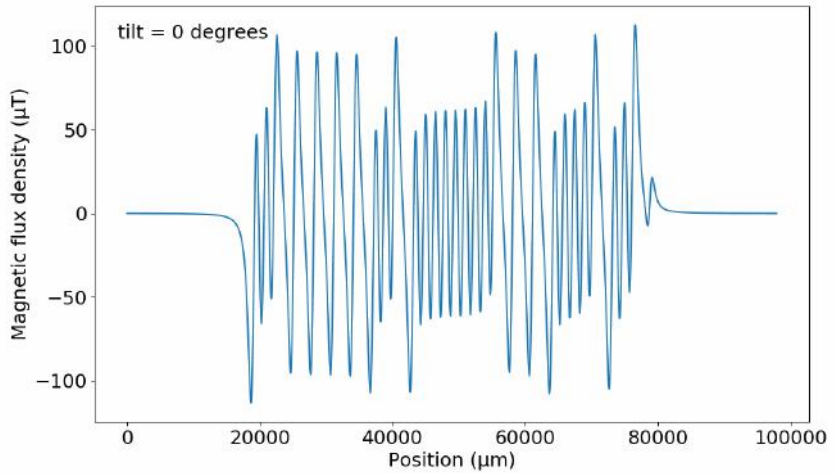

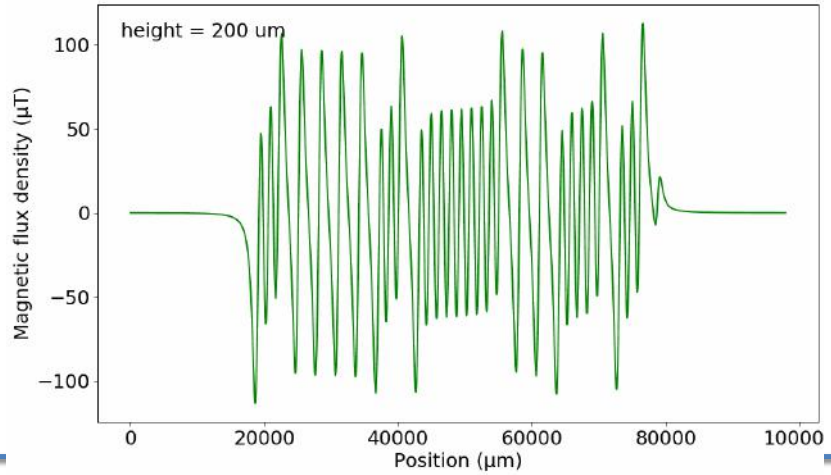

S.Abrunhosa. S.Cardoso, et.al
IEEE Trans. Magn. 58 (8), 4002304 (2022)

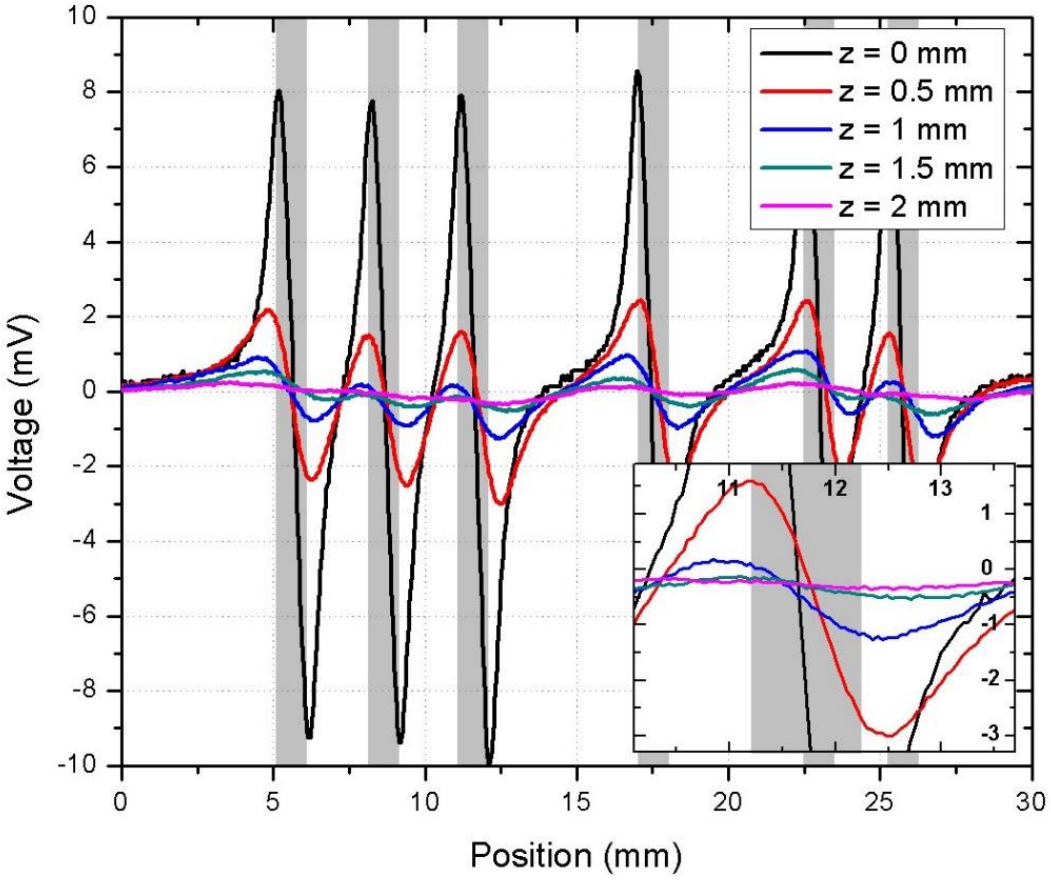

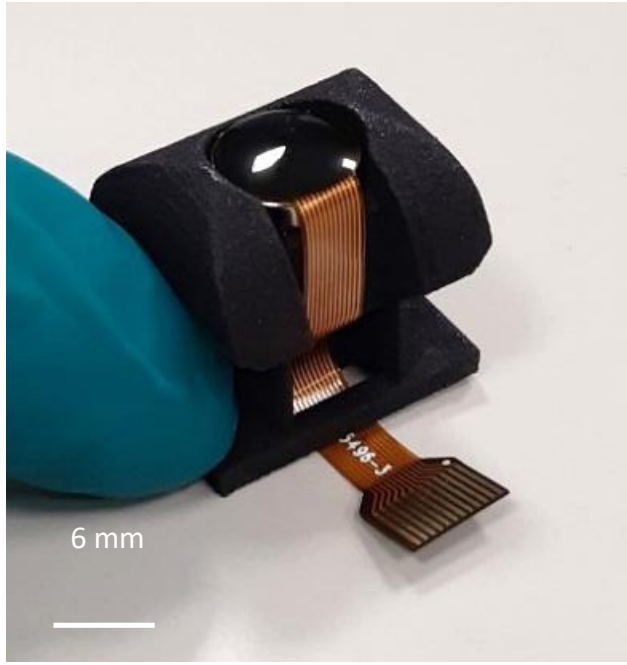

Hiden codes detectable
through 2 mm of material

S.Abrunhosa. S.Cardoso, et.al
IEEE Trans. Magn. 58 (8), 4002304 (2022)

Applications

If no time:
move to

Industrial Robotics

Measurement range:
Several kN to 10 N

Main goals:

- Improve safety around robots
- Allow human-machine interaction

Humanoid Robotics

Measurement range:
10 N to 100 µN

Main goals:

- Improve object manipulation capacities
- Facilitate human-machine interaction

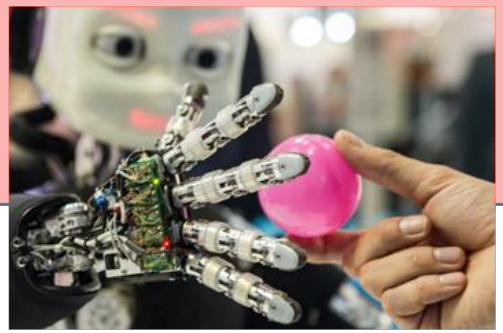

Surgical Robotics

Measurement range:
100 µN to 10 nN

Main goals:

- Improve object manipulation
- Reduce operation related damage

If no time: move to

The Vizzy hand

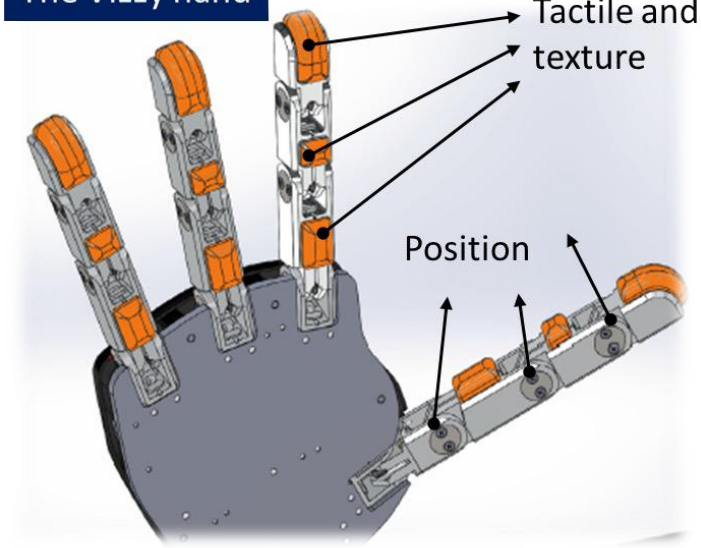

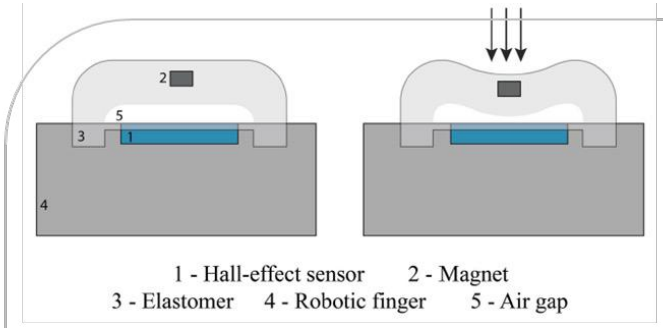

3D Hall effect pressure sensors

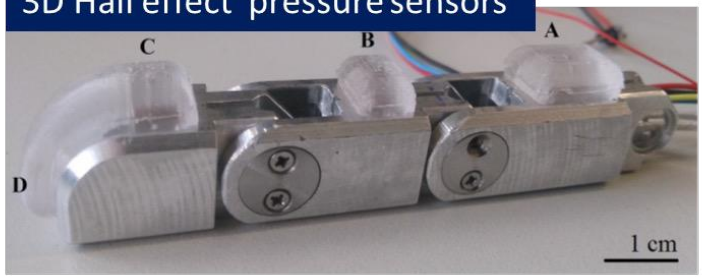

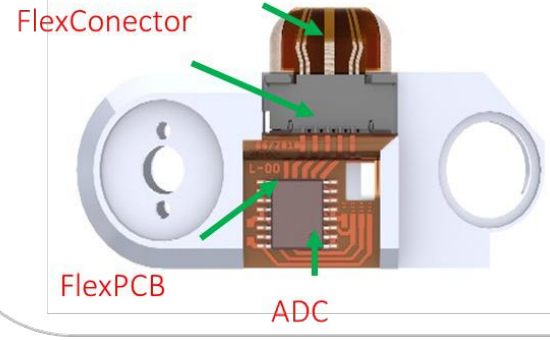

Flexible 2D GMR pressure sensors

Distributed GMR/TMR sensors

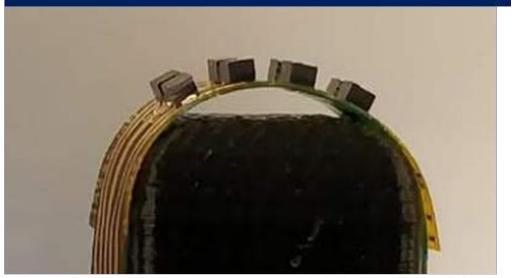

2D MR sensors mounted by flip-chip

Cilia + 2D GMR tactile and pressure sensors

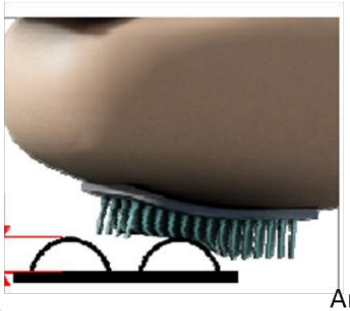

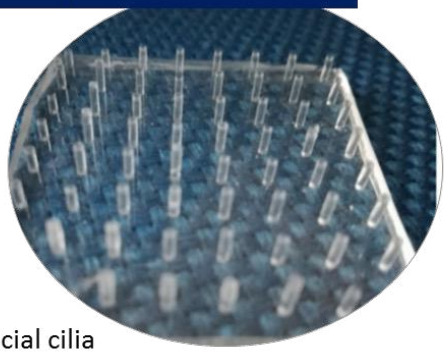

Artificial cilia

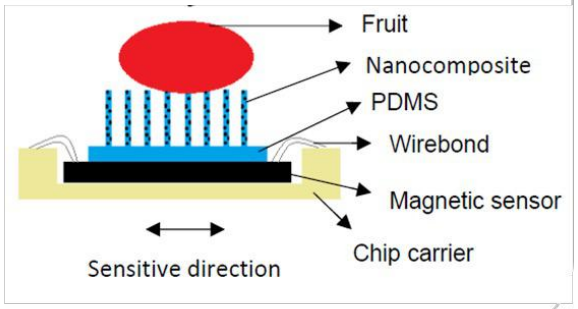

TACTILE INSPIRED IN NATURE

Magnetic cilia bending **induces** magnetic profile variation

MR sensor transduces variation into an electrical signal

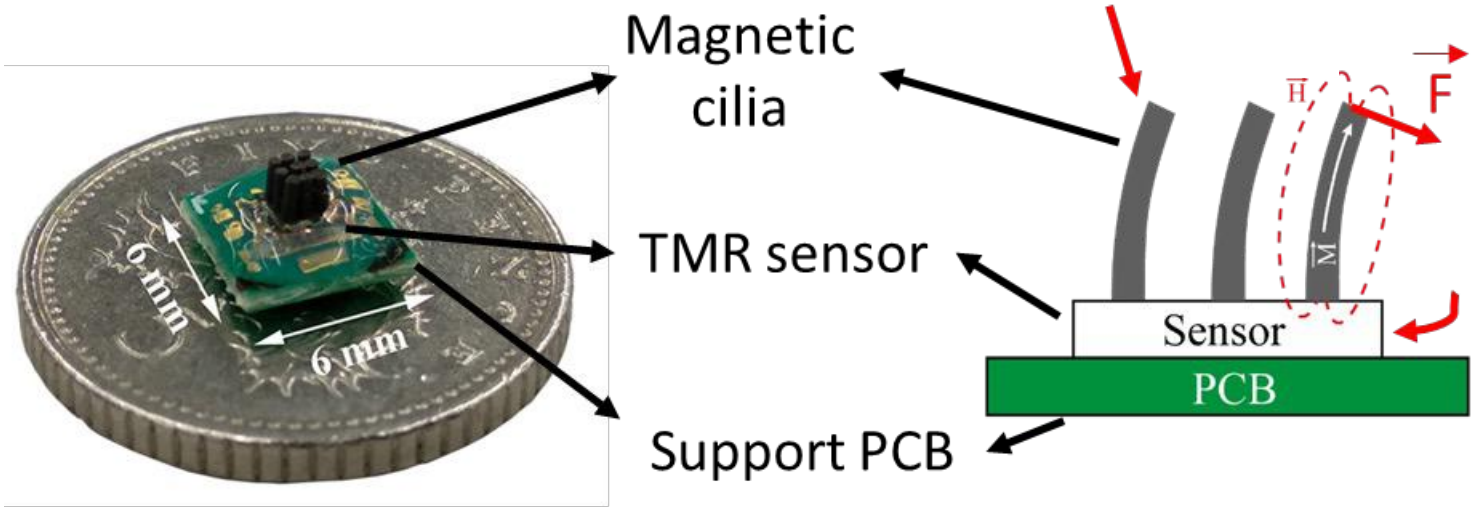

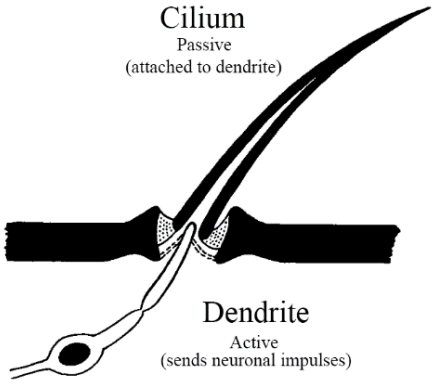

A. Alfadhel and J. Kosel, Advanced Materials, 27, 7888–7892, 2015.
P. Ribeiro, et.al. IEEE Robotics and Automation Letters, 2, 971–976, 2017.

2D WHEATSTONE BRIDGE – NO ANNEALING

INESC MN
Microsistemas & Nanotecnologias

2D monolithic TMR sensor
In Wheatstone bridge

Die dimensions: 3x3 mm^2

80 MTJs per bridge branch
R_{eq}: 384 kΩ

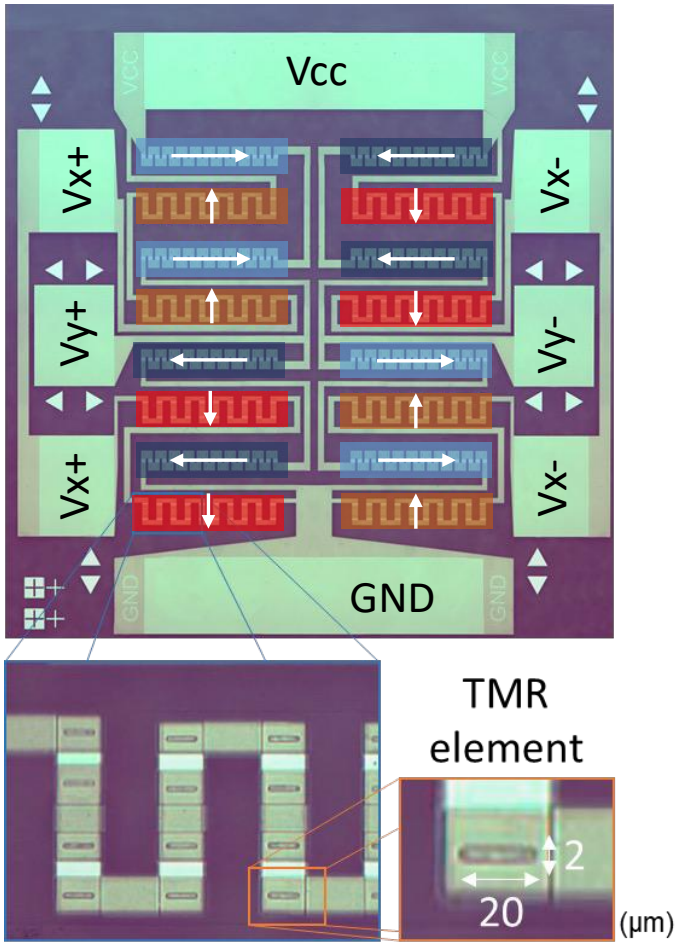

X bridge

2 TMR stack depositions

Y bridge

2 TMR stack depositions

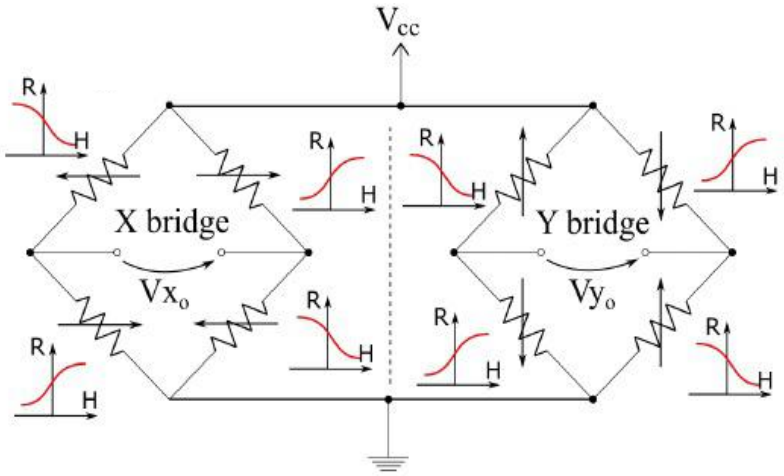

No wafer annealing needed!

J. Phys. D: Appl. Phys. 50 (16), 165001 (2017)

J.Mag.Magn.Mat. 412, 181–184 (2016)

2D WHEATSTONE BRIDGE

INESC MN
Microsistemas & Nanotecnologias

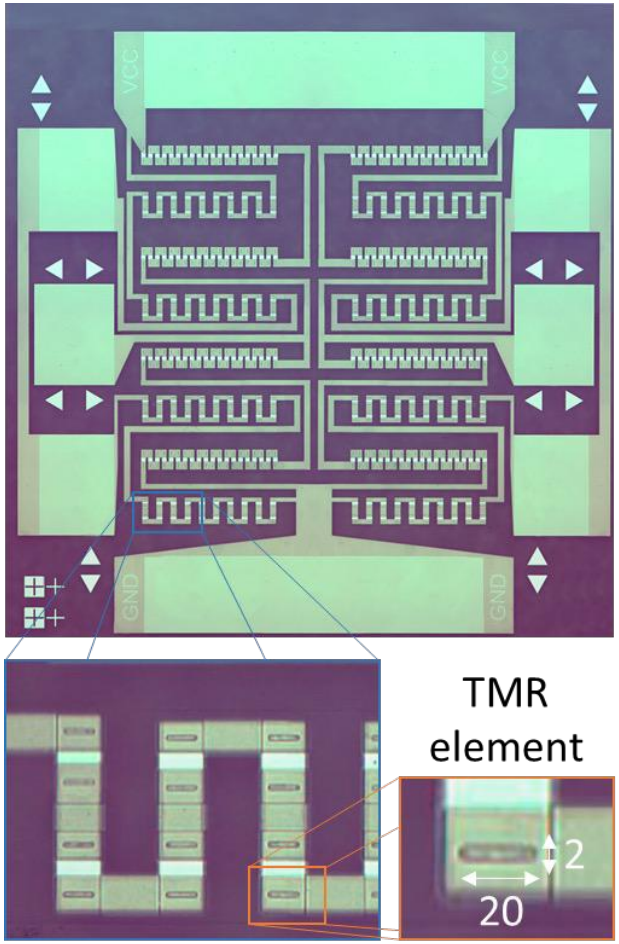

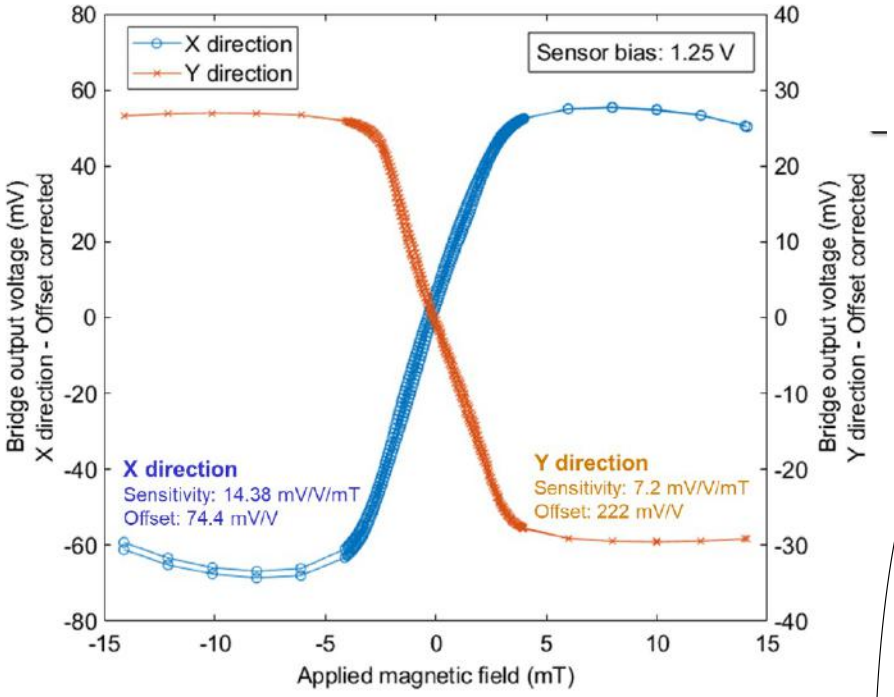

Sensitive direction	Sensitivity (mV/V/mT)		Offset voltage (mV/V)	
	Minimum	Maximum	Minimum	Maximum
X	7.7	16.1	74	416
Y	6.9	9.8	218	728

"Perfect" X sensor
"Perfect" Y sensor
are needed…

Offset issues

External electronics to compensate for this offset

CILIA SIMULATION – 3 LEVELS

Institute for Systems and Robotics Lisboa | CRISP | Advanced Robotics @ Queen Mary ARQ | INESC MN Microsistemas & Nanotecnologias

Mechanical simulation (FEM – with COMSOL)

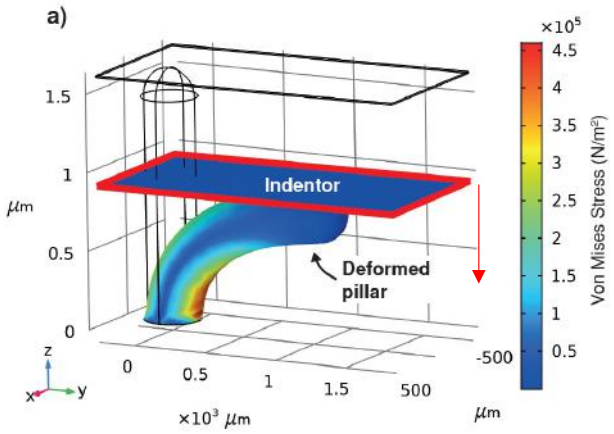

Simulation: indentor iteratively lowered against cilia
Steps of 100 µm
Discretized into cross-sections

Deformation

Magnetic moment simulation

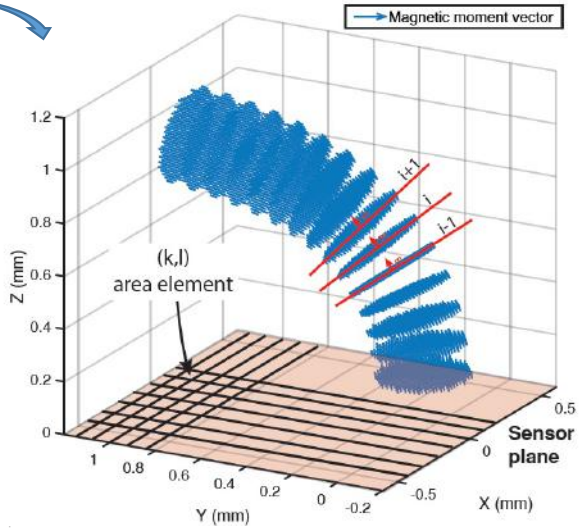

$$\mathbf{v_{i-1}} = \overrightarrow{i-1, i};\ \mathbf{v_{i+1}} = \overrightarrow{i, i+1}$$

$$\mathbf{v_i} = \frac{\mathbf{v_{i+1}} + \mathbf{v_{i-1}}}{2}.$$

Estimation of **m** direction

$$\mathbf{H_j}(r_{j,(k,l)}) = \frac{1}{4\pi}\left(\frac{3\mathbf{r_{j,(k,l)}}(\mathbf{m_j}\cdot\mathbf{r_{j,(k,l)}})}{|\mathbf{r_{j,(k,l)}}|^5} - \frac{\mathbf{m_j}}{|\mathbf{r_{j,(k,l)}}|^3}\right)$$

H (x direction) over surface

Magnetic field

Magnetic moment simulation

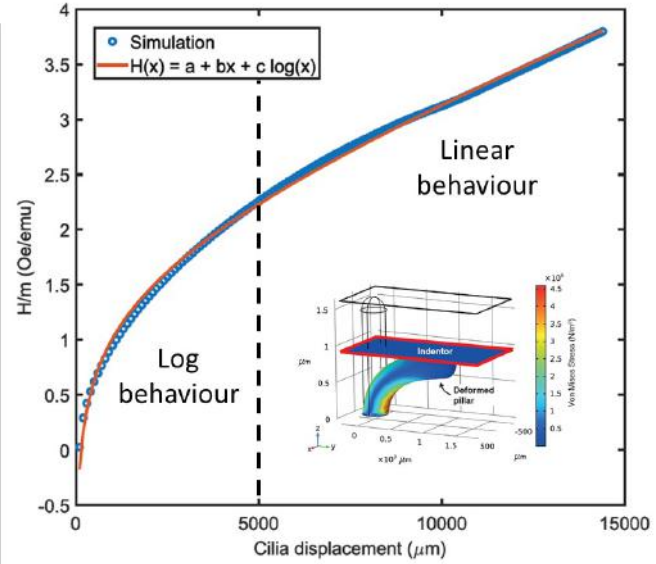

$$\langle \mathbf{H_{inc}} \rangle = \frac{\sum_{k=1}^{N_k}\sum_{l=1}^{N_l}\sum_{j=1}^{N}\mathbf{H_j}(r_{j,(k,l)})}{N_k N_l}$$

Average field over sensor area

$$\langle H \rangle(x) = ax + b\log(x) + c$$

Best fitting function describing field

RESULTS – FRUIT SURFACE ASSESSMENT

INESC MN
Microsistemas & Nanotecnologias

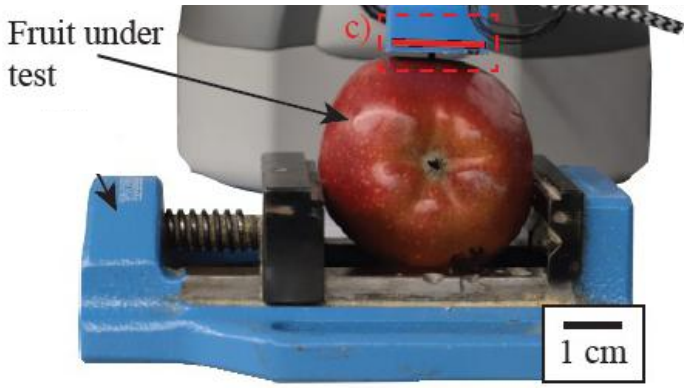

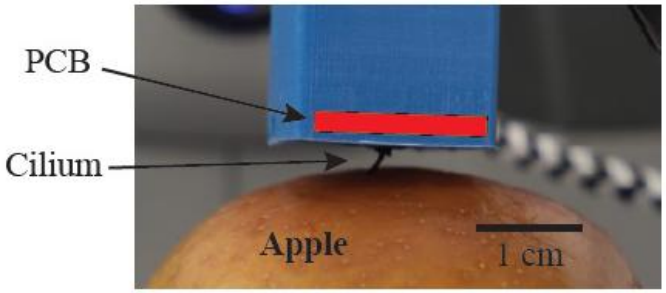

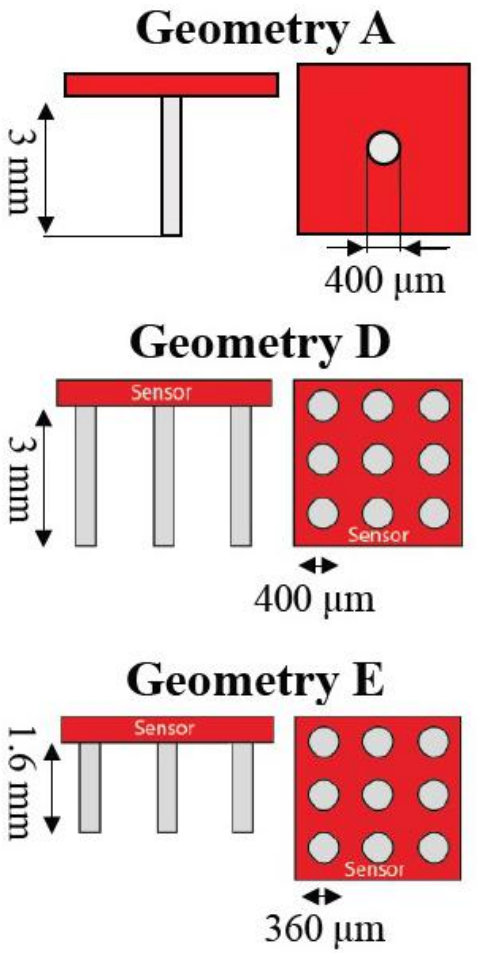

Proof of concept
Fruit quality classifier

Braeburn apples
- 12 ripe fruits
- 12 senescent fruits

Sabrina strawberries
- 12 ripe fruits
- 12 senescent fruits

Data acquisition
- Data rate: 1 kSPS
- Scan speed: 1 mm/s
- 10 consecutive scans in each area
- 2 areas per fruit

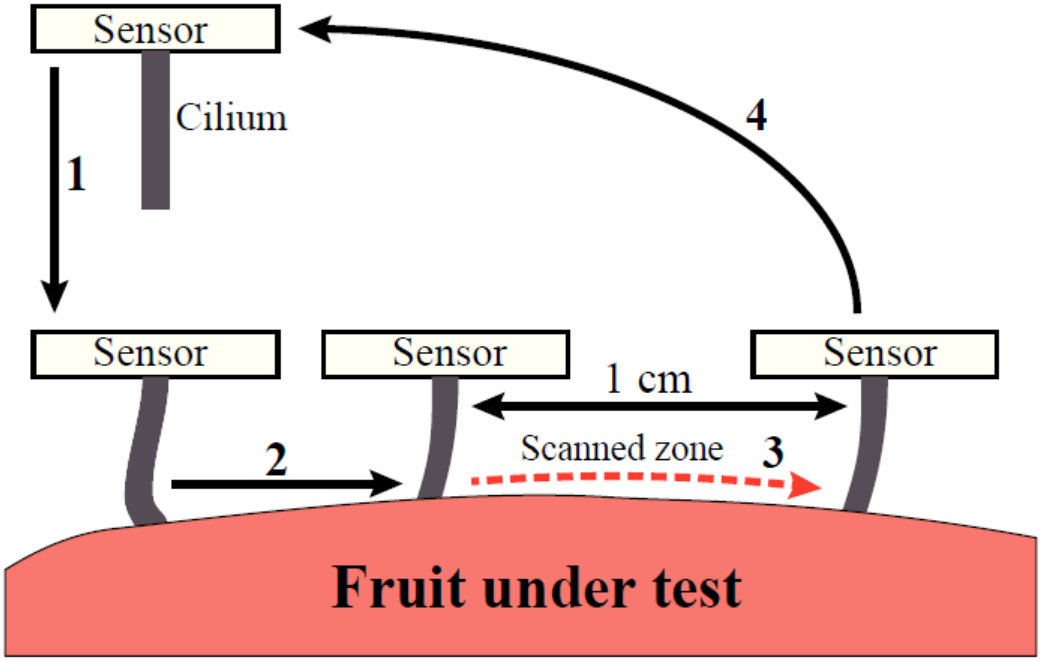

FRUIT QUALITY SENSING - RESULTS

Raw signal upon scanning

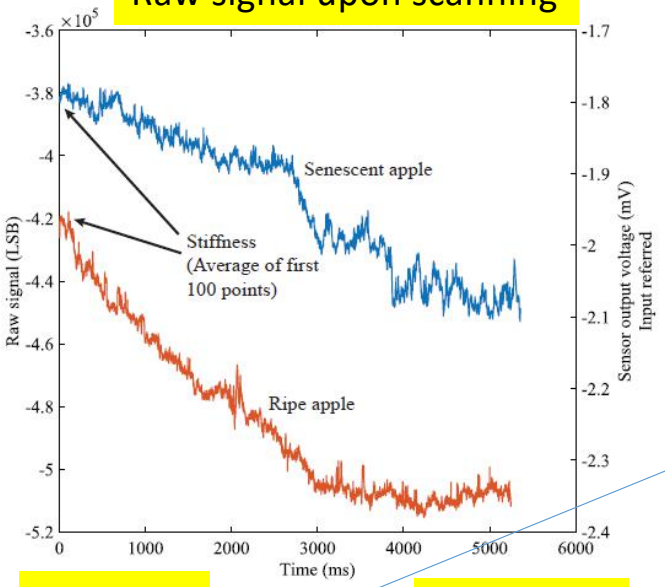

Waviness

Roughness

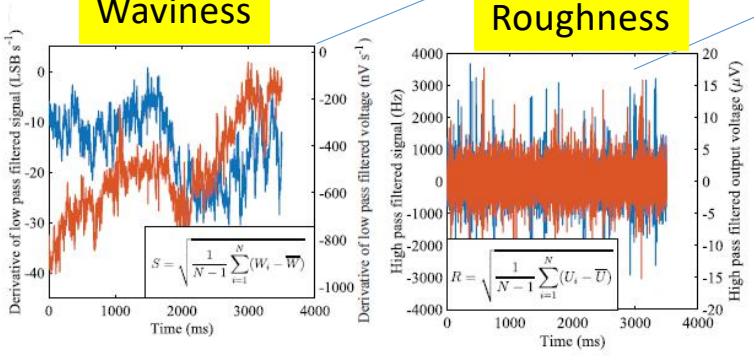

3 features were extracted from the signal

FEATURE	WHAT IS MEASURED	PHYSICAL CHARACTERISTIC
Stiffness (E)	Sensor signal with achieved contact	Fruit hardness
Waviness (S)	Std. deviation of 100 point moving average	Deformation over fruit surface
Roughness (R)	Std. deviation of high-pass filtered (f > 150 Hz) signal	Fruit surface texture

Fruit can be classified into two classes

- **Ripe**
- **Senescent**

FRUIT QUALITY SENSING - RESULTS

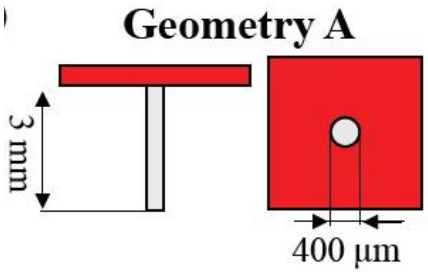

Stiffness (E) → **Fruit hardness**

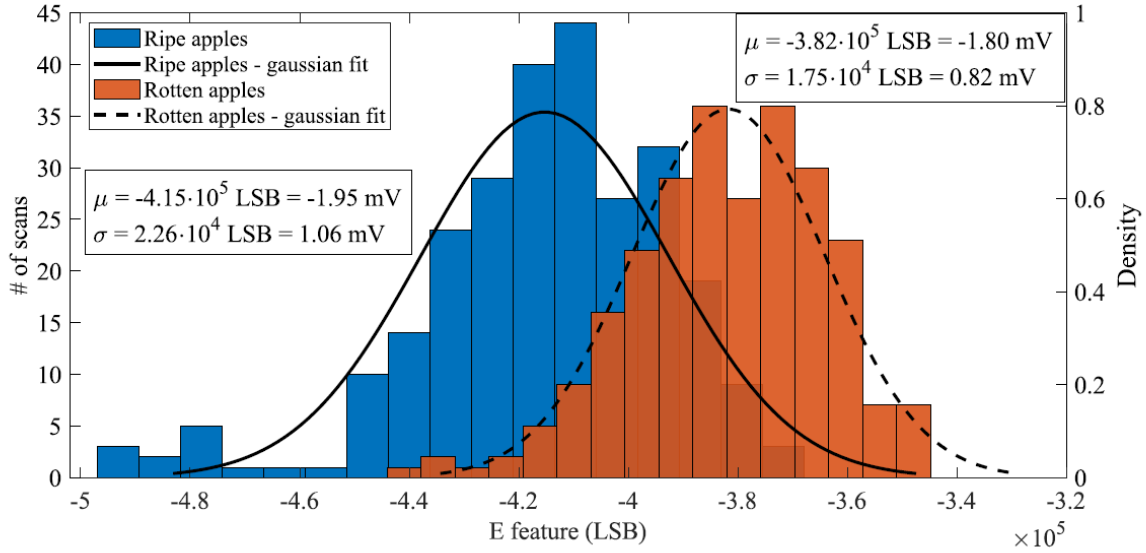

Figure 6.4: Computed E parameter histogram from all scans of apples scanned using a geometry A ciliary sensor.

Gaussian classifier
(i.e. Gaussian Näive Bayes)

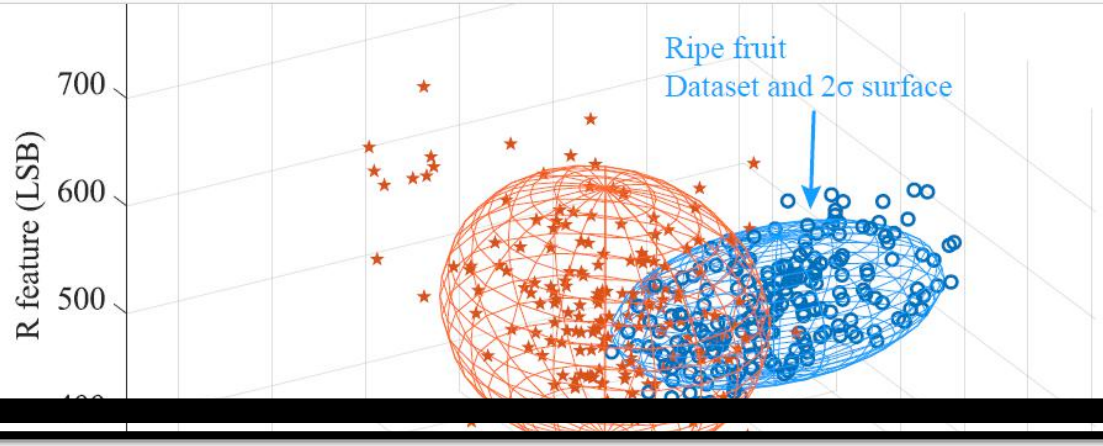

Combining R, S, E

Sensor	Fruit	1 feature (E)	2 features ($E+R$)	3 features ($S+E+R$)
B	Apple	0.83	0.92	0.96
	Strawberry	0.63	0.79	0.71
D	Apple	0.71	0.88	0.88
	Strawberry	0.67	0.67	0.71
E	Apple	0.58	0.71	0.71
	Strawberry	0.63	0.83	0.83

Table 6.3: Accuracy vs number of features used for classification with Gaussian Näive Bayes algorithm.

FRUIT QUALITY SENSING - RESULTS

Apple

Strawberry

Conf. A

h = 3 mm
ϕ = 400 µm

	True positive	True negative	Accuracy
Naïve Bayes	11/12	12/12	0.96
Random Forest	10/12	12/12	0.92

	True positive	True negative	Accuracy
Naïve Bayes	7/12	10/12	0.71
Random Forest	8/12	11/12	0.79

Conf. B

h = 1.6 mm
ϕ = 320 µm

	True positive	True negative	Accuracy
Naïve Bayes	10/12	11/12	0.88
Random Forest	10/12	11/12	0.88

	True positive	True negative	Accuracy
Naïve Bayes	10/12	7/12	0.71
Random Forest	10/12	10/12	0.83

Conf. C

h = 3 mm
ϕ = 400 µm

	True positive	True negative	Accuracy
Naïve Bayes	9/12	8/12	0.71
Random Forest	9/12	11/12	0.83

	True positive	True negative	Accuracy
Naïve Bayes	10/12	10/12	0.83
Random Forest	10/12	10/12	0.83

INESC MN
Microsistemas & Nanotecnologias

“From farm to fork”

Final food inspection

Integrated Food control & management system

If no time: move to

Magnetic Biosensors

Magnetic Biosensors and biomedical interfaces

INESC MN

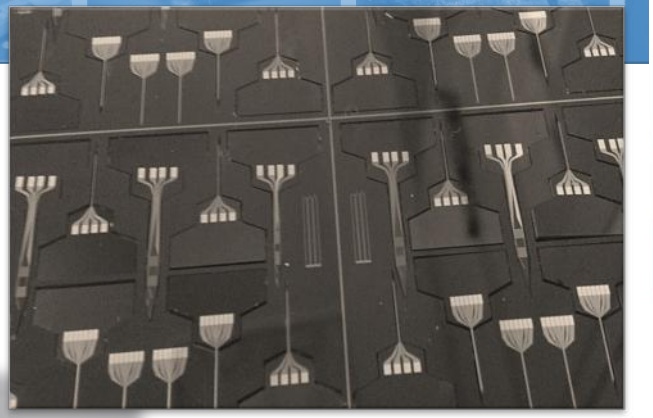

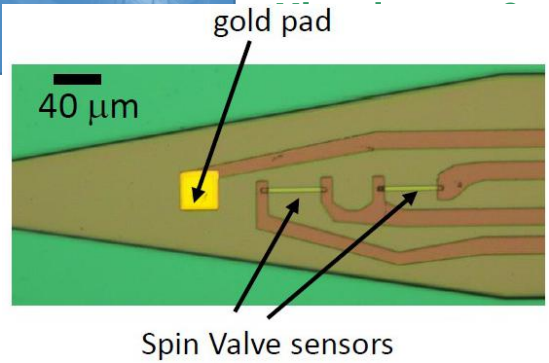

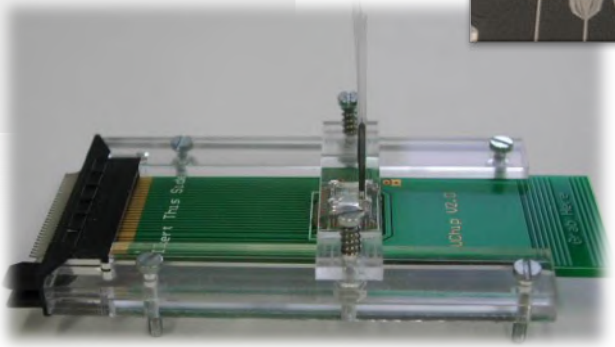

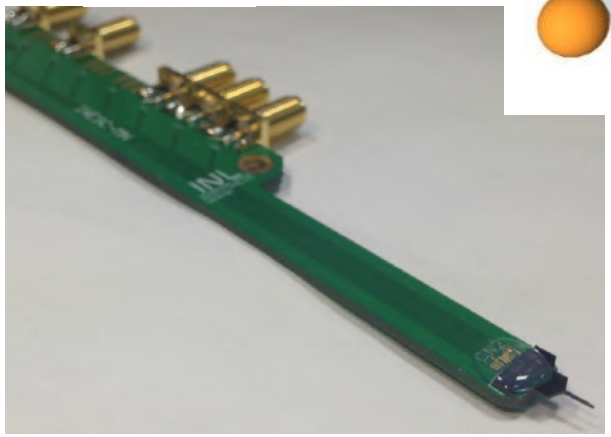

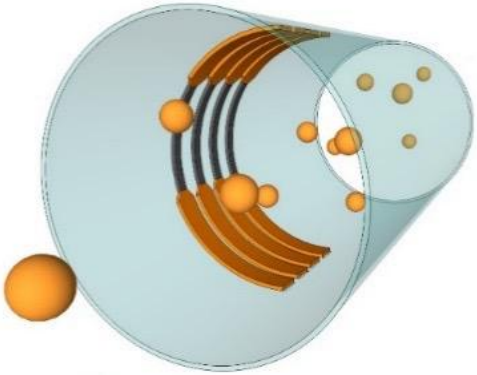

Needle sensors
Flexible MR Sensors

Magnetoresistive biochip concept

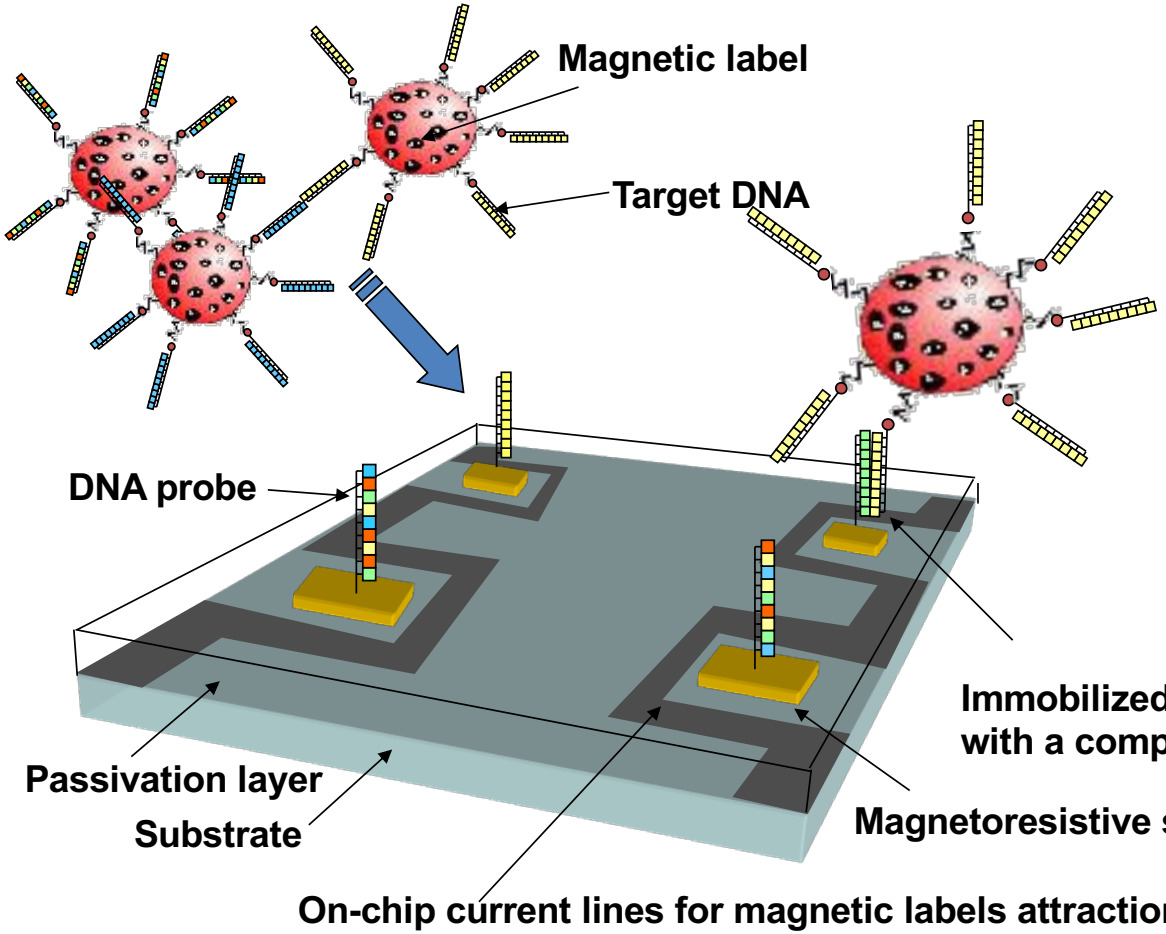

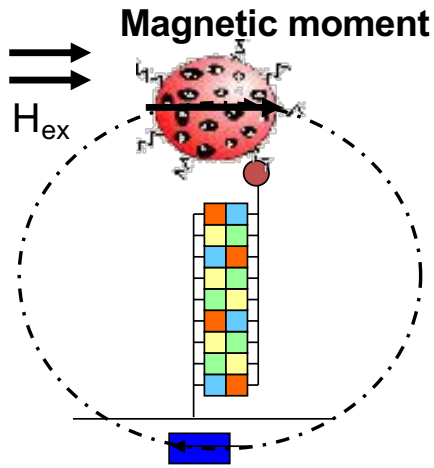

Biosensors and Bioelectronics, *210, 114302 (2022),*
Lab-on-Chip *18, 2593-2603 (2018);*
Trends in Biotechnology, August 2004
IEEE Magnetics Letters, *10 (1) (2019);*
Anal. Bioanal. Chem. *(2019) 411, pp. 1839 (2019);*
ACS Nano *11 (11), pp 10659–10664 (2017)*
Lab-on-Chip, 11 (13), 2255 – 2261 (2011)
Analytical Methods, ***8***, *119-128 (2016);*
Lab-on-Chip, 2012, 12 (3), 546 – 557 (2011)
Biosensors and Bioelectronics *11, 100149, (2022)*

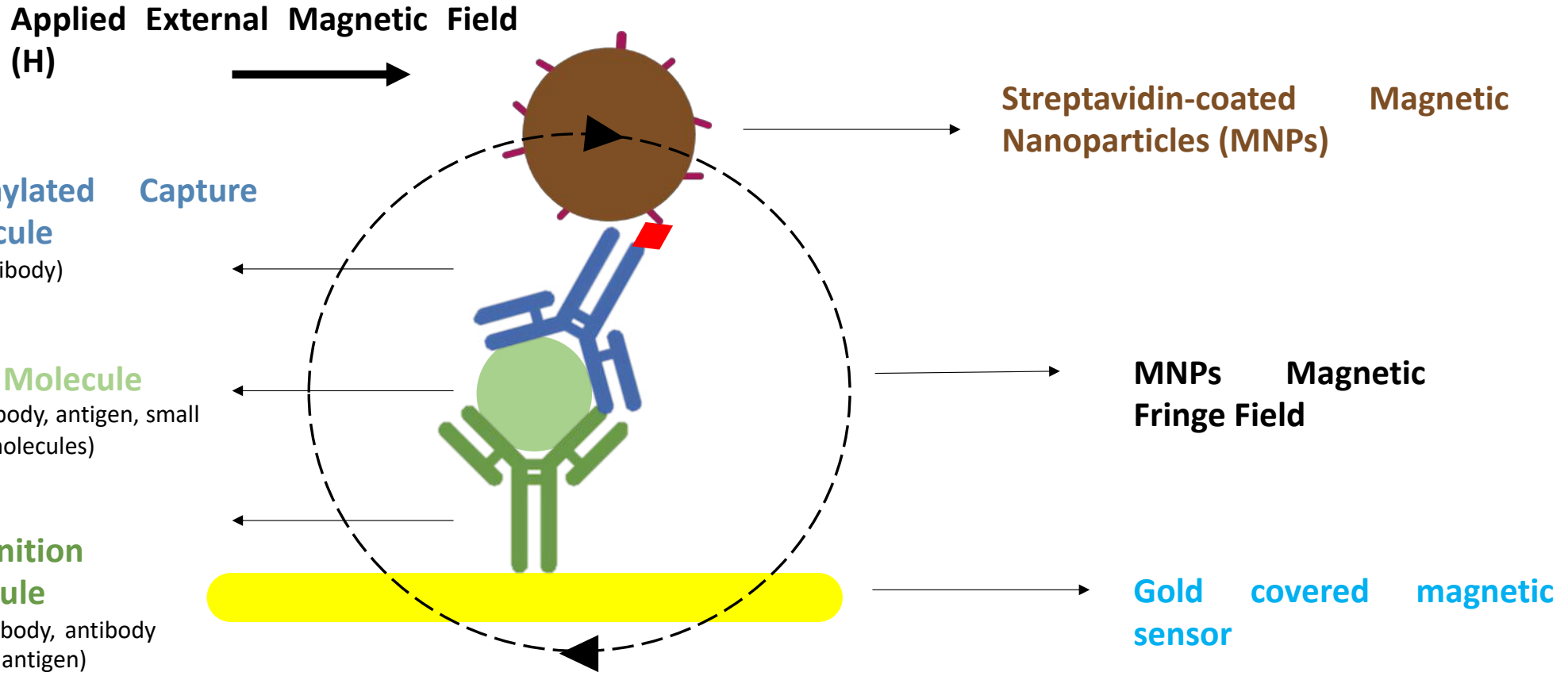
Applied External Magnetic Field (H)
Streptavidin-coated Magnetic Nanoparticles (MNPs)
Biotinylated Capture Molecule
(e.g. antibody)
Target Molecule
(e.g. antibody, antigen, small organic molecules)
Recognition Molecule
(e.g. antibody, antibody mimetic, antigen)
MNPs Magnetic Fringe Field
Gold covered magnetic sensor

Technology:
MR-based Biochips and Static Platform

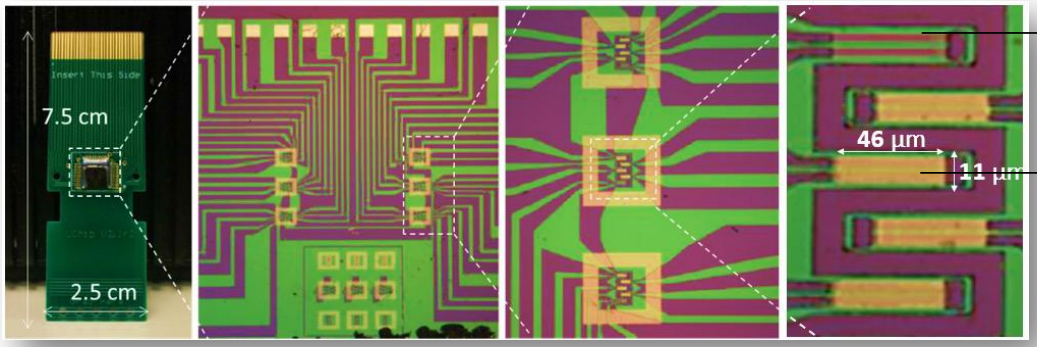

Spin valve (SV) sensors

Gold thin film over SV

Static Platform

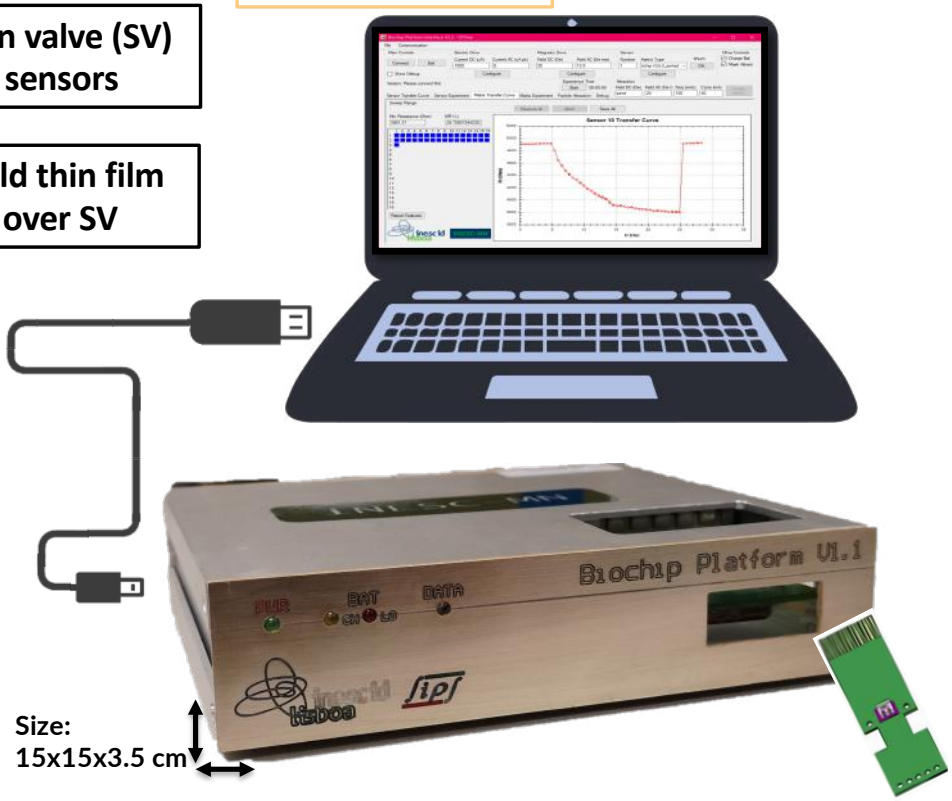

- Highly sensitive
- Multiplexing capability
- Distinct sensing regions
- Disposable Biochips

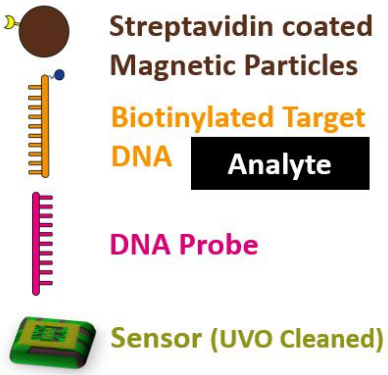

Functionalization

If no time: move to

Control sensor

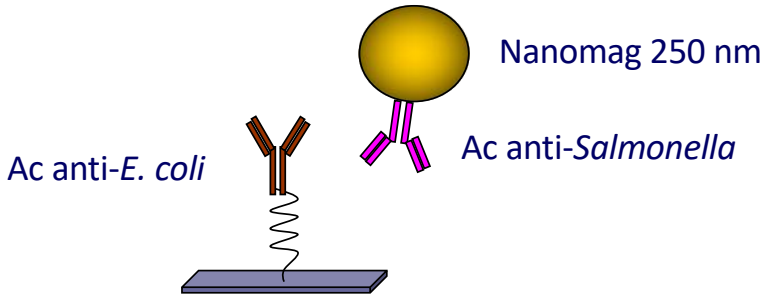

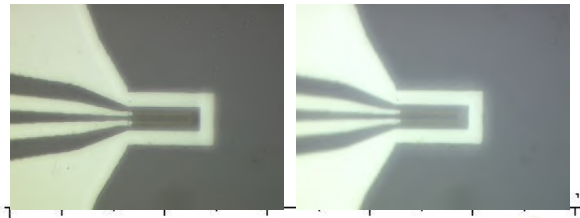

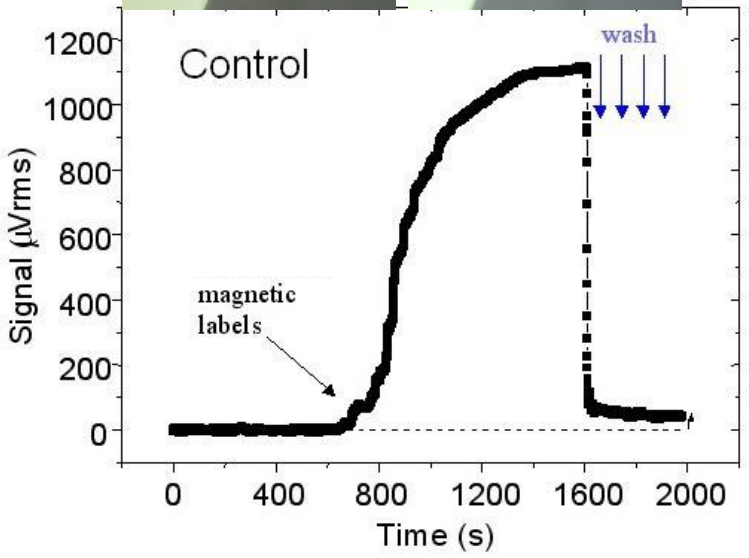

Final ~ initial

Signal sensor

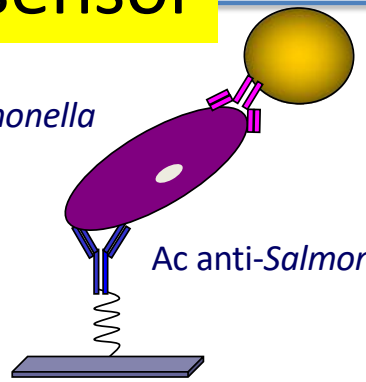

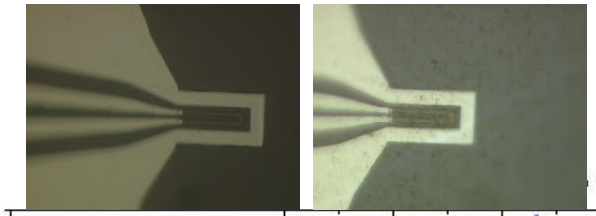

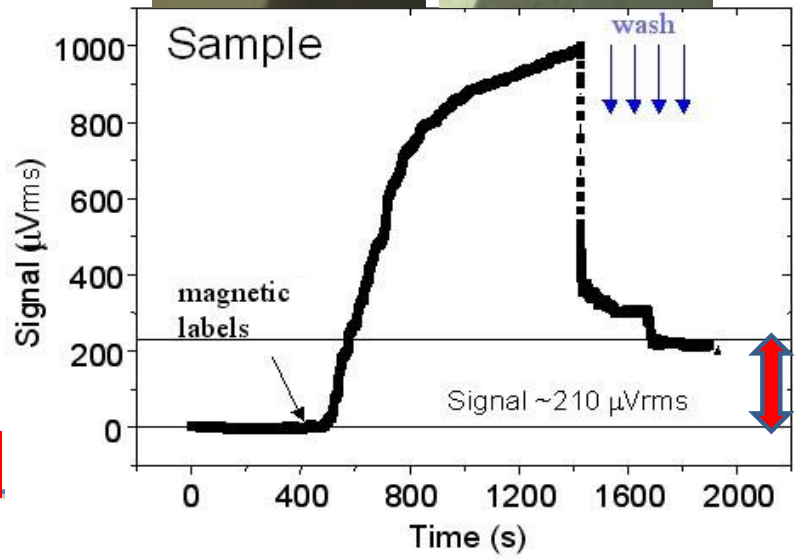

α salmonela concentration

INESC MN
Microsistemas & Nanotecnologias

Biosensors and Bioelectronics 210 (2022) 114302

Contents lists available at ScienceDirect

Biosensors and Bioelectronics

journal homepage: www.elsevier.com/locate/bios

Zika and dengue viruses

INESC MN
Microsistemas & Nanotecnologias

Combined detection of molecular and serological signatures of viral infections: The dual assay concept

Débora C. Albuquerque [a,b,c,*], Verónica C. Martins [b], Elisabete Fernandes [c], Líbia Zé-Zé [d,e], Maria João Alves [d], Susana Cardoso [a,b]

[a] IST - Instituto Superior Técnico, University of Lisbon, Lisboa, 1049-001, Portugal
[b] INESC-MN-Instituto de Engenharia de Sistemas E Computadores – Microsistemas e Nanotecnologias, Lisboa, 1000-029, Portugal
[c] INL, International Nanotechnology Laboratory, Braga, 4715-330, Portugal
[d] INSA- National Institute of Health Doutor Ricardo Jorge, Centre for Vectors and Infectious Diseases Research, Águas de Moura, 2965-575, Portugal
[e] BioISI - Biosystems and Integrative Sciences Institute, Edifício TecLabs, Campus da FCUL, Campo Grande, Lisboa, 1749-016, Portugal

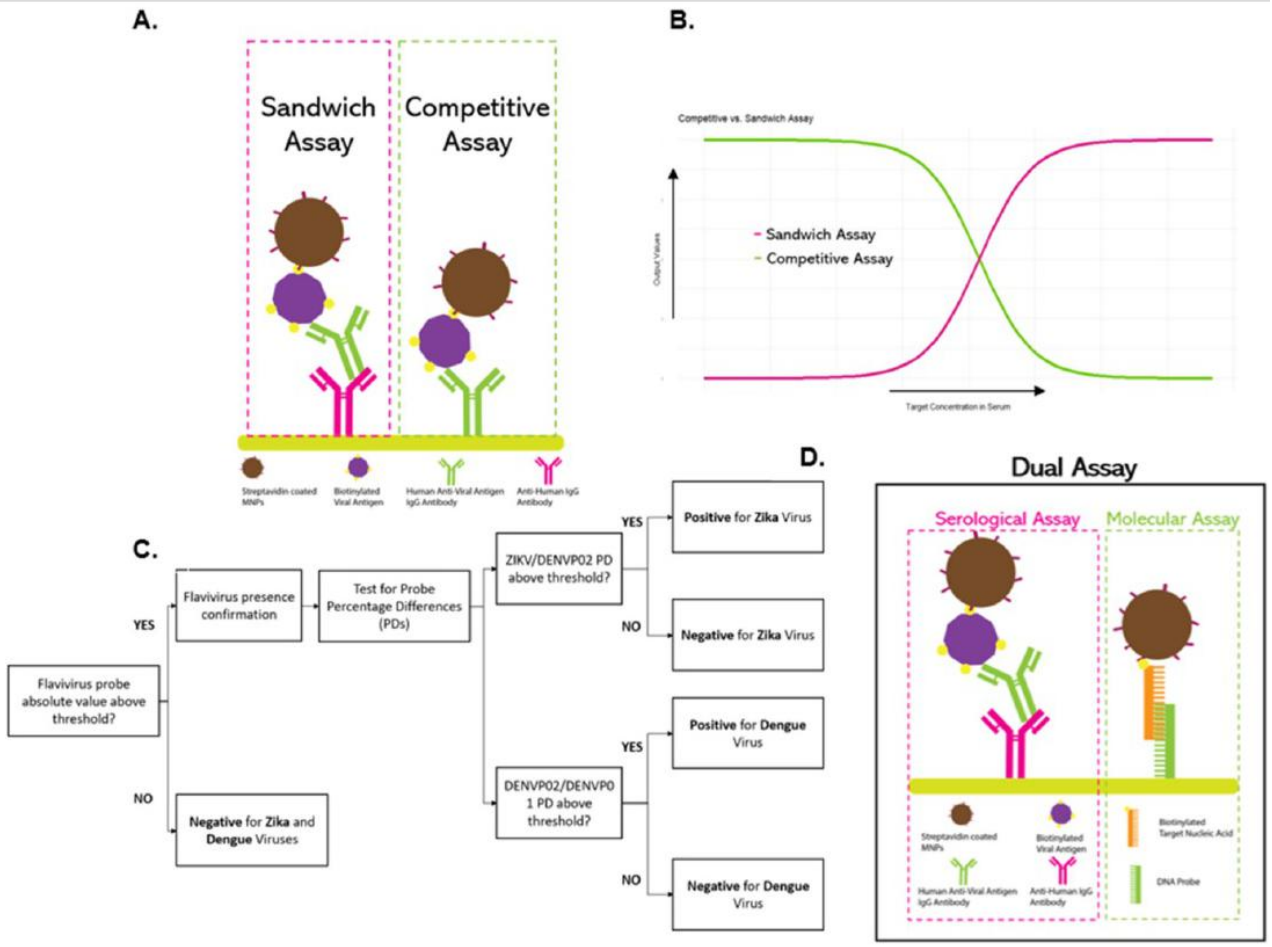

Molecular Assays: Viral RNA target Detection

Specific Detection

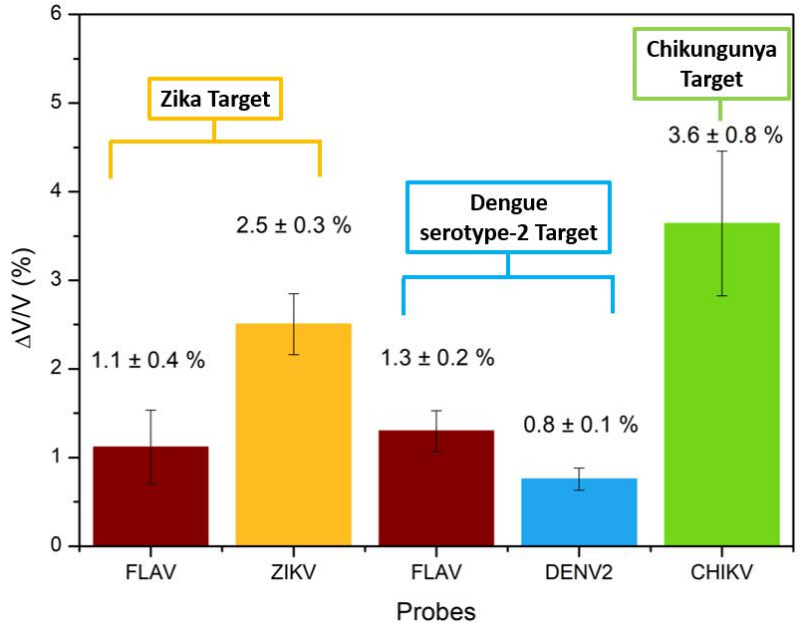

Non-specific Detection

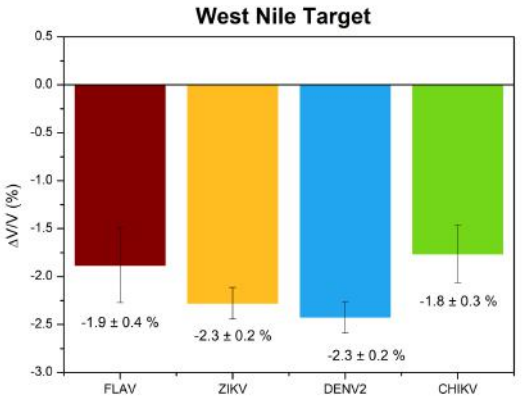

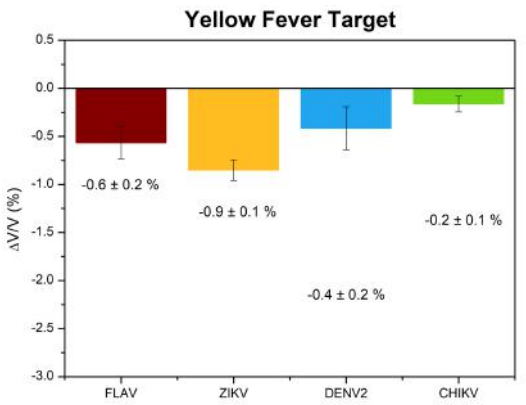

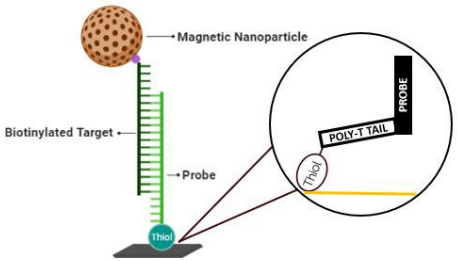

- **Successful detection of ZIKV, DENV-2 and CHIKV, with high signal specificity**
- **No signal detection for non-specific flaviviruses. High probe specificity**

INESC MN

Microsistemas e Nanotecnologias

Magnetic cytometer

INESC MN

Microsistemas & Nanotecnologias

Labels magnetization

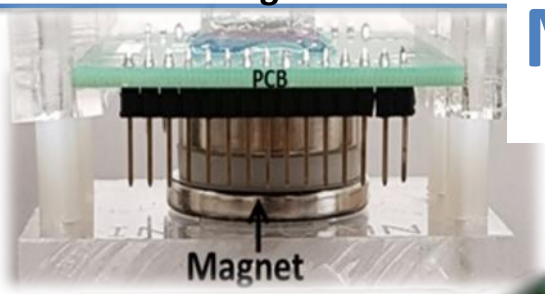

Microfluidics technology

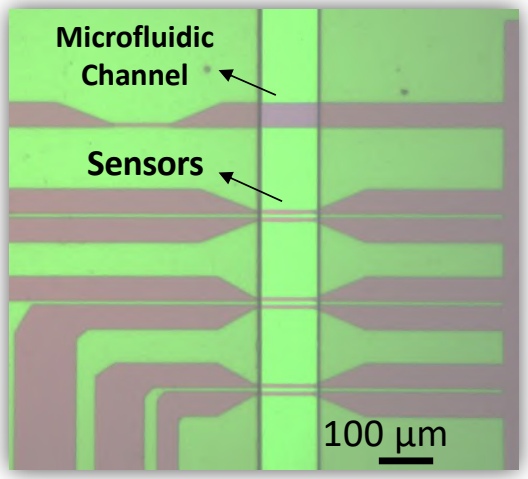

Detection principle

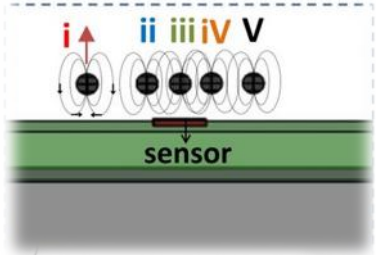

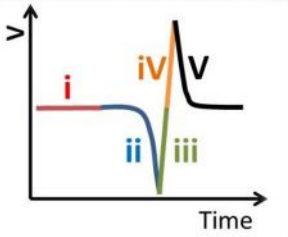

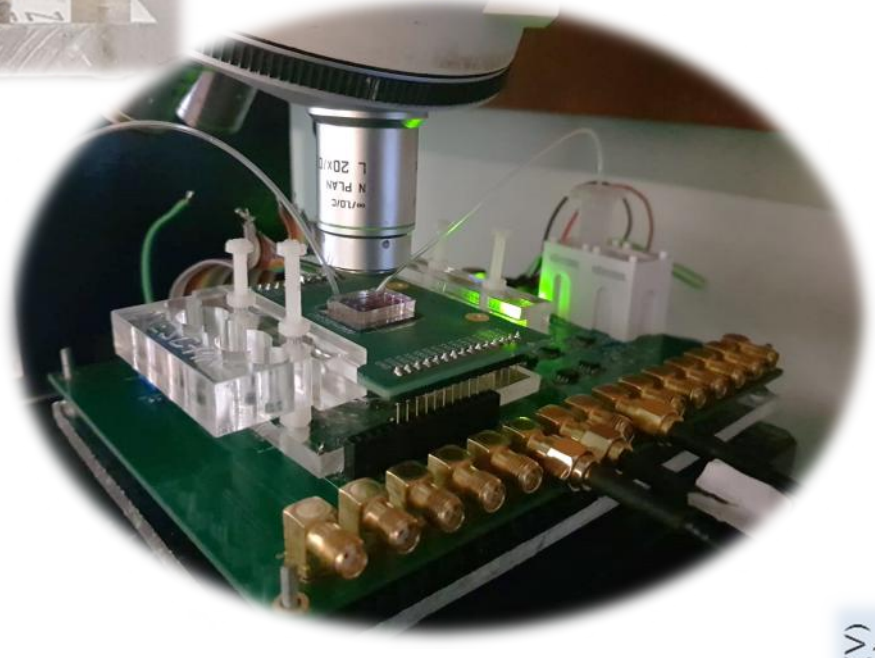

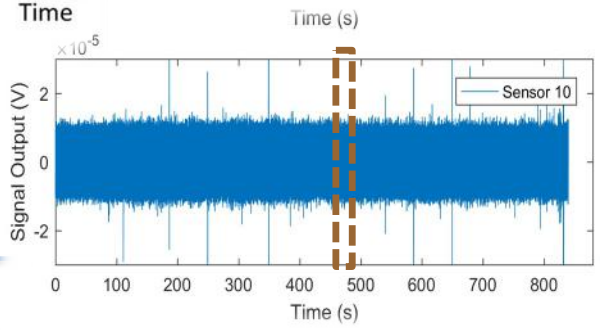

Detection signals

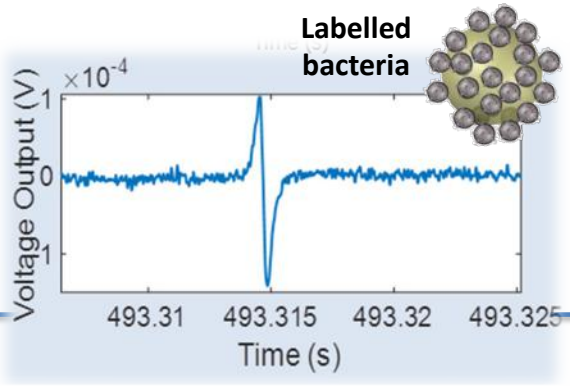

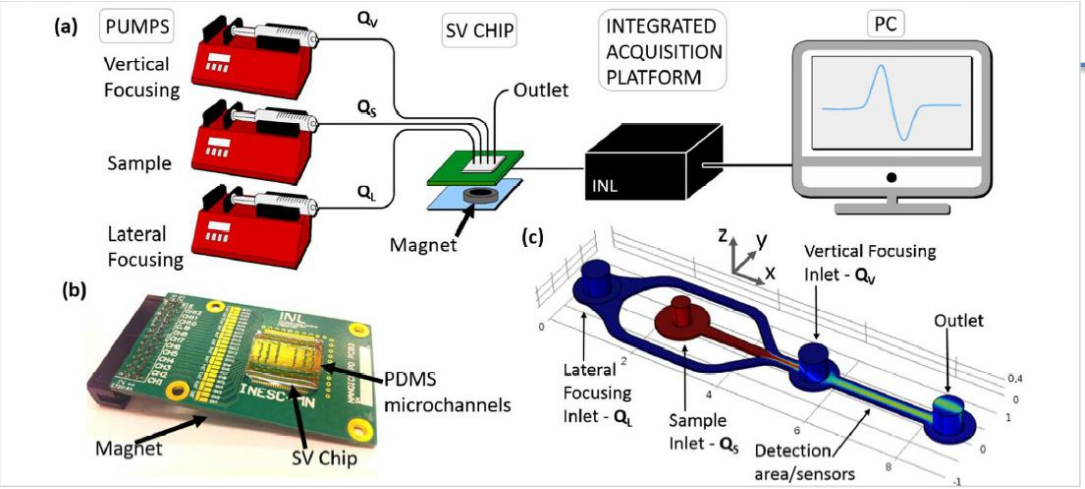

- Labelled cell
- Beads free in solution

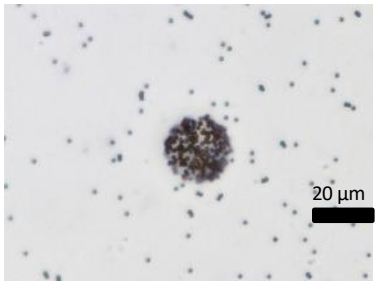

Lab-on-Chip 18, 2593-2603 (2018);

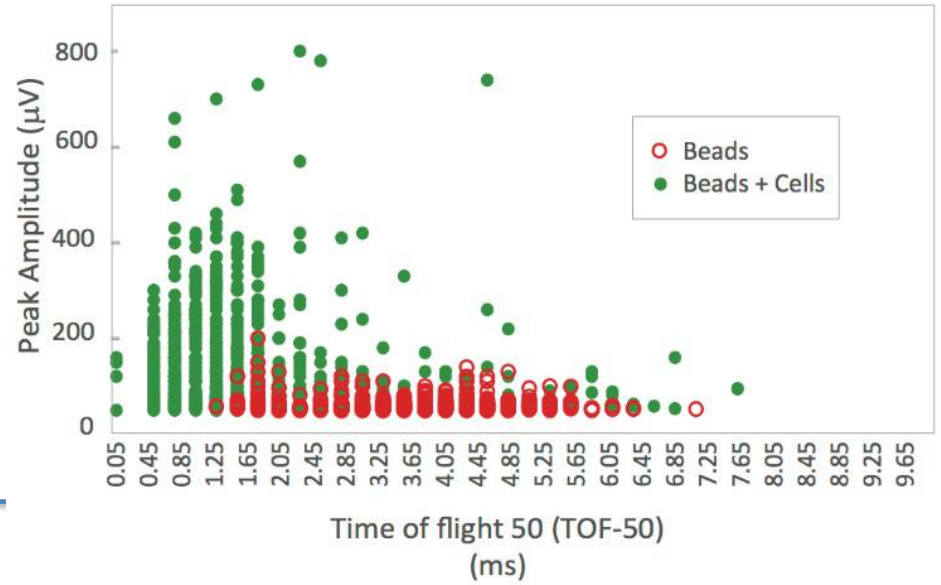

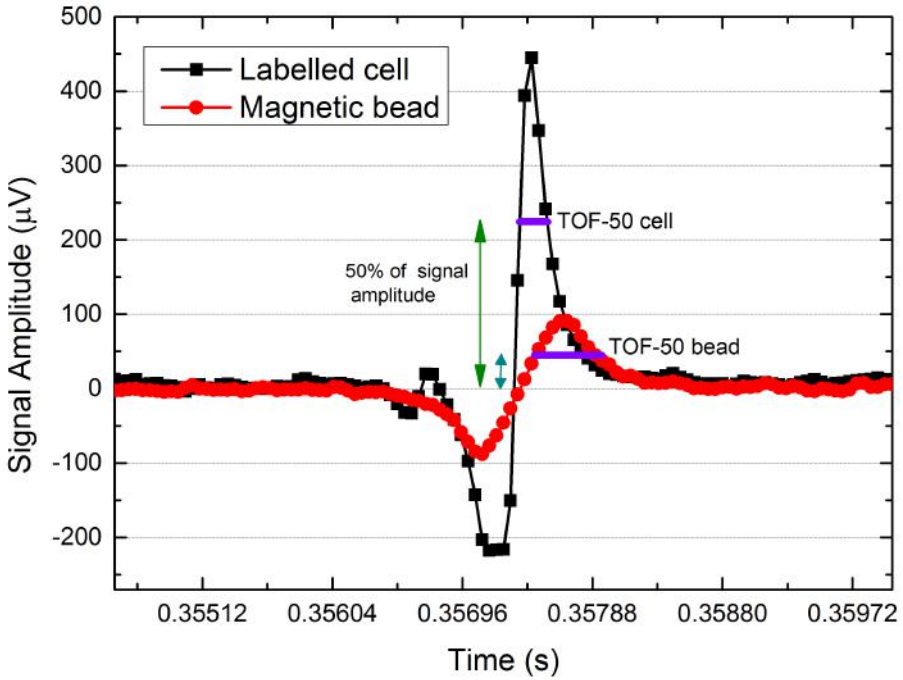

Contents lists available at ScienceDirect

Biosensors and Bioelectronics: X

journal homepage: www.journals.elsevier.com/biosensors-and-bioelectronics-x

INESC MN
Microsistemas & Nanotecnologias

On-site magnetic screening tool for rapid detection of hospital bacterial infections: Clinical study with *Klebsiella pneumoniae* cells

Ana R. Soares [a,b,*], R. Afonso [b,c], V.C. Martins [a], C. Palos [d], P. Pereira [d], Diogo M. Caetano [b,c], Davide Carta [a,b], S. Cardoso [a,b]

[a] Instituto de Engenharia de Sistemas E Computadores – Microsistemas e Nanotecnologias (INESC MN), Rua Alves Redol 9, 1000-029, Lisbon, Portugal
[b] Instituto Superior Técnico, Universidade de Lisboa, Av. Rovisco Pais 1, 1049-001, Lisbon, Portugal
[c] Instituto de Engenharia de Sistemas E Computadores - Investigação e Desenvolvimento, Rua Alves Redol 9, 1000-029, Lisbon, Portugal
[d] HBA – Hospital Beatriz Ângelo, Av. Carlos Teixeira 3, 2674-514, Loures, Portugal

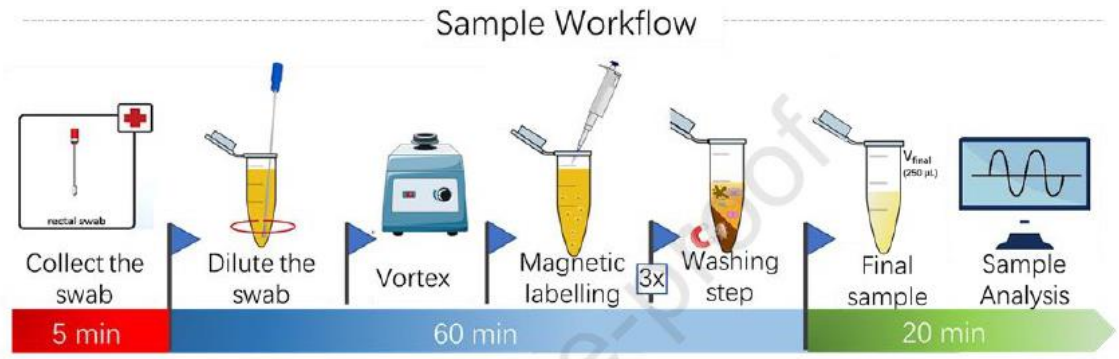

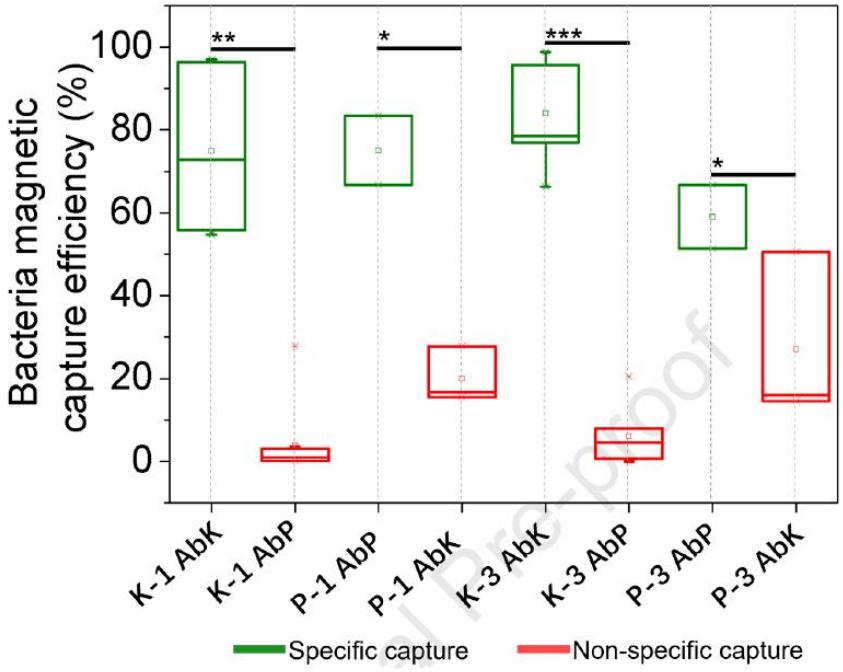

If no time: move to

INESC MN
Microsistemas & Nanotecnologias

Summary

xMR sensors

– thin film control at sub nm level

- noise

- thermal stability

- detectivity

Applications

Spintronic sensors team


Prof. @IST

Susana Cardoso


Prof. @IST
@INL since 2008

Paulo P. Freitas


Rita Macedo


Chamseddine Bouhafs

INESC MN
Microsistemas & Nanotecnologias

Physics Eng
Electrical Eng
BioNano
Materials Eng

PhD Students

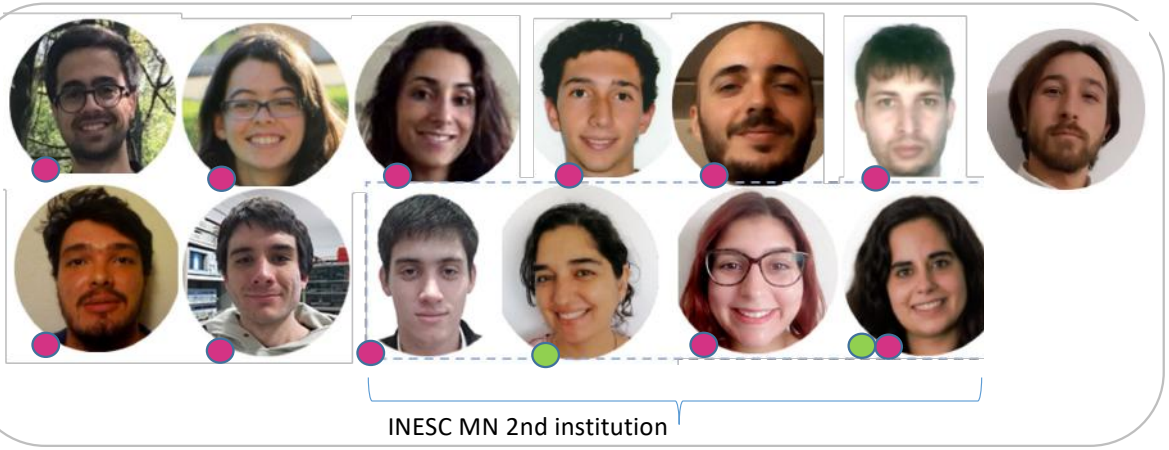

MSc Students

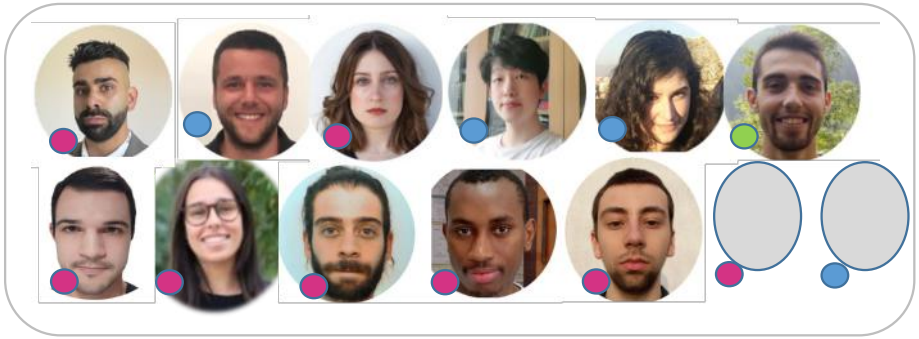

Junior Engineers

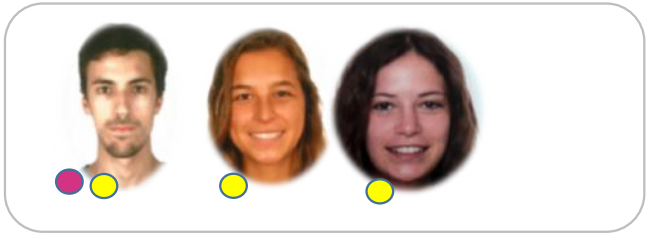

Visiting students


IOP Beijing


IMG-Basque


Ablute-PRR-H4PT

AGH Poland

ETH

Univ Bath

Acknowledgments

INESC MN
Microsistemas & Nanotecnologias

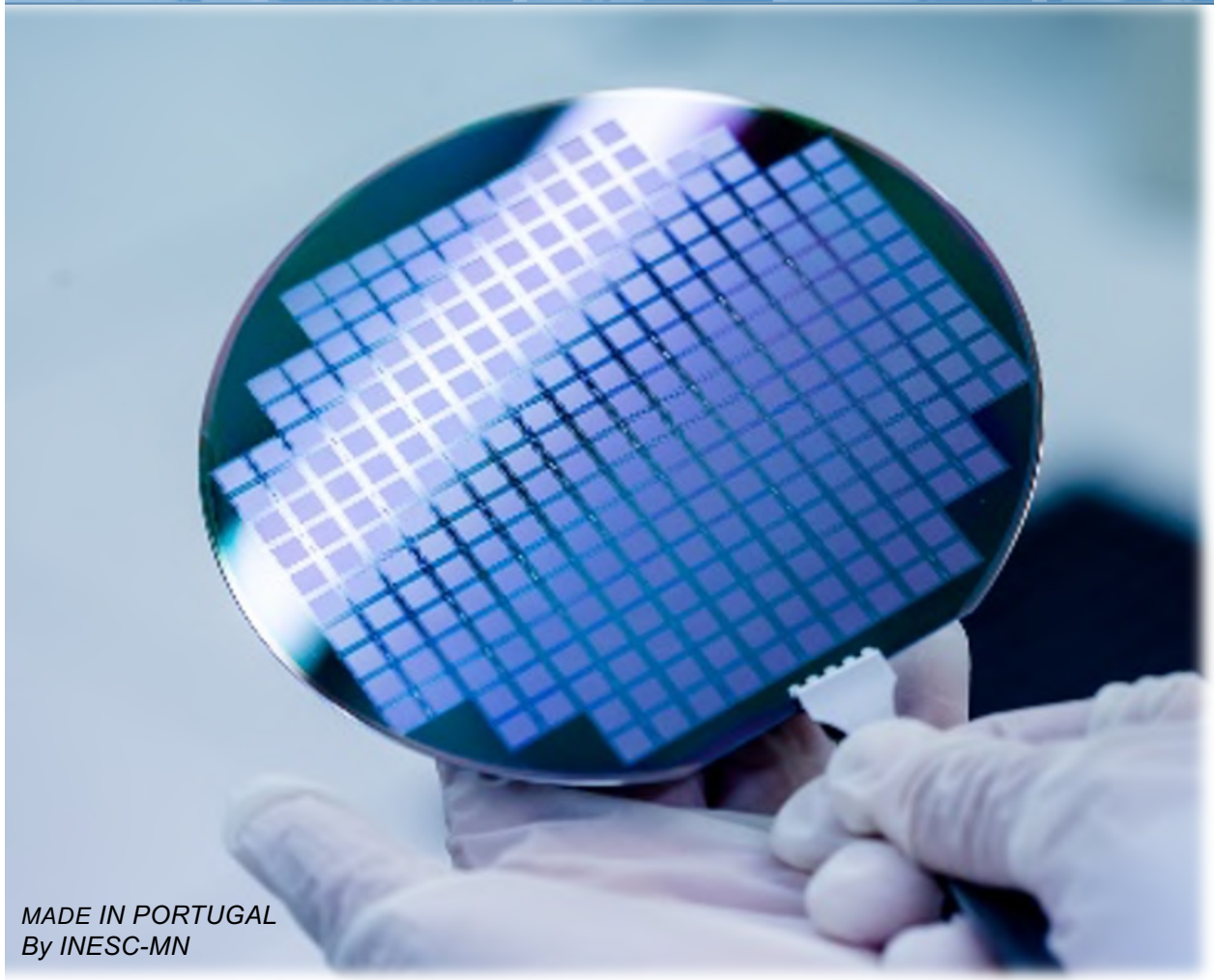

MADE IN PORTUGAL
By INESC-MN

Mag-ID H2020-EIC-FTI-870017
MASMA H2020-EIC-SMEInst n. 858934
MagScopy4IHC LISBOA-01-0145-FEDER-031200

INESC MN
Microsistemas &
Nanotecnologias

Technological challenges:

- Compatibility with electronics => Wheatstone Bridge

REQUIRED: WHEATSTONE BRIDGE

TMR sensor acts as a variable resistor

Simplest way to measure:

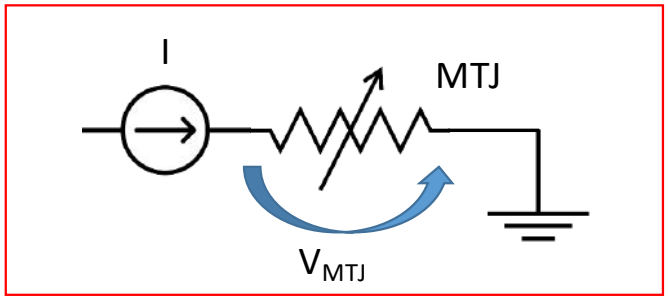

Disadvantages:

- Current source is difficult to implement
- Prone to supply noise
- Output is not zero when field is zero

Wheatstone bridge

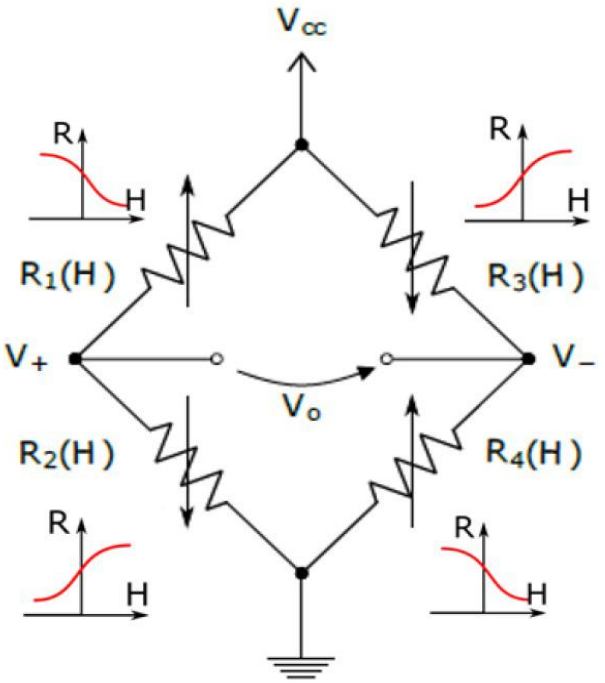

$$V_o = \left(\frac{R_2(H)}{R_1(H) + R_2(H)} - \frac{R_4(H)}{R_3(H) + R_4(H)} \right) V_{cc}$$

Advantages:

- Bipolar output
- Noise immunity
- Easy biasing (V const)

Disadvantage:

- Requires 4 TMR sensors
- **Anti-parallel sensitivities**

Full bridge with mechanical mounting

INESC MN
Microsistemas & Nanotecnologias

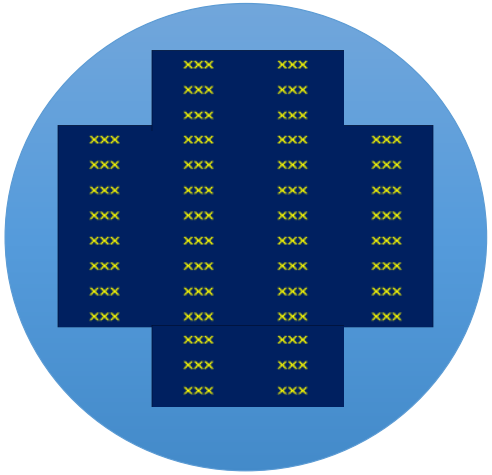

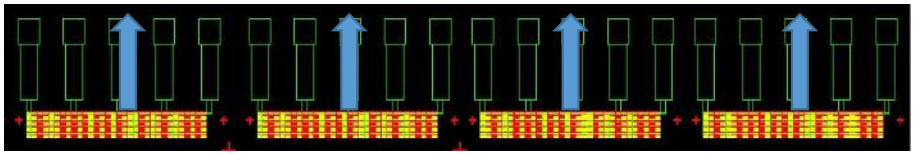

1 deposition step for TMR definition
The same annealing for all wafer

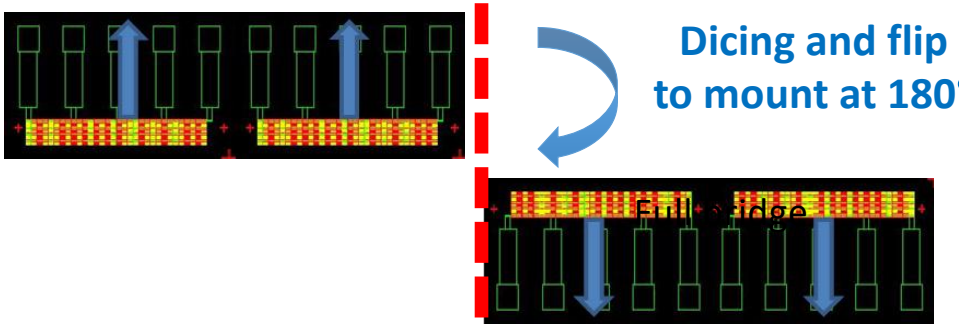

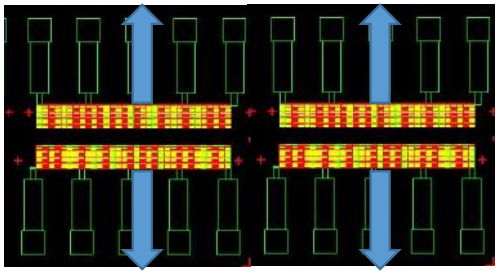

Full Weatstone Bridge

Full bridge with 2 depositions

INESC MN
Microsistemas &
Nanotecnologias

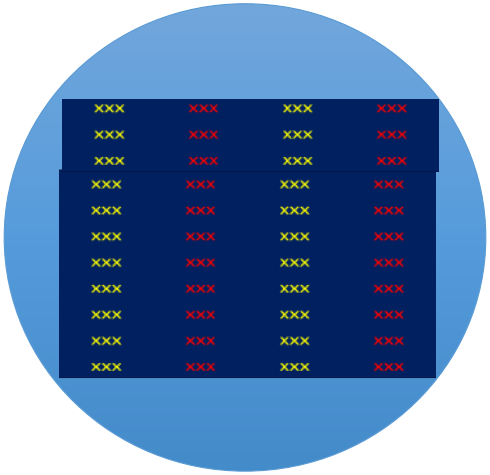

2 deposition steps for TMR definition

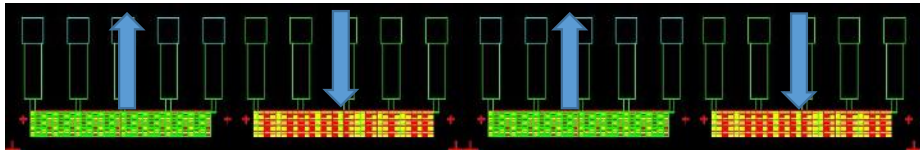

INESC MN
Microsistemas & Nanotecnologias

Full Wheatstone Bridge Architectures		Device Footprint	Production Cost	Performance
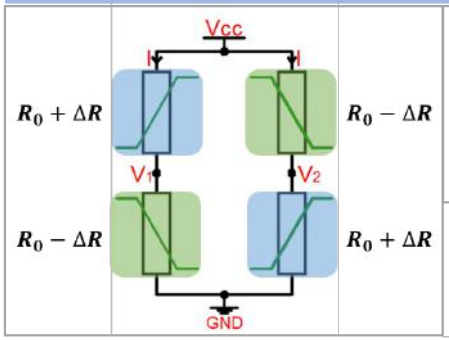	Single xMR Stack Deposition — Discrete Assembling	🔴	🟢	🟡
	Single xMR Stack Deposition — Sensor/Source Arrangement	🟡	🟢	🟢
	Single xMR Stack Deposition — Local Assisted Annealing Current / Laser	🟡	🔴	🟢
	Multi xMR Stack Deposition — Annealing free xMR stack	🟢	🔴	🟢
	Multi xMR Stack Deposition — Asymmetric SAF reference structure	🟢	🔴	🟢

Discrete Assembling

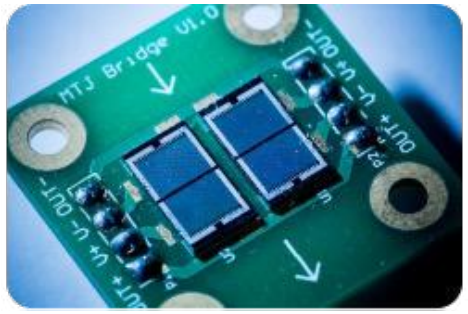

Sensor/Source Arrangement

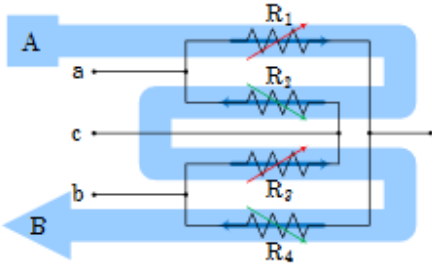

C. Reig et al., *Sensors.*, 9, 7919 (2009)

Local Assisted Annealing

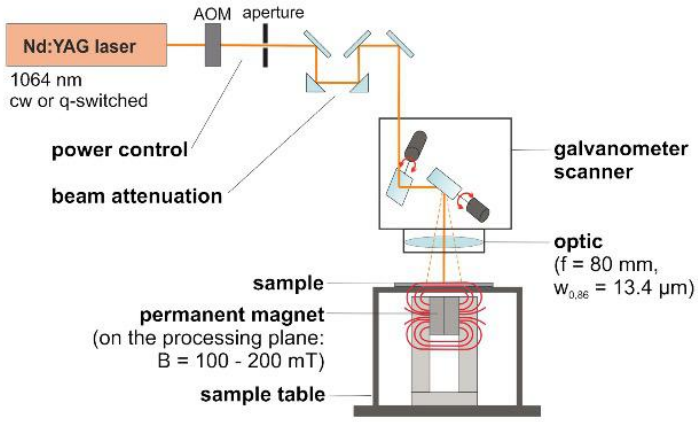

Berthold et al., *Appl. Surf. Sci.*, 302, 159 (2014)
J. Cao et al., *Journal of Applied Physics*, 107, 09E712 (2010)

Asymmetric SAF reference structure

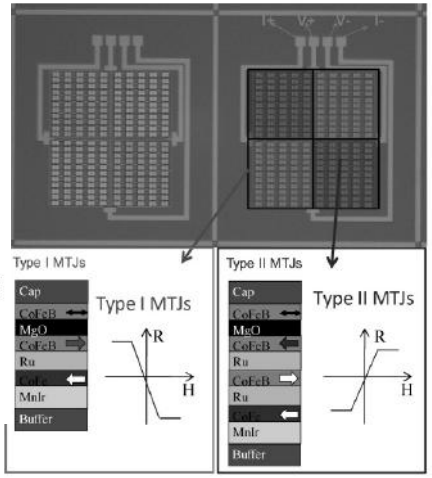

R. Ferreira et al., *IEEE Trans. Magn.*, 48, 4107 (2012)